UNIVERSITY
OF TRENTO - Italy
DEPARTMENT OF INDUSTRIAL ENGINEERING

XXXIV cycle

Doctoral School in Materials, Mechatronics
and Systems Engineering

Flexible and 3D printable conductive composites for pressure sensor applications

Mayara Cristina Bertolini

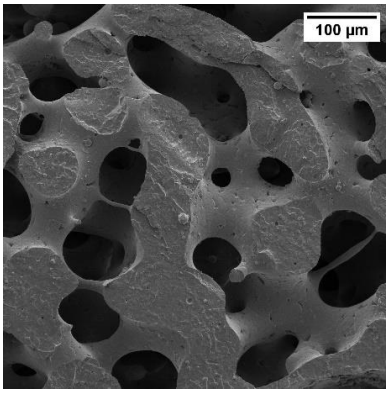

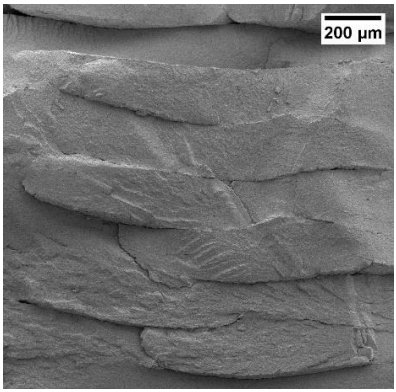

September 2022

FLEXIBLE AND 3D PRINTABLE CONDUCTIVE COMPOSITES

FOR PRESSURE SENSOR APPLICATIONS

Mayara Cristina Bertolini

E-mail: mayara.bertolini@unitn.it

Approved by:

Prof. Alessandro Pegoretti, Advisor
Department of Industrial Engineering
University of Trento, Italy.

Prof.Guilherme Mariz de Oliveira Barra, Advisor abroad
Department of Mechanical Engineering
Universidade Federal de Santa Catarina, Brazil.

Ph.D. Commission:

Prof. Giuliana Gorrasi
Department of Industrial Engineering
Università degli Studi di Salerno,Italia.

Prof. Dachamir Hotza,
Department of Mechanical Engineering
Universidade Federal de Santa Catarina, Brazil.

Documento assinado digitalmente
Guilherme Mariz de Oliveira Barra
Data: 24/01/2023 16:36:32-0300
CPF: ***.718.428-**
Verifique as assinaturas em https://v.ufsc.br

University of Trento,

Department of Industrial Engineering

September 2022

University of Trento - Department of Industrial Engineering

Doctoral Thesis

Mayara Cristina Bertolini - 2022
Published in Trento (Italy) – by University of Trento

ISBN: - - - - - - - - -

“I am among those who think that science has great beauty”

Marie Curie

Abstract

The aim of this study was the development of flexible and highly electrically conductive polymer composites via compression molding and fused filament fabrication for possible applications as piezoresistive or piezoelectric materials for pressure sensors. Composites based on blends of poly(vinylidene fluoride)/thermoplastic polyurethane (PVDF/TPU) as matrix and containing various fractions of carbon black-polypyrrole (CB-PPy) as conductive filler were prepared. Several characterization techniques were performed in order to evaluate the mechanical, thermal, chemical and electrical properties, morphology and printability of the investigated materials.

First, PVDF/TPU blends with different compositions were prepared by melt compounding followed by compression molding. The results showed that the flexibility aimed for the final materials was improved with the addition of TPU to PVDF composites. SEM images evidenced the achievement of a co-continuous blend comprising 50/50 vol% of PVDF/TPU. The blends composed of PVDF/TPU 38/62 vol% and the co-continuous blend of PVDF/TPU 50/50 vol% were selected as matrices for the preparation of compression molded and 3D printed composites in order to achieve an optimal compromise between electrical conductivity, mechanical properties and printability.

Various amounts of carbon black-polypyrrole, from 0 up to 15%, were added to the selected blends in order to rise the electrical conductivity of the composites and to possible act as nucleating filler for the β crystalline phase of PVDF in order to increase its piezoelectric response. The addition of CB-PPy increased the electrical conductivity of all composites. However, the electrical conductivity of composites based on PVDF/TPU 50/50 vol% co-continuous blends was higher than those found for PVDF/TPU 38/62 vol% composites at the same filler content. Indeed, the electrical percolation threshold of the conductive co-continuous composite blends was 2%, while the electrical percolation threshold of the composites with the nonco-continuous composite blends was 5%. With respect to the mechanical properties, the incorporation of the filler into the blends leaded to more rigid materials with higher

elastic modulus, lower elongation at break and higher storage modulus. The storage modulus (G') and complex viscosity (η*) of the composites increased with the addition of CB-PPy. The rheological percolation threshold was found to be 3% for PVDF/TPU/CB-PPy 38/62 vol% and 1% for PVDF/TPU/CB-PPy 50/50 vol%, indicating that higher amount of filler could compromise the processability of the composites. The addition of CB-PPy also resulted in a reduction on the T_g and T_m values of the composites due to the reduction of the mobility of the polymeric chains.

Based on the electrical conductivity and mechanical behavior of the composites, three different compositions were selected for the extrusion of filaments to be used in a 3D printing process. Overall, the 3D printed parts presented lower mechanical and electrical properties because of the presence of voids, defects and overlapping layers that can hinder the flow of electrons. The electrical conductivity values of PVDF/TPU/CB-PPy 38/62 vol% composites containing 5% and 6 wt% of CB-PPy 3D printed samples are one to seven orders of magnitude lower than those found for compression molded composites with the same composition. Even if the electrical conductivity value for PVDF/TPU 38/62 vol% compression molded composite with 6% of CB-PPy was as high as $1.94x10^{-1}$ $S•m^{-1}$, the 3D printed composite with same composition showed a very low electrical conductivity of $6.01x10^{-8}$ $S•m^{-1}$. On the other hand, the 3D printed co-continuous composite PVDF/TPU 50/50 vol% with 10% of filler displayed a high value of electrical conductivity of $4.14×10^{0}$ $S•m^{-1}$ even after the printing process.

Moreover, the piezoresistive responses of the composites were investigated. For PVDF/TPU/CB-PPy 38/62 vol% composites, the compression molded and 3D printed samples with 5% and 6% of CB-PPy exhibited good piezoresistive response. However, only the composites with 6% displayed high sensitivity and gauge factor values, large pressure range and reproducible piezoresistive responses under 100 cycles for both methods. On the other hand, for PVDF/TPU/CB-PPy co-continuous composites only the compression molded sample with 5% of CB-PPy presented good and reproducible piezoresistive responses.

The crystallinity and β phase content of PVDF were investigated for the composites. Althought the degree of crystallinity of the samples decreased with the addition of CB-PPy, the percentage of β phase in PVDF was increased. The

piezoelectric coefficient d_{33} of the samples increased with the percentage of β phase. The addition of 6% or more of CB-PPy was necessary to increase significatively the piezoelectric coefficient (d_{33}) of the composites. The β phase content and piezoelectric responses of PVDF were lower for samples prepared by FFF.

Finally, as a collateral research, the electromagnetic interference shielding effectiveness (EMI-SE) were measured for all composites. Composites with higher electrical conductivity showed better shielding of the electromagnetic radiation. In addition, composites based on the co-continuous blend displayed higher EMI shielding efficiency than 38/62 vol% composites. The main mechanism of shielding was absorption for all composites. Specimens prepared by FFF displayed diminished EMI-SE responses when compared to compression molded samples.

Riassunto

Lo scopo di questo studio è lo sviluppo di compositi polimerici flessibili e ad elevata conducibilità elettrica tramite stampaggio a compressione e manifattura additiva (fused filament fabrication) per possibili applicazioni come materiali piezoresistivi o piezoelettrici in sensori di pressione. In particolare, sono stati preparati compositi a base di miscele di poli(vinilidene fluoruro)/poliuretano termoplastico (PVDF/TPU) come matrice e contenenti varie frazioni di nerofumo-polipirrolo (CB-PPy) come riempitivo conduttivo. Sono state utilizzate diverse tecniche di caratterizzazione al fine di valutare le proprietà meccaniche, termiche, chimiche ed elettriche, la morfologia e la stampabilità dei materiali ottenuti.

In primo luogo, miscele PVDF/TPU con diverse composizioni sono state preparate mediante mescolatura allo stato fuso seguita da stampaggio a compressione. I risultati hanno mostrato che la flessibilità del PVDF viene notevolemente migliorata dall'aggiunta di TPU. Le immagini SEM hanno evidenziato il raggiungimento di una miscela co-continua per una composizione 50/50% in volume di PVDF/TPU. Le miscele composte da PVDF/TPU 38/62 vol% e la miscela co-continua di PVDF/TPU 50/50 vol% sono state selezionate come matrici per la preparazione di compositi per stampaggio a compressione e manifattura additiva al fine di ottenere un compromesso ottimale tra conducibilità, proprietà meccaniche e stampabilità.

Alle miscele selezionate sono state aggiunte varie quantità di nerofumo-polipirrolo, dallo 0 al 15%, per aumentare la conducibilità elettrica dei compositi ed eventualmente fungere da additivo nucleante per la fase β cristallina del PVDF al fine di aumentarne la risposta piezoelettrica. L'aggiunta di CB-PPy ha aumentato la conduttività elettrica di tutti i compositi. Tuttavia, la conduttività elettrica dei compositi basati su miscele co-continue di PVDF/TPU 50/50% in volume era superiore a quella trovata per compositi PVDF/TPU 38/62% in volume con lo stesso contenuto di riempitivo. Infatti, la soglia di percolazione elettrica delle miscele conduttive era del 2%, mentre la soglia di percolazione elettrica dei compositi con miscele composite non continue era del 5%. Per quanto riguarda le proprietà meccaniche, l'incorporazione

del riempitivo nelle mescole ha portato a materiali più rigidi con modulo elastico più elevato, allungamento a rottura inferiore e modulo conservativo più elevato. Il modulo conservativo (G') e la viscosità complessa (η*) dei compositi sono aumentate con l'aggiunta di CB-PPy. La soglia di percolazione reologica è risultata essere del 3% per PVDF/TPU/CB-PPy 38/62 vol% e dell'1% per PVDF/TPU/CB-PPy 50/50 vol%, indicando che una maggiore quantità di riempitivo potrebbe compromettere la processabilità dei compositi. L'aggiunta di CB-PPy ha comportato anche una riduzione dei valori di T_g e T_m dei compositi a causa della riduzione della mobilità delle catene polimeriche.

Sulla base della conduttività elettrica e del comportamento meccanico dei compositi, sono state selezionate tre diverse composizioni per l'estrusione di filamenti da utilizzare in un processo di stampa 3D. Nel complesso, le parti stampate in 3D presentavano proprietà meccaniche ed elettriche inferiori a causa della presenza di vuoti, difetti e strati sovrapposti che possono ostacolare il flusso di elettroni. I valori di conducibilità elettrica dei compositi PVDF/TPU/CB-PPy 38/62 vol% contenenti il 5% e il 6% di CB-PPy di campioni stampati in 3D sono da uno a sette ordini di grandezza inferiori a quelli trovati per i compositi stampati a compressione con la stessa composizione. Anche se il valore di conducibilità elettrica per il composito stampato a compressione PVDF/TPU 38/62 vol% con il 6% di CB-PPy era pari a $1{,}94 \times 10^{-1}$ S•m^{-1}, il composito stampato in 3D con la stessa composizione ha mostrato un valore molto basso di conducibilità elettrica, pari a $6{,}01 \times 10^{-8}$ S•m^{-1}. D'altra parte, il composito PVDF/TPU 50/50 vol% stampato in 3D con il 10% di riempitivo ha mostrato un elevato valore di conducibilità elettrica, pari a $4{,}14 \times 10^{0}$ S•m^{-1}, anche dopo il processo di stampa.

Inoltre, sono state studiate le risposte piezoresistive dei compositi. Per i compositi PVDF/TPU/CB-PPy 38/62 vol%, i campioni stampati a compressione e stampati in 3D con il 5% e il 6% di CB-PPy hanno mostrato una buona risposta piezoresistiva. Tuttavia, solo i compositi con il 6% hanno mostrato valori di sensibilità e gauge factor elevati, ampio intervallo di pressione e risposte piezoresistive riproducibili in 100 cicli per entrambi i metodi. D'altra parte, per i compositi co-continui PVDF/TPU/CB-PPy solo il campione stampato a compressione con il 5% di CB-PPy ha presentato risposte piezoresistive adeguate e riproducibili.

La cristallinità e il contenuto di fase β del PVDF sono stati studiati per i compositi. Sebbene il grado di cristallinità dei campioni diminuisca con l'aggiunta di CB-PPy, la percentuale di fase β in PVDF risulta aumentata. Il coefficiente piezoelettrico d_{33} dei campioni aumenta anch'esso con la percentuale di fase β. L'aggiunta del 6% o più di CB-PPy è stata necessaria per aumentare significativamente il coefficiente piezoelettrico (d_{33}) dei compositi. Il contenuto di fase β e le risposte piezoelettriche del PVDF sono inferiori per i campioni ottenuti mediante stampa 3D.

Infine, come ricerca collaterale, è stata misurata l'efficacia della schermatura contro le interferenze elettromagnetiche (EMI-SE) per tutti i compositi. I compositi con una maggiore conduttività elettrica hanno mostrato una migliore schermatura della radiazione elettromagnetica. Inoltre, i compositi basati sulla miscela co-continua hanno mostrato un'efficienza di schermatura EMI maggiore rispetto ai compositi a 38/62% in volume. Per tutti i compositi, il principale meccanismo di schermatura è l'assorbimento. I campioni preparati mediante manifattura additiva hanno mostrato risposte EMI-SE inferiori rispetto ai campioni stampati a compressione.

Resumo

O objetivo deste estudo foi o desenvolvimento de compósitos poliméricos flexíveis e altamente condutores elétricos preparados por moldagem por compressão e por fabricação de filamentos fundidos (FFF) para possíveis aplicações como materiais piezoresistivos ou piezoelétricos para sensores de compressão. Compósitos baseados em misturas de poli(fluoreto de vinilideno)/poliuretano termoplástico (PVDF/TPU) como matriz e contendo várias frações de negro de fumo-polipirrol (CB-PPy) como aditivo condutor foram preparados. Diversas técnicas de caracterização foram realizadas para avaliar as propriedades mecânicas, térmicas, químicas e elétricas, morfologia e printabilidade dos materiais investigados.

Primeiro, blendas de PVDF/TPU com diferentes composições foram produzidas por mistura por fusão seguida de moldagem por compressão. Os resultados mostraram que a flexibilidade desejada para os materiais foi melhorada com a adição de TPU aos compósitos de PVDF. As imagens SEM evidenciaram a obtenção de uma blenda co-contínua com 50/50 vol% de PVDF/TPU. As blendas compostas de PVDF/TPU 38/62 vol% e a blenda co-contínua de PVDF/TPU 50/50 vol% foram selecionadas como matrizes para a preparação de compósitos moldados por compressão e impressos em 3D a fim de alcançar uma ótima combinação entre condutividade, propriedades mecânicas e printabilidade.

Várias quantidades de negro de fumo-polipirrol, de 0 a 15%, foram adicionadas às blendas selecionadas para aumentar a condutividade elétrica dos compósitos e possivelmente atuar como agente nucleante para a fase cristalina do PVDF a fim de aumentar sua resposta piezoelétrica. A adição de CB-PPy aumentou a condutividade elétrica de todos os compósitos. No entanto, a condutividade elétrica dos compósitos baseados em blendas co-contínuas PVDF/TPU 50/50 vol% foi maior do que as encontradas para os compósitos de PVDF/TPU 38/62 vol% com mesma concentração de aditivo. De fato, o limiar de percolação elétrico dos compósitos com blenda co-contínua foi de 2%, enquanto o limiar de percolação elétrico dos compósitos compostos da blenda não contínua foi de 5%. Com relação às propriedades mecânicas, a incorporação do aditivo condutor nas blendas resultou em

materiais mais rígidos com maior módulo de elasticidade, menor alongamento na ruptura e maior módulo de armazenamento. O módulo de armazenamento (G') e a viscosidade complexa (η*) dos compósitos aumentaram com a adição de CB-PPy. O limiar de percolação reológico foi de 3% para PVDF/TPU/CB-PPy 38/62 vol% e 1% para PVDF/TPU/CB-PPy 50/50 vol%, indicando que uma quantidade maior de carga poderia comprometer a processabilidade dos compósitos. A adição de CB-PPy também resultou na redução dos valores de T_g e T_m dos compósitos devido à redução da mobilidade das cadeias poliméricas.

Com base na condutividade elétrica e no comportamento mecânico dos compósitos, três composições diferentes foram selecionadas para a extrusão de filamentos para serem posteriormente utilizados no processo de impressão 3D. No geral, as peças impressas em 3D apresentaram propriedades mecânicas e elétricas inferiores devido à presença de vazios, defeitos e camadas sobrepostas que podem dificultar o fluxo de elétrons. Os valores de condutividade elétrica dos compósitos impressos em 3D de PVDF/TPU/CB-PPy 38/62 vol% contendo 5% e 6% de CB-PPy são de uma a sete ordens de grandeza menores do que os encontrados para os compósitos com a mesma composição moldados por compressão. Mesmo que o valor da condutividade elétrica para o compósito PVDF/TPU 38/62 vol% com 6% de CB-PPy moldado por compressão foi de $1{,}94 \times 10^{-1}$ S•m^{-1}, o compósito impresso em 3D com a mesma composição mostrou um valor muito baixo de condutividade elétrica de $6{,}01 \times 10^{-8}$ S•m^{-1}. Por outro lado, o compósito co-contínuo de PVDF/TPU 50/50 vol% com 10% de aditivo impresso em 3D apresentou um alto valor de condutividade elétrica de $4{,}14 \times 10^{0}$ S•m^{-1} mesmo após o processo de impressão.

Além disso, as respostas piezoresistivas dos compósitos foram investigadas. Para os compósitos PVDF/TPU/CB-PPy 38/62 vol%, as amostras moldadas por compressão e impressas em 3D com 5% e 6% de CB-PPy exibiram boa resposta piezoresistiva. No entanto, apenas os compósitos com 6% de aditivo apresentaram valores elevados de sensibilidade e gauge factor, atuação em ampla faixa de pressão e respostas piezoresistivas reprodutíveis durante a aplicação de 100 ciclos de compressão/descompressão para ambos os métodos de fabricação. Por outro lado, para os compósitos co-contínuos de PVDF/TPU/CB-PPy apenas a amostra moldada

por compressão com 5% de CB-PPy apresentou respostas piezorresistivas boas e reprodutíveis.

A cristalinidade e o teor de fase β do PVDF foram investigados para os compósitos. Embora o grau de cristalinidade das amostras tenha diminuído com a adição de CB-PPy, a porcentagem de fase β no PVDF aumentou. O coeficiente piezoelétrico d_{33} das amostras aumentou com a porcentagem de fase β. A adição de 6% ou mais de CB-PPy foi necessária para aumentar significativamente o coeficiente piezoelétrico (d_{33}) dos compósitos. O conteúdo de fase β e as respostas piezoelétricas do PVDF foram menores para as amostras preparadas por FFF.

Por fim, como pesquisa colateral, a eficiência de blindagem contra interferência eletromagnética (EMI-SE) foi medida para todos os compósitos. Compósitos com maior condutividade elétrica apresentaram melhor blindagem da radiação eletromagnética. Além disso, os compósitos baseados na blenda co-contínua apresentaram maior eficiência de blindagem contra EMI do que os compósitos de PVDF/TPU 38/62 vol%. O principal mecanismo de blindagem foi a absorção para todos os compósitos. As amostras preparadas por FFF apresentaram respostas de EMI-SE menores quando comparadas às amostras moldadas por compressão.

Table of contents

List of Figures

List of Tables

List of abbreviation and acronyms

3D	three dimensional
3DP	three dimensional printed
A	absorption
ABS	poly(acrylonitrile-co-butadiene-co-styrene)
AM	additive manufacture
ASTM	American society for testing and materials
ATR	attenuated total reflectance
$BaTiO_3$	barium titanate
CB	carbon black
CM	compression molded
CNT	carbon nanotubes
d_{33}	piezoelectric constant
DSC	differential scanning calorimetry
FTIR	fourier transform infrared
XRD	X-ray diffraction
E'	storage modulus
E"	loss modulus
ECPC	electrically conductive polymer composites
EDS	energy dispersive X-ray spectroscopy
DMTA	dynamic mechanical thermal analysis
EMI-SE	electromagnetic interference shielding effectiveness
FFF	fused filament fabrication
G'	storage modulus
G"	loss modulus
GF	gauge factor
GR	graphene
GO	graphene oxide
ICP	intrinsically conductive polymer
MFI	melt flow index

MR	multiple reflection
MWCNT	multi-walled carbon nanotubes
η^*	complex viscosity
PA	polyamide
PANI	polyaniline
PC	polycarbonate
PS	polystyrene
PCL	polycaprolactone
PETG	polyethylene terephthalate
PLA	polylactic acid
PMMA	poly(methyl methacrylate)
PPy	polypyrrole
PTH	polythiophene
PVDF	poly(vinylidene) fluoride
R	reflection
SE_A	shielding effectiveness by absorption
SEM	scanning electron microscopy
SE_R	shielding effectiveness by reflection
tan δ	loss tangent
T_g	glass transition temperature
THF	tetrahydrofuran
T_m	melting temperature
TPU	thermoplastic polyurethane

Chapter I

1. Introduction

The addition of carbonaceous nanofillers into polymeric matrices have been widely reported to improve electrical and thermal conductivity, mechanical strength, modulus of elasticity and toughness of electrically conductive polymer composites (ECPCs). In fact, combining characteristics of electrically conductive particles and polymeric matrices is an efficient way to prepare ECPCs with superior properties when compared to the neat components. Moreover, the final properties of ECPCs are also a result of the fabrication method. The direct dispersion of the conductive filler into the polymeric matrix by melt compounding is commonly used to prepare conductive composites with a good balance of mechanical and functional properties. Furthermore, fused filament fabrication (FFF), one of the most important 3D printing technology, is an interesting approach for the preparation of complex shapes with ECPCs with enhanced properties and low cost.

Flexible and highly conductive polymer composites have been widely studied for numerous technological applications in strain and pressure sensing, flexible electronic devices, smart sensors, soft robotics and electromagnetic interference shielding. In this context, the development of flexible pressure sensors with high sensitivity, fast responses, extended lifetime and low cost have been investigated. Pressure sensors are based on different types of working principles including piezoresistivity, piezocapacitivity, piezoelectricity and inductivity. Among them, piezoresistive sensors convert the applied compressive force into changes in electrical resistivity, while piezoelectric sensors produce voltage responses to the applied pressure. The performance of pressure sensors can be quantified by the sensitivity of the sensor and gauge factor that are related to the ability and accuracy of the sensor in converting the external stimulus into a measurable output signal.

The main challenge in developing sensors based on ECPCs is the reduction of the electrical percolation threshold in order to achieve high responses at minimum filler content thus preserving the mechanical properties and processability of the matrix. Some studies have been reported on the preparation of polymer blends to be used as matrices in polymeric composites to reduce the percolation threshold. Co-continuous blends have been investigated due to the possible selective localization of the conductive filler in one phase or at the interface of the co-continuous phases of the blend.

Furthermore, a proper choice of the materials used to fabricate ECPCs plays an important role on the final properties of the composites. Among polymeric materials, poly(vinylidene fluoride) (PVDF) offers interesting possibilities for the production of ECPCs for pressure sensors applications because of its low cost, low melting point and potential piezoelectric properties. However, it manifests low elongation at break, limited stretchability and it is a semi-crystalline polymer that is difficult to be printed because of warping and shrinking during the crystallization process. Moreover, its relatively high elastic modulus does not allow the production of soft pressure sensors. In this framework, blending PVDF with thermoplastic polyurethane (TPU), which is an amorphous, stretchable and printable material, is the selected strategy to overcome these drawbacks. Moreover, PVDF can exist in five different crystalline phases, however, the one with higher dipole moment and piezoelectric properties is the polar β phase, while commercial PVDF is predominantly composed of the nonpolar α phase. In this context, the addition of carbon nanofillers have been also taylored to assist the formation of the β phase in the PVDF matrix.

The aim of this work is the fabrication of flexible and electrically conductive composites composed of a blend of poly(vinylidene fluoride) and thermoplastic polyurethane (PVDF/TPU) as matrix and containing different fractions of carbon black-polypyrrole (CB-PPy) as conductive filler for possible applications as piezoresistive pressure sensors and piezoelectric materials. The composites were prepared by melt compounding followed by compression molding and fused filament fabrication. As a collateral research, the electromagnetic interference shielding capability of the final composites was also tested.

Firstly, polymer blends of PVDF/TPU were prepared in different compositions. The blends composed of PVDF/TPU 38/62 vol% and PVDF/TPU 50/50 vol% were selected as matrices for the preparation of compression molded and 3D printed composites by adding various amounts of CB-PPy, from 0 up to 15%, in order to achieve the best relationship between mechanical properties, electrical conductivity and printability.

In order to evaluate the mechanical properties of the investigated blends and composites, quasi static tensile tests were performed and the elastic modulus and fracture behavior were determined. Dynamic mechanical thermal analysis (DMTA) tests were carried out to obtain the storage (E') and loss (E'') moduli and galss transition (T_g) values were calculated from the tan δ peaks. The filler dispersion and distribution and the morphology of the blends and conductive composites were investigated by scanning electron microscopy (SEM). The effects of composition on the rheological behavior of the composites were analysed also by rheology measurements. In addition, density measurements were carried out to calculate the percentage of voids in 3D printed specimens.

Moreover, differential scanning calorimetry (DSC) was performed to assess the melting temperature, T_m, of the specimens and impact of blend composition and the addition of CB-PPy on the PVDF crystallinity. Fourier transform infrared (FTIR) spectroscopy was performed to evaluate the chemical structure, interaction between the materials and crystalline phases of PVDF. Also, X-ray diffraction analysis (XRD) were performed to investigate the effect of filler content in PVDF phase transformation.

The electrical behavior of the materials was assessed by electrical resistivity measurements. In addition, the piezoresistive responses of samples were evaluated simultaneously applying controlled loads and measuring the electrical resistivity. The piezoelectric properties of the composites were estimated by measuring the d_{33} constant. Additionally, electromagnetic interference shielding effectiveness (EMI-SE) properties were investigated for compression molded and 3D printed composites.

In summary, the main objective of this study was the development of flexible and highly conductive polymer composites for possible application as piezoresistive and piezoelectric pressure sensors. PVDF/TPU blends were prepared

in order to achieve the intended flexibily and reduce the electrical percolation threshold of the composites. Carbon black-polypyrrole was added as conductive filler to rise the electrical conductivity of the composites and to possible act as nucleating filler for the β crystalline phase of PVDF in order to increase its piezoelectric properties. In addition, this work aims to compare the results obtained for composites prepared by compression molding and FFF technique to evaluate the effect of the processing on the materials properties.

Chapter II

2 Background

2.1 Electrically conductive polymer composites (ECPCs)

Combining the characteristics of electrically conductive particles and polymeric matrices is an efficient way to prepare ECPCs that offers superior properties when compared to the neat components [1-3]. In fact, ECPCs have been widely investigated due to their notable electrical, mechanical and thermal properties. The final properties of ECPCs is also a consequence of the preparation method. The electrically conductive particles are commonly dispersed in a polymer matrix by *in situ* polymerization, solution casting and melt compounding followed by compression molding. Melt compounding is the direct dispersion of the electrically conductive filler in the polymer melt matrix applying a shearing force with the advantages of reduced costs and large scale production [1, 4]. Moreover, the fused filament fabrication (FFF) based on the currently large developed 3D printing technology is an interesting strategy for producing ECPCs with enhanced properties and low cost [5].

The addition of nanofillers, such as carbon nanotubes (CNT), carbon black (CB), graphene (GR) and others, into polymeric matrices have been reported to improve electrical and thermal conductivity, mechanical strength, modulus of elasticity and toughness of components fabricated by melt mixing and FFF [6-12]. ECPCs have been potentially used in numerous technological applications including chemical sensors [8], flexible electronic devices [9, 10, 13-15], electrical circuit printing [16, 17], electromagnetic interference (EMI) shielding [11, 18-24]. Moreover, the stimulus responsive behavior of ECPCs can be used to monitor and detect external changes making them promising candidates to fabricate electronic devices and smart sensor, such as strain and pressure sensors [1]. For instance, Christ et al. [15] printed a flexible

circuit with high elasticity and excellent pressure sensitive properties using a filament composed of thermoplastic polyurethane (TPU) and multi-walled carbon nanotubes (MWCNT). The sensitivity and detectable range of the sensor resulted to be significantly affected by the content of MWCNTs in the composite. Ahmed et al. [14] prepared polymeric composites of poly(methyl methacrylate)/carbon nanotubes (PMMA/CNT) by FFF for flexible electronic devices evaluating the mechanical, thermal and electrical properties of the composites. Alsharari et al. [10] investigated the variation of electrical conductivity with the applied strain for polylactic acid/thermoplastic polyurethane/graphene (PLA/TPU/GR) composites. Kim et al. [5] has efficiently prepared 3D printed poly(vinylidene fluoride/barium titanate ($PVDF/BaTiO_3$) composites with enhanced piezoelectric constant for sensors applications. Furthermore, Dul et al. [23] evaluated the effect of compression molding and FFF on EMI shielding properties of hybrid composites of acrylonitrile butadiene styrene/graphene-carbon nanotube (ABS/GNO-CNT).

The critical filler concentration in electrically conductive composites is known as percolation threshold, Figure 2-1, which represents the concentration needed to promote a significant increase in the electrical conductivity of the composite and it represents the onset of a conductive network into the insulating polymeric matrix [25]. One of the challenges in the development of electrically conductive polymer composites is the reduction of the percolation threshold to achieve the highest electrical conductivity values at the lower filler concentration in order to avoid loss of mechanical properties and printability of the insulating polymeric matrix and to reduce costs. The addition of the nanofillers into insulating polymeric matrices can significantly affect the rheology and printability of the filament as the nanoparticles reduce the mobility of the polymer chain and tend to aggregate at high content [18, 26]. The melt flow index (MFI) of ECPCs abruptly increases with increasing the filler concentration [27]. In fact, Dorigato at al. [27] claimed that the printability of ABS/MWCNT composites was partially impaired for conductive filler concentration above 4 wt%. Furthermore, a ductile to brittle transition with increasing the conductive filler content have been reported for ECPCs [27-30]. In general, tensile modulus and strength values increase with the conductive filler, while elongation at break decreases.

Moreover, the final properties of the composites depend not only on the conductive fillers but also on the polymer matrix. Thermosets, thermoplastics and thermoplastic elastomers have been reported for fabrication of ECPCs for various applications.

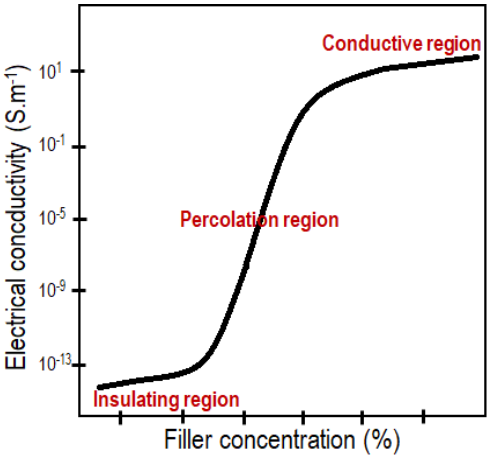

Figure 2-1: Electrical conductivity of polymer composites as function of filler content.

A great effort has been made to improve the quality and properties of ECPCs, reduce percolation threshold and overcome printing limitation of their components fabricated via FFF [9, 14, 27, 30, 31]. For this purpose, different strategies have been investigated such as the production of electrically conductive composites comprising two or more conductive fillers into insulating polymer matrix, the use of modified conductive fillers and the preparation of polymer blends to be used as matrix in polymeric composites [1, 11, 14, 28, 32-34]. Recently, many works have been published on the preparation of co-continuous immiscible polymer blends to reduce percolation threshold in ECPCs and to improve mechanical properties and printability of composites filaments [28, 32, 34-39]. Schematic representations of continuous, discontinuous and co-continuous phases are displayed in Figure 2-2. Figure 2-2 (a) shows the discontinuous phase of Polymer 2 disperse in the continuous phase

composed by Polymer 1 and Figure 2-2 (c) show the discontinuous phase of Polymer 1 disperse in the continuous phase composed by Polymer 2, while Figure 2-2 (b) displays both polymers forming a co-continuous phase structure. The reduction of the percolation threshold in co-continuous blends is related to double percolation because the conductive particles are preferable localized in one of the phases or at the interface of the co-continuous phases [1, 28, 35-38, 40-42]. In fact, conductive fillers as carbon nanotubes and carbon black have been found to be selectively distributed at the interface or in one of the co-continuous phases in polymer blends due to the different affinity of the filler for each blend component [34, 35, 37, 38, 40, 42]. The localization of conductive filler in co-continuous polymer blends is affected by thermodynamic, kinetic factors and the melt viscosity [38, 42]. Therefore, the insulating polymer selection, blend composition and conductive filler are an important key to achieve the highest electrical and mechanical properties of the polymer system at the lowest conductive filler content.

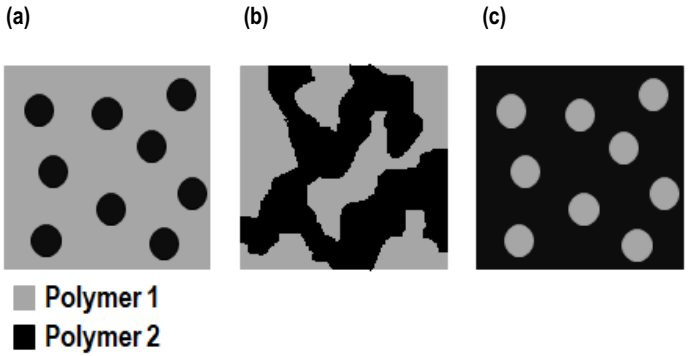

Figure 2-2: Schematic illustration of immiscible blends morphology for (a) and (b) discontinuos and (c) co-continuos polymer blends.

The development of material filaments for 3D printing based on co-continuous polymer blends containing conductive filler can be an interesting alternative to produce structural and highly conductive components for technical applications. Although the production of polymeric blends to control the morphology

and properties of ECPCs have been already proposed [28, 34-37, 40, 42], only a few studies are reported on its use in the fused filament fabrication (FFF) technology [33].

In this context, this study proposes the fabrication of electrically conductive composites of poly(vinylidene fluoride)/thermoplastic polyurethane blends as matrix comprising carbon black-polypyrrole as conductive filler by melt compounding and fused filament fabrication for possible applications as piezoresistive pressure sensors and piezoelectric materials. As a collateral research, the final composites were also tested as electromagnetic interference shielding materials.

2.2 Additive Manufacturing (AM)

Additive manufacturing (AM), also called 3D printing, is a very promising technology for prototyping manufacture due to its low cost, reduced lead time and production of complex structures without a mold tooling and without the typical waste from traditional manufacturing techniques [8-12, 33, 43, 44]. The first AM process was created in 1986 and it has attracted great attention in several fields of industry including aerospace, automotive, architecture, biomedical, semiconductor, flexible electronics, sensor and antennas [11, 12, 26, 29, 44, 45]. In additive manufacturing, the 3D object is created from a digital model that is sliced into a number of cross-sections or layers and the final object is built by the deposition of the material layer by layer [29, 44, 46-48].

According to the American Society for Testing and Materials (ASTM), additive manufacturing includes several technologies suitable for various materials, such as polymers, metals, ceramics and nanocomposites. The AM technologies can be divided into seven main categories according to the type of the material, physical state and type of energy used during the printing process and include: i) materials extrusion, ii) powder bed fusion, iii) photopolymerization, iv) binder jetting, v) material jetting, vi) direct energy deposition and vii) sheet lamination [26, 46, 47]. Among material extrusion technologies, fused filament fabrication (FFF) is the most popular because of its convenience, possibility of large scale production and reduced cost [8, 11, 26, 33, 44-47, 49, 50].

2.2.1 Fused filament fabrication (FFF)

Fused filament fabrication technology was invented by Scott Crump in 1989 [26, 29]. This technology has become very popular among other additive manufacturing techniques because of low processing and equipment cost, design flexibility, portability, easily scalable and low material waste [9, 12, 46, 49, 51].

Recently, FFF has been considered a promising way to fabricate electrically conductive polymeric composites [49]. In this technique, the 3D part is first designed using a computer program and saved as STL file that is sequentially imported into a slicing software [26, 51]. The printing operation is based on the sliced file and consists of a thermoplastic filament extruded through a heated nozzle that moves in x, y and z directions and the material layers are deposited in a heated glass bad [8, 26, 46, 51]. The schematic of FFF process is presented in Figure 2-3.

The final quality of printed parts is affected by several parameters including nozzle temperature, extrusion rate, raster angle, layer thickness, infill density, infill pattern and build orientation [26, 45]. Studies have shown anisotropy of objects produced by FFF as mechanical and electrical properties of printed parts depend on the growing direction. In addition, specimens produced via FFF present mechanical properties and electrical conductivity lower than specimens prepared by compression molding because of the presence of voids and defects [27-30, 32].

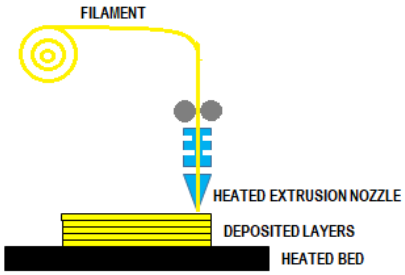

Figure 2-3: Schematic representation of the fused filament fabrication process.

The most common commercial filaments employed in FFF are the polymers such as poly(lactic acid) (PLA) and poly(acrylonitrile-co-butadiene-co-styrene) (ABS) [8, 11, 12, 26, 33, 43, 44, 51]. However, there are several other filaments commercially available such as polyamide (nylon), polycarbonate (PC), polystyrene (PS) and polyethylene terephthalate glycol-modified (PETG) [8, 12, 43, 51]. Moreover, recent advances in filament fabrication technology have also allowed using high-performance materials with functional properties, for instance, mechanical, electrical and thermal properties [43, 51, 52]. In this framework, the development of electrically conductive polymer composites (ECPCs) filaments is a good strategy for manufacturing multi-functional components using FFF technology.

2.3 Mechanical pressure sensors

Sensors are widely used in various fields of industry and medicine to measure temperature, pressure, energy and other physical parameters [53]. Numerous types of sensors have been produced and flexible pressure sensors are getting great attention in the field of soft robotics, wearable and flexible electronics, prosthetics, health monitoring and human-machine interface [1, 3, 10, 54, 55]. Such applications require flexible pressure sensors with high sensitivity, fast responses, long lifetime and low cost. A recent study affirms that the pressure sensors global market is expected to increase from $8.8 billion in 2018 to $15.97 billion in 2028. Currently, the major pressure sensor suppliers are Bosch, Denso, Sensata, and Amphenol [55].

A pressure sensor is a device that converts an external stimulus into electrical or other type of output signals [1, 55, 56]. These devices are based on different types of working principles such as piezoresistivity, piezocapacity, piezoelectricity, inductivity, and triboelectricity [7, 56]. Among the mentioned transduction approaches, piezoresistive and piezoelectric sensors are the most widely studied for transducing a mechanical stimulus to changes in resistance or producing an electrical voltage, respectively, in response to an applied pressure [2, 3, 7]. While the changes in the materials resistance in piezoresistive sensors depends on a

conductive network, see Figure 2-4 (a), piezoelectric responses result from oriented and permanent dipoles in the material [1, 7], see Figure 2-4 (b).

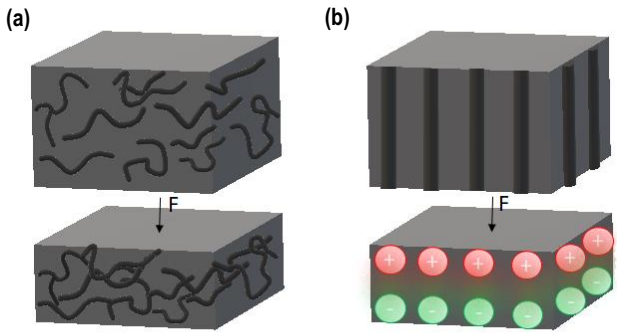

Figure 2-4: Representation of (a) piezoresistive and (b) piezoelectric sensors operation.

The choice of materials used to fabricate pressure sensors plays an important role on their final properties. Although traditional sensors made of metals, ceramics or semiconductive materials can be highly sensitive and accurate, they show some limitations on mechanical properties such as low stretchability, fragility and rigidity. On the other hand, sensors based on electrically conductive polymeric composites (ECPCs), whose schematic representation is reported in Figure 2-5, are currently getting much attention due to their light weight, high flexibility, easy processing, corrosion resistance, low cost and easier integration into devices [1, 2, 41, 57].

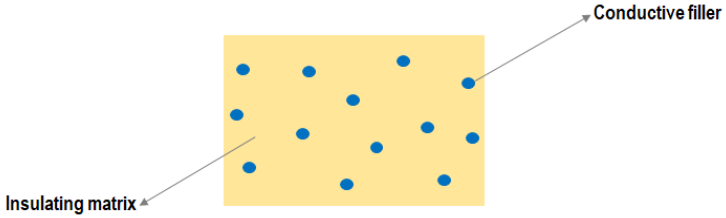

Figure 2-5: Schematic representation of an electrically conductive polymeric composite (ECPC).

The final properties and sensitivity of sensors based on ECPCs rely not only on the concentration of conductive filler and on intrinsic properties of polymers and fillers, such as electrical conductivity, thermal properties, degree of crystallinity, miscibility and so on, but also on the type of conductive network, composite morphology, interaction between the components, dispersion and distribution of filler. Moreover, the processing method plays a significant role on the final properties of the sensor [2, 3]. Although preparation methods as solution casting, electrospinning, in situ polymerization are used to produce materials with good sensing performances, a facile fabrication method for industrial scale production is still a challenge [2, 9, 15]. In this context, a promising technology for fabrication of flexible pressure sensors is the fused filament fabrication (FFF) technique offering the advantages of low cost, versatility and large scale production [7, 10, 58]. The development of functional filaments for FFF based on electrically conductive composites allow the fabrication of materials with conductive, structural and sensor functionalities with high sensitivity [1, 2, 5, 15, 26, 53]. Some researches show the advantages of preparing electronic devices composed of ECPCs via FFF that are able to detect electrical conductive variations under flexure, strain and compressive forces [9, 10, 14, 16]. For instance, Leigh et al. [16] studied the fabrication of capacitive and piezoresistive sensors of polycaprolactone/carbon black (PCL/CB) using the FFF technique. In this framework, combining the FFF technology with piezoelectric properties of PVDF and elastomeric properties of TPU is an interesting strategy to fabricate high flexible pressure sensors.

2.3.1 Piezoresistive sensors

Piezoresistive sensors are the most widely studied types of pressure sensors due to their simple device structure, broad range of detection, easy read-out mechanism, low energy consumption, high linearity and easy fabrication [7, 54]. Their working principle is based on the piezoresistive effect and they operate by converting external pressure stimuli into a measurable resistance variation [7, 55, 57, 59].

The piezoresistive effect was discovered by Lord Kelvin in 1856 and it is described by the variation of electrical resistance in a conductive material in response of an applied mechanical force [1, 7]. The piezoresistive effect in semiconductors was studied by Smith many decades later and his investigations greatly contributed to the progress of piezoresistive based sensors [55].

There are different mechanisms related to materials piezoresistance behavior. The resistance variation can be associated to a geometry change in the material. For instance, without any external stimuli, the material resistance can be calculated by Equation 1:

$$R = \rho \frac{L}{A} \tag{1}$$

where ρ is the resistivity, L is the length and A is the cross-sectional area of the specimen. When an external load is applied, the change in the resistance is expressed by Equation 2:

$$\frac{\Delta R}{R} = (1 + 2\nu)\varepsilon + \frac{\Delta \rho}{\rho} \tag{2}$$

where v is the materials Poisson ratio, ε is the strain and $\Delta\rho/\rho$ is the resistivity change [7, 54]. Pressure and strain sensors work basically with the same mechanism, the only difference is the sensing direction. While a pressure sensor works in through the thickness (z) direction, the strain sensor acts in planar (x and y) directions [57, 60]. Piezoresistivity can also be originated from a variation of density and mobility of charges due to a change in the band gap in interatomic spacing produced by the

applied stress. It has been observed in silicon, graphene and carbon nanotubes [61-63]. Furthermore, piezoresistance can also be caused by quantum tunneling conduction in electrically conductive composites where the conductive fillers are insulated by a polymer layer creating an insulating barrier. However, when a mechanical stimulus is applied the fillers promote a tunneling pathway thus significantly reducing the composite overall resistance [7]. Moreover, in the context of piezoresistive polymeric composites, change in resistance derives from a combination of three main mechanisms: changes in fillers band structure, tunneling resistance and variation of percolation paths [54]. Usually, the main mechanisms for sensors based on electrically conductive polymeric composites (ECPCs) is related to the creation of a percolation path and the electrical response of these materials under loading-unloading cycles depend on the compressive applied force.

The required sensing performance of piezoresistive sensors depends on the specific application and it is evaluated by considering various parameters including sensitivity, stretchability, durability, linearity, selectivity, detection limit, hysteresis and response time [54]. The sensitivity is related to the ability and accuracy of the sensor in converting the external applied pressure into electrical signals and it is defined as (Equation 3):

$$S = \frac{\Delta R/R_0}{\Delta P} \quad (3)$$

where S is the sensor sensitivity, ΔR is the resistance change, R_0 is the initial resistance and ΔP is the variation of external applied pressure. The sensitivity units are $k.Pa^{-1}$ when the external force is pressure. It can also be calculated as the slope of relative electrical resistance curves as a function of compressive stress [64-66]. The performance of piezoresistive sensors can be also determined by the gauge factor (GF), which evaluates the response of the material related to the applied deformation. The GF can be obtained from Equation 4 or by the slope of electrical resistance curves as function of strain and it is dimensionless [1, 2, 7, 9, 15, 41, 54, 64-68].

$$GF = \frac{\Delta R/R_0}{\varepsilon} \quad (4)$$

where ε is the applied strain. Stretchability is the maximum tensile strain sustained during stable performance and durability is the ability of preserving mechanical integrity and electrical responses under repeated loading-unloading cycles. Linearity of responses leads to easy calibration and detection limit is the smallest stimuli that a sensor can respond accurately [54]. Hysteresis can be observed after successively loading-unloading cycles and it is related to the viscoelastic behavior of polymers and interaction between components in sensors based on polymer composites [54, 69]. The response time is the time required for a measurable response [54].

Although conventional piezoresistive materials, such as metals and semiconductors, are cost-effective, they have low sensitivity and narrow sensing ranges, poor stretchability, nonlinearity and large hysteresis [54]. For this reason, piezoresistive pressure sensors based on electrically conductive polymeric composites have been widely investigated for their good processability, low cost, fast and linear response, and high reproducibility [1, 2, 41, 57, 69]. ECPCs based sensors can be prepared by distributing the conductive filler into the polymeric matrix (filling-type), as show in Figure 2-6, or creating a conductive layer of filler between two polymeric films (sandwich-like). Filling-type piezoresistive sensors are commonly chosen due to their high mechanical properties, good processability, low cost and large scale production [1]. When in an undeformed state, a filling-type composite consists of conductive particles dispersed in an insulating polymer matrix and its electrical conductivity is limited by the low conductivity of the polymeric insulating matrix. The application of an external load induces the elastic deformation of the matrix, thus decreasing the distance between the conductive particles of the fillers until they approach each other creating a percolation path and thus sharply increasing the composite electrical conductivity, as displayed in Figure 2-6. However, when the compression force is released, the composite viscoelastically recovers its undeformed shape and the initial electrical conductivity is restored [1, 3, 4, 59, 69, 70]. Typically, piezoresistive composites present the highest electromechanical responses at filler content close to the percolation threshold [2]. Nevertheless, during the loading-unloading cycles the conductive filler network can be irreversibly modified and hysteresis effects might be observed after repeated loading-unloading cycles, which

is also related to the polymers viscoelasticity and interaction between polymers and fillers [41, 54, 69, 71].

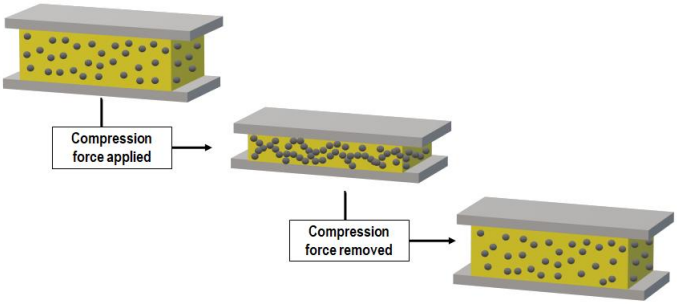

Figure 2-6: Schematic representation of piezoresistive sensors operation.

2.4 Piezoelectric properties

Piezoelectricity is a physical property related to some crystals, ceramics and biomaterials. It was first studied in 1880 by the brothers Paul-Jacques and Pierre Curie [55, 57]. When a mechanical force is applied, the electric dipole moments are separated and the two surfaces of the material become charged positively and negatively creating a piezopotential, see Figure 2-4 (b). Therefore, the free electrons flow through the external circuit to reach a balanced state again [7, 53, 55, 57]. Piezoelectric materials have been frequently used as transducers for pressure sensing applications due to the fact they can produce electrical potential variations as response to external stress with high sensitivity and fast response time.

The energy conversion efficiency of these materials can be assessed by the piezoelectric coefficient (d_{33}). Several researches have been carried on the development of flexible piezoelectric sensors with high d_{33}, including the use of piezoelectric polymers or polymer composites and building piezoelectric inorganics on flexible substrates [7]. Piezoelectric ceramics are commonly used because of its high

$d_{33;}$ however, they show very low flexibility. On the other hand, piezoelectric polymers are a promising class of material for developing piezoelectric sensors due to its physical and chemical properties, including high flexibility [7, 72]. A potential piezoelectric polymer is poly(vinylidene fluoride) (PVDF) which also possess non-toxicity, lightweight, flexibility and low cost. Moreover, fused filament fabrication technology has a great potential to produce multifunctional materials including piezoelectric composites [73].

2.5 Electromagnetic interference (EMI) shielding

Electromagnetic interference (EMI) refers to the radiated and conducted electromagnetic signals that can disturb the operation of electronic instruments and generate radiative damage to living species [18, 19, 21].

Nowadays, the technological growth is increasing the number of electronic devices, such as portable computers, mobile phones, radars, sensors, electrodes, wearable smart devices, transmitters and son on, in several areas including aerospace industry, wireless communication, household, medical and military, thus contributing for the enhancement of the electromagnetic interference. In this context, the development of EMI shielding materials to dissipate and attenuate the EMI radiation is being widely studied [11, 18, 19, 21, 23, 74]. EMI shielding materials can reflect, absorb and dissipate the electromechanical waves in a specific range of frequencies, however, the reflection mechanism is a source of secondary pollution since the radiation is reflected back to the environment [19-22, 36]. For this reason, materials that can attenuate the EMI by absorption are more attractive [20, 22]. The traditional shielding materials are metallic sheets due to their high electrical conductivity, high magnetic permeability and high number of free electron charge carriers that make their shielding properties very effective [21, 22]. However, their working principle is based on the reflection mechanisms and they have the disadvantages of poor mechanical flexibility, electrochemical corrosion, increased weight and density and costly processing methods [19, 21, 23]. On the other hand, electrically conductive polymer composites (ECPCs) are getting much attention as EMI shielding materials because

of their light weight, low cost, ease of processing, corrosion resistance [11, 18, 21, 23, 24, 74]. Moreover, they work primarily by absorbing the electromagnetic radiation and dissipate it in the conductive filler particles, which is interesting for numerous applications [21, 22].

ECPCs comprising carbon-based fillers, such as carbon black, graphene, carbon nanotubes, carbon fibers and so on, have been extensively studied as EMI shielding materials [19, 23]. Their EMI shielding effectiveness (SE) depends on several factor including the electrical conductivity of the filler, dielectric constant and aspect ratio [20]. However, the effect of carbonaceous fillers on electrical and shielding properties of immiscible polymer blends are not very explored, especially when processed by FFF.

ECPCs for EMI shielding are usually fabricated via conventional processing routes such as solvent casting and melt mixing followed by compression molding that can allow the fabrication of components with high SE. Melt mixing is an advantageous manufacturing method for composite compounds due to its extensive availability in polymer industries and simplicity. Nevertheless, a large scale and freedom in design processing technique for manufacturing specimens with complex geometries is still a challenge. For this reason, the recent developed FFF technique is attracting much interest for manufacturing ECPCs parts for EMI shielding and it remains a topic to be studied [11, 18, 19, 22-24, 74].

2.6 Poly(vinylidene fluoride)/thermoplastic polyurethane (PVDF/TPU) blends

Among polymer materials, poly(vinylidene fluoride) (PVDF) is an interesting choice for producing pressure sensors because of its low cost, low melting point and potential piezoelectric properties [46]. However, it has low elongation at break, elevated rigidity and limited stretchability aimed for flexible applications. These drawbacks can be overcome by blending PVDF with an elastomeric material with similar type of properties [32]. Moreover, in the 3D printing context, there are some drawbacks in processing PVDF by FFF technique since PVDF is a semi-crystalline polymer that is difficult to be printed because of warping and shrinking during the

crystallization process [33, 46]. One of the published strategies to overcome printing limitations of semi-crystalline polymers is producing an immiscible blends with an amorphous polymer to decrease the overall crystallinity of the blend.

On the other hand, thermoplastic polyurethane (TPU) is an amorphous, stretchable and printable material [10, 75]. PVDF and TPU are incompatible at all compositions [75]. Materials based on poly(vinylidene fluoride) and thermoplastic polyurethane have been reported due to the possibility of producing high-performance engineering materials for numerous industrial applications [32, 75, 76]. Studies show that hybrid materials of PVDF and TPU offers unique advantages of mechanical properties, such as stretchability and flexibility, and pyroelectric/piezoelectric properties, while maintaining excellent sensing performance [57, 76].

2.6.1 Poly(vinylidene fluoride) (PVDF)

Poly(vinylidene fluoride), (PVDF), is a promising choice for the production of piezoelectric materials for different applications including self-powered devices, capacitors, biomedicals, electromagnetic shielding and sensors with high sensitivity, wide frequency and good electromechanical responses [5, 53, 69, 77-80]. In this context, PVDF is an interesting candidate to be used as matrix to produce electrically conductive composites for sensing applications also because of its good mechanical properties, chemical resistance, high dielectric permittivity, pyroelectric/piezoelectric properties, easy processing and low cost [2, 5, 32, 69, 75, 76, 79, 81-83]. Furthermore, this polymer is an interesting choice for the preparation of composite filaments for FFF because of its low cost, low melting point and thermoplastic behavior [5, 46].

PVDF is composed of repeated units of vinylidene difluoride, as displayed in Figure 2-7. It is a semi-crystalline polymer that can exist in five different crystalline phases: α, β, γ, δ and ε [79, 80, 83], see Figure 2-8. The predominant phase in commercial PVDF is the nonpolar α phase due to the fact it is thermodynamically more stable than the other phases [81, 84]. However, PVDF piezoelectric properties are related to the polar phases β and γ, being β the one with the higher dipole moment and, therefore, the higher piezoelectric response [5, 53, 72, 77, 79-81, 84-87].

The energy conversion efficiency of the piezoelectric materials can be evaluated by the piezoelectric constant or piezoelectric charge coefficient, d_{33}. The constant refers to the materials electric response to an applied force in units of electrical charge (in Coulomb) per unit force (in Newton) [7, 72, 86]. Generally, inorganic piezoelectric materials have high d_{33} but low flexibility, while piezoelectric polymers display high flexibility and easy integration with functional devices even though their d_{33} are not as high as the inorganic materials [7, 82]. Between polymers, PVDF is a frequent choice as piezoelectric and dielectric material because of its substantial higher dielectric constant around 10 when compared to the usual 2-5 of other polymers [88].

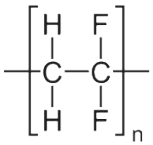

Figure 2-7: Chemical structure of poly(vinylidene fluoride) (PVDF).

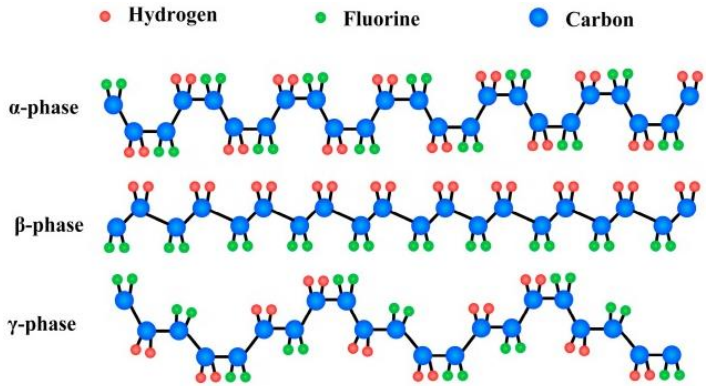

Figure 2-8: Schematic representation of the chain conformations of α, β and γ semi-crystalline phases of PVDF. Reproduced from [89].

Several methods have been studied to increase the content of β phase in PVDF polymers to enhance its piezoelectric properties such as mechanical stretching, high electrical field poling, crystallization under high pressure, polymer blending, electrospinning, thermal annealing and addition of nanofilers [5, 77, 79, 81, 83, 86, 90-93]. In this framework, the dispersion of nanofillers to induce the formation of an electroactive phase and enhance piezoelectric properties of PVDF has attracted much attention lately [53, 73, 77-79, 81, 82, 90, 91, 93]. In this context, the addition of carbon nanofillers have been reported because of their high compatibility with polymeric matrices, high surface area, mechanical properties, electron transport and superior polymer-filler interfacial interactions [53, 79, 83]. For instance, Georgousis et al. reported the enhancement of PVDF β phase with the addition of 6 wt% and 8 wt% of CNT by melting mixing [94]. Fakhri et al. prepared composites of PVDF comprising Au- and Cu-doped graphene oxide (GO/Au and GO/Cu) with high electroactive phases content and high dielectric constant [81].

Furthermore, PVDF properties are related not only to the polymer phase, but also to the degree of crystallinity, microstructure and processing conditions [2]. Hot pressing PVDF samples was show by Seena et al. [83] to rise PVDF overall polar phases, particularly the β phase. Apart from traditional manufacturing methods, 3D printing techniques are capable of producing complex 3D geometries and structures with technological functionalities [77, 95]. However, processing PVDF via fused filament fabrication is still a challenge due to its elevated shrinking during the crystallization process and the large coefficient of thermal expansion that leads to warping deformation [33, 46]. Moreover, its printed parts have low elongation at break and low stretchability, thus limiting its applications.

2.6.2 Thermoplastic polyurethane (TPU)

Thermoplastic polyurethane (TPU) is a copolymer that consists of linear blocks of soft and hard segments as shown in Figure 2-9. The soft segments are composed of long and low polar polyol chains that provide flexibility and elasticity. On

the other hand, the rigid segments are composed of shorter and high polar urethane groups that form hydrogen bonds working as a reinforcing structure [6, 25, 59].

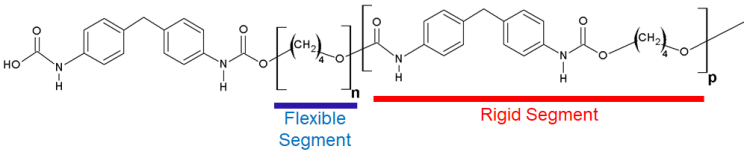

Figure 2-9: Chemical structure of thermoplastic polyurethane (TPU).

The different properties of these segments makes TPU one of the most versatile engineering polymers that combines the processability of thermoplastics with elastomeric properties such as low stiffness and high strain at failure [48, 59, 75]. TPU also offers advantages of chemical resistance, abrasion resistance, good adhesion and good compatibility with carbonaceous nanofillers [2, 32, 59, 75]. Because of its thermoplastic behavior, TPU can also be processed by additive manufacturing via fused filament fabrication technology. However, its elevated flexibility makes difficult to transmit through the filament the pressure necessary for the extrusion [48]. To overcome this limitation, blending TPU with PVDF is proposed in this work.

2.7 Carbon black-polypyrrole (CB-PPy)

Carbon black (CB) is a carbon based nanomaterial with great mechanical, thermal and electrical properties; and a more economical alternative among other carbon fillers [96]. Polypyrrole (PPy) is an intrinsic conductive polymer with good mechanical and electrical properties, insoluble in water and stable under diverse environment conditions [97]. Previous studies demonstrate the efficiency of producing conductive polymeric composites comprising carbon black-polypyrrole (CB-PPy) as conductive filler [6, 96].

2.7.1 Carbon black

Recently, carbon-based nanofillers have been successfully added into polymeric matrices to fabricate electrically conductive composites due to their exceptional mechanical, thermal and electrical properties [8, 11, 18, 23, 27, 98]. Among reported carbon nanofillers, such as carbon nanotubes (CNT), carbon black (CB) and graphene (GR) [8, 59], carbon black offers the advantages of high surface area, easier dispersion and lower cost in comparison to CNT and GR [82].

Carbon black is composed of small spherical particles of carbon fused into aggregates, see Figure 2-10, and it is formed in the gas phase by thermal decomposition of hydrocarbons. The mechanical and electrical properties of CB depends on its structure that is related to the shape and degree of aggregate branching. Increasing the carbon black structure leads to improved properties, such as higher modulus, hardness, viscosity, dispersability and electrical conductivity [21].

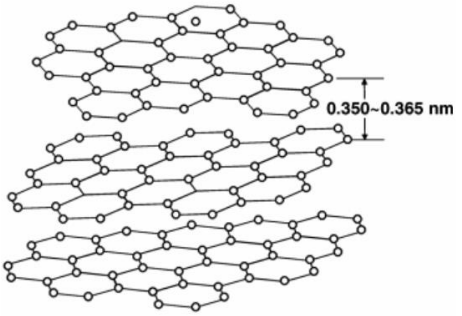

Figure 2-10: Representation of carbon black atomic structure. Adapted from [99].

CB has been already reported as a conductive filler for sensing applications. The sensing mechanism of conductive polymeric composites is related to the conductive particle dimensionality. In the case of carbon black, the spherical particles are 0-dimensional and the conductive path is built by a large number of weak

contacts between the particles leading to an easily broken network under stretch that increases the sensors sensibility. However, under unloading, the conductive network is fast recovered resulting in good recoverability of the sensor. On the other hand, 1- or 2-dimensional particles, for instance carbon nanotubes, are less sensitive to strain stimulus due to the formation of a stronger network related the particles entanglement. Moreover, some damages in the CNT conductive network are not recovered resulting in poor recoverability of the sensor [1].

Among the advantages of using carbon black as conductive filer, CB was found to be selectively dispersed in one phase or at the interface of immiscible co-continuous polymeric blends thus reducing the percolation threshold of ECPCs [34, 39]. Furthermore, carbon black has been reported to act as a nucleating agent improving the β crystalline phase in PVDF composites [78, 82, 90].

2.7.2 Polypyrrole (PPy)

Numerous studies have demonstrated the use of polypyrrole for sensing applications [4, 100-105]. Indeed, investigations on intrinsically conductive polymers (ICPs) are getting great attention since their discovery in the late 1970s due to their potential for several technological applications including soft electronics, solar cell, intelligent textiles, biomedical applications, electromechanical sensing, electromagnetic interference (EMI) shielding and so on [25, 97]. Different from traditional polymers that are used as insulators, intrinsically conductive polymers have a significant electrical conductivity due to their conjugated π-electron system, alternate single and double bonds, that creates a conduction path. The most common ICPs are polyacetylene (PA), polyaniline (PANI), polypyrrole (PPy) and polythiophene (PTH) [97]. Among them, polypyrrole (PPy), see Figure 2-11, has been widely studied because of its high electrical conductivity, environmental and chemical stability, biocompatibility and easy of synthesis [25, 97, 105]. PPy is obtained as a black powder by chemical oxidative polymerization of pyrrole monomers [106]. Because of its high charge density and reduced cost, PPy is an alternative for costly carbonaceous and metallic nanofillers. However, when PPy is used as a conductive filler, high amounts are required to increase significantly the electrical conductivity of the composite [4]. In

fact, Merlini et al. developed poly(vinylidene fluoride)/polypyrrole (PVDF/PPy) blends for pressure sensing reaching the highest sensitivity at 9 wt% of PPy [107].

In the present study, the strategy used for developing highly conductive polymer composites is using a combination of carbon black dopped with polypyrrole as conductive filler.

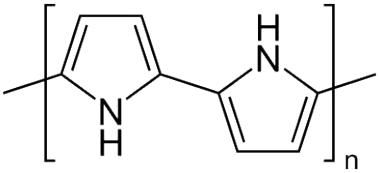

Figure 2-11: Chemical structure of polypyrrole.

Chapter III

3. Experimental

3.1 Materials

Polymeric blends of poly(vinylidene fluoride) (PVDF) and thermoplastic polyurethane (TPU) were prepared in different proportions. Various amounts of the conductive filler carbon black doped with polypyrrole (CB-PPy) was added to selected blends for the production of electrically conductive polymeric composites.

3.1.1 Poly(vynilidene fluoride) (PVDF)

The poly(vinylidene fluoride) used in this study, (PVDF 24 Amboflon®), was purchased from Ambofluor GmbH (Hamburg, Germany) in the form of pellets. According to the product data sheet, this PVDF possess a relative density of 1.78 $g.cm^{-3}$, a melt flow index of 18-26 $g \bullet 10min^{-1}$ and a melting temperature of 165-175 °C.

3.1.2 Thermoplastic polyurethane (TPU)

An ether based thermoplastic polyurethane (Desmopan® DP 6064 A) was provided by Covestro Italia srl (Milano, Italy). According to the product data sheet, this TPU possess a relative density of 1.09 $g \bullet cm^{-3}$ and an injection molding temperature of 200-220 °C.

3.1.3 Carbon black-polypyrrole (CB-PPy)

Carbon black doped with polypyrrole containing 80 wt% of carbon black was purchased from Sigma Aldrich. According to the product data sheet, this CB-PPy additive possess an electrical conductivity of $3x10^1$ $S \cdot cm^{-1}$ and a relative density of 2.22 $g \cdot cm^{-3}$.

3.2 Melt compounding

PVDF/TPU blends were prepared by melt mixing using a Thermo-Haake Polylab QC Rheomix internal mixer consisting of an internal volume of 50 cm^3 equipped with counter-rotating rotors. PVDF and TPU polymers were previously dried overnight at 60 °C. The processing was carried out at 180 °C with a rotor speed of 50 rpm for 15 minutes. The compositions of the produced blends are displayed in Table 3-1 and pictures of the internal mixer are shown in Figure 3-1.

Table 3-1: Formulations of PVDF/TPU blends.

Sample	Blend composition	
	PVDF (vol%)	TPU (vol%)
PVDF	100	0
TPU	0	100
PVDF/TPU	59	41
PVDF/TPU	50	50
PVDF/TPU	48	52
PVDF/TPU	38	62

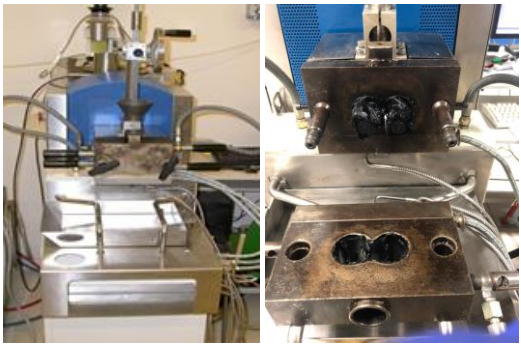

Figure 3-1: Photographs of Haake® internal mixer and mixing chamber.

The carbonaceous filler carbon black doped with polypyrrole (CB-PPy) was incorporated into the selected matrices by melt mixing using the internal mixer. First, predetermined amounts of PVDF and TPU were added in the mixing chamber and after 2 minutes, the conductive filler was introduced and left mixing for 13 minutes more. The composition of each mixture is shown in Table 3-2. For compression molded samples, filler contents up to 15% were added to the selected matrices to evaluate the effect of the filler quantity on the materials properties. According to the electrical conductivity measurements and calculation of the percolation threshold, three compositions were selected to be printed via FFF.

Table 3-2: Formulations of PVDF/TPU/CB-PPy composites.

PVDF/TPU 38/62 vol%	PVDF/TPU 50/50 vol%
% CB-PPy	
3	1
5	2
6	3
7	5
10	6
15	10

3.3 Compression molding

The mixtures reported in Table 3-1 and Table 3-2 were compression molded in square plaques (120 × 120 mm^2) with a thickness of 2 mm at 180 °C applying a pressure of 3.9 MPa for 10 min by a Carver Laboratory press (Carver, Inc. Wabash, IN, USA), see Figure 3-2. Compression molded samples were cut in specific formats, see Figure 3-3, for different tests.

According to the testing results, specific compositions were selected for the preparation of filaments to be used as feeding material in the fused filament fabrication (FFF).

Figure 3-2: Carver® laboratory hot plates press.

Figure 3-3: Compression molded samples used for different tests.

3.4 Filament extrusion

The samples shown in Table 3-3 were selected for filament extrusion and the subsequent fused filament fabrication (FFF) process. The mixtures prepared by melt mixing were immersed in liquid nitrogen before grinding. Then the obtained powders were extruded using a single screw extruder displayed in Figure 3-4 provided by Friul Filiere SpA, model Estru 13 operating at 30 rpm with four temperature zones of 130, 170, 175 and 180 °C (die). The extruded filament was then collected on a rolling belt (see Figure 3-4 (c)) at 20 mm•s^{-1}. The final diameter of the collected filaments displayed in Figure 3-5 was set to 1.75 ± 0.10 mm.

Table 3-3: Formulations of samples selected for filament extrusion and fused filament fabrication.

Samples
PVDF
PVDF/TPU/CB-PPy 38/62 vol% % CB-PPy
0%
5%
6%
PVDF/TPU/CB-PPy 50/50 vol% % CB-PPy
10%

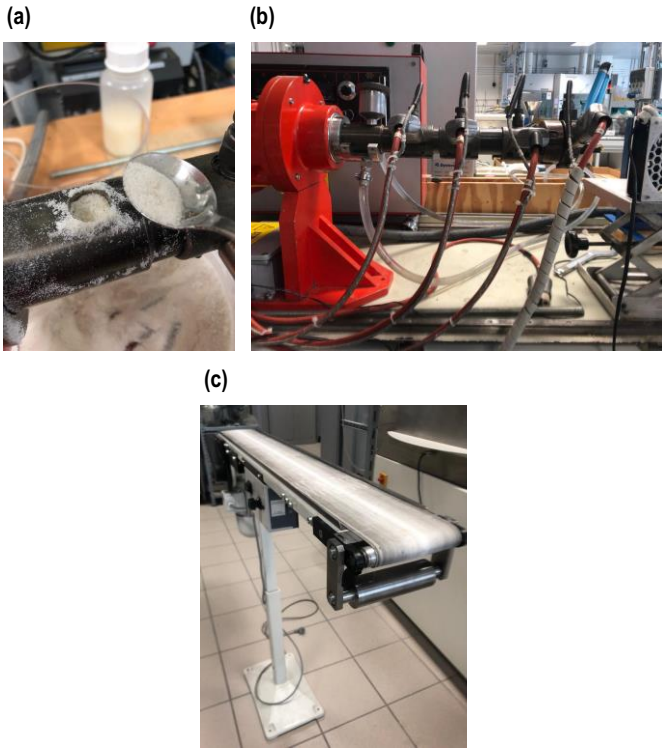

Figure 3-4: Photographs of (a) extruder feeding zone, (b) single screw extruder with four temperature zones and (c) rolling belt collector.

Figure 3-5: Extruded filaments with different compositions.

3.5 Fused Filament Fabrication (FFF)

The extruded filaments with composition displayed in Table 3-3 were used to feed FFF 3D printing machines. In particular, the samples were printed by using i) a prototype 3D printer Sharebot Next Generation desktop (Sharebot NG, Nibionno, LC, Italy), see Figure 3-7, and ii) a Sethi S3 3D printer (Sethi3D, Campinas SP, Brazil), see Figure 3-7, both based on the fused filament fabrication (FFF) technology. Before 3D printing, the specimens geometry was drawn using AutoCAD and sliced using the open-source software Slic3r. The design and printing parameters adopted for the FFF process were settled using Slic3r and they are shown in Table 3-4. The specimens were build-up along horizontal alternate (H45) direction, as shown in Figure 3-8, where the first layer was oriented at 45° with respect to the origin and the following layers were deposited at 90° with respect to the previous one. The samples were printed in dumbbell format according to the ISO 527 type 1BA standard with a gauge length of 30 mm, a width of 5 mm and a thickness of 2 mm, see Figure 3-9; circular disks with 15 mm of diameter and 2 mm of thickness, see Figure 3-10, and square plates of 45x45x2 mm.

Figure 3-6: Image of the Sharebot 3D printer Next Generation.

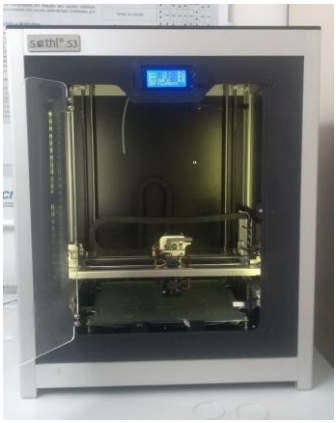

Figure 3-7: Image of the Sethi S3 3D printer.

Table 3-4: FFF printing parameters.

Parameter	Value
Nozzle temperature	230 °C
Bed temperature	40 °C
Nozzle diameter	0.4 mm
Nozzle speed	16 mm·s^{-1} (dumbbell)/ 40 mm·s^{-1} (circular)
Layer height	0.2 mm
Number of layers	10
Infill type and density	Rectangular 100 %
Raster angle	+45°/-45°

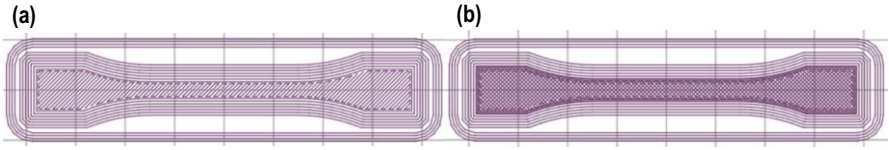

Figure 3-8: Schematic representation of dumbbell specimens ISO 527 type 1BA for (a) the first layer and (b) after the deposition of the second layer

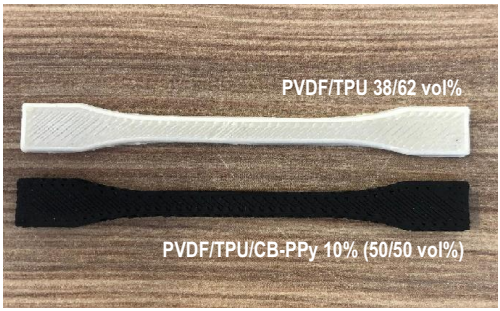

Figure 3-9: 3D printed samples in ISO 527 type 1BA dumbbell format.

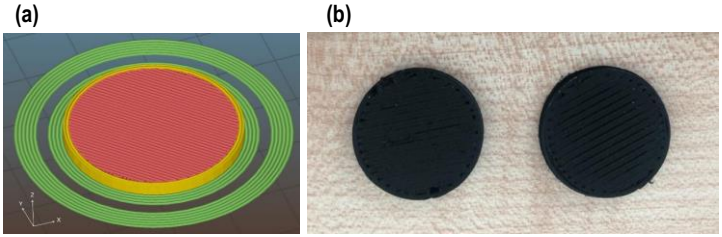

Figure 3-10: (a) Schematic representation of circular specimen and (b) 3D printed circular samples of PVDF/TPU/CB-PPy 10% (50/50 vol%).

3.6 Testing techniques

3.6.1 Density measurement and percentage of voids

Density measurements were used to investigate the presence of voids in the printed parts. The density of 3D printed samples was experimentally measured by weighting the circular samples (15x2 mm) in the air and calculated according to Equation 5:

$$\rho_{ap} = \frac{m}{V} \quad (5)$$

where ρ_{ap} is the apparent density (g.cm^{-3}), m is the measured weight (g) and V is the volume (cm^3) as measured from the geometrical dimensions. Three specimens of each sample were measured. The theoretical density ρ_{th} of the samples was then predicted based on the rule of mixture, Equation 6:

$$\rho_{th} = \rho_{\mathrm{PVDF}} \times V_{\mathrm{PVDF}} + \rho_{TPU} \times V_{\mathrm{TPU}} + \rho_f \times V_f \qquad (6)$$

where ρ_{PVDF}, ρ_{TPU} and ρ_f are the density of the PVDF, TPU and of the conductive filler CB-PPy, respectively, while V_{PVDF}, V_{TPU} and V_f are the volume fraction of each matrix and of the conductive filler. In addition, the content of voids (V%) in the specimens was calculated by Equation 7:

$$V\% = \frac{\rho_{th} - \rho_{ap}}{\rho_{th}} \times 100 \qquad (7)$$

3.6.2 Quasi static tensile test

Mechanical properties were measured by quasi static tensile tests using an electromechanical testing machine Instron® 5969 with a 50 kN load cell. The elastic modulus of the specimens was evaluated using an electrical extensometer model 2620-601 with a gauge length of 12.5 mm at a crosshead speed of 1 mm•min^{-1} until 1% of deformation. Fracture properties were determined at a crosshead speed of 100 mm•min^{-1} without any extensometer. Five specimens of each composition were analysed in dumbbell format according to ISO 527 type 1BA with gauge length of 30 mm, width of 5 mm and thickness of 2mm.

3.6.3 Scanning electron microscopy (SEM) and energy dispersive X-ray spectroscopy (EDS)

Scanning electron microscopy (SEM) observations were performed to investigate the morphology of the blends and of the conductive composites. Also,

dispersion and distribution of the conductive filler CB-PPy in the PVDF/TPU matrices were investigated. In addition, SEM coupled with energy dispersive X-ray spectroscopy (EDS) was also performed to assist in the phases identification. The analysis was carried out on different regions of previous fractured surfaces of two samples of each composition using a Tescan VEGA3 field emission scanning electron microscope at an acceleration voltage of 5.0 kV coupled with an Oxford Instrument X-act model 51-ADD0007. The samples were covered with a thin conductive gold coating before the analysis.

In addition, SEM and EDS analyses were also performed after etching out the TPU phase in the blends and composites. The etching process was carried out immersing samples of 20x20x2 mm in THF for 4 hours in a sonication bath and then drying them at room temperature for 24 hours.

3.6.4 Dynamic mechanical thermal analysis (DMTA)

Dynamic mechanical thermal analysis (DMTA) was carried out under tensile mode using a Netzsch DMA 242 E device in order to obtain the storage (E') and loss (E'') moduli as a function of temperature. Also, the T_g values were calculated from the tan δ maximum peak (ratio between E'' and E') for neat polymers, blends and composites comprising various amount of CB-PPy. Rectangular specimens with 20x5x2 mm^3 with a gauge length of 10 mm were tested. The tests were performed on one specimen of each composition from – 80 °C to 100 °C applying a maximum dynamic strain of 50 microns at a heating rate of 3 °C•min^{-1} and frequency of 1 Hz.

3.6.5 Rheology measurements

The rheology measurements were performed using a Discovery DHR 1 rheometer from TA Instrument Inc. in oscillatory mode using parallel plates with 25 mm of diameter and 1.0 mm of gap for samples with filler content lower than 10% and 1.2 mm of gap for samples with 10% or higher filler content. The analysis was carried

out at 180 °C under nitrogen atmosphere in the frequency range from 0.1 to 100 Hz at a strain amplitude of 0.1% (linear viscoelastic region).

3.6.6 Fourier transform infrared (FTIR) spectroscopy

Fourier transform infrared (FTIR) spectra were recorded through the attenuated total reflectance (ATR) method using a ZnSe crystal by an Agilent Cary 660 spectrometer in a scanning range from 4000 to 650 cm^{-1} in order to evaluate the chemical structure, interaction between the materials and crystalline phases of PVDF. The samples were analyzed in form of films, which were prepared by compression molding the mixtures applying a pressure of 3.9 MPa for 5 min at 180 °C using a BOVENAU P15 ST hydraulic press.

3.6.7 X-ray diffraction analysis (XRD)

X-ray diffraction analysis (XRD) was performed using an Italstructures IPD3000 diffractometer with a standard sealed-tube source of Copper [Cu] anode and a multilayer flat monochromator on the incident beam selecting CoKa. The instruments is equipped with a Dectris Mythen 1K detector and it operates in Bragg-Brentano geometry. The measures were taken with a fixed incident beam with an angle of 6°, while the Dectris Mythen 1K detector moved for the 2θ angles ranging from 10 to 120°.

3.6.8 Differential scanning calorimetry (DSC)

Differential scanning calorimetry (DSC) testes were carried out by a Perkin Elmer JADE DSC in order to obtain the melting temperature of the samples and to investigate the crystallinity of PVDF. The analysis was performed under a nitrogen flow of 100 $ml.min^{-1}$ and heating/cooling rate of 10 °$C.min^{-1}$ in the temperature range from 20 to 250 °C. The mass of analyzed samples was around 10 mg.

3.6.9 Electrical conductivity

The electrical conductivity of the high-conductive samples was measured according to the ASTM D4496-04 standard with a four-probe configuration. The voltage source was a DC power supply produced by ISO-TECH (IPS303DD) and the current flow was measured between external electrodes by a pocket multimeter electrometer (ISO-TECH IDM 67) with an internal electrode (i.e. 3.69 mm). The samples were cut in rectangular specimens of 36.9x5x2 mm^3 and the measurements were taken on both side on three specimens per sample. For the high-resistive samples a two-probe standard method was performed by a Keithley 6517A electrometer/high resistance meter connected to a resistivity test fixture Keithley 8009. The thickness of the samples was 2.0 mm and the tests were performed on both sides of each sample.

3.6.10 Electromechanical test

The electromechanical measurements were performed to evaluate the piezoresistive behavior of samples by simultaneously applying controlled loads and measuring the electrical resistivity. Loading-unloading cycles were carried out using a MTS Acumen universal testing machine by MTS Eden Prarie MN (see Figure 3-11 (a)) equipped with a load cell of 0.5 kN. Concurrently, the specimen's resistance was measured by a Keithley 6517A electrometer (see Figure 3-11 (c)) using an in-house developed software. First, the circular specimens with 15 mm of diameter were placed between two copper electrodes as shown in Figure 3-11 (b) and the assembly located inside an electrically insulated chamber where three different maximum loads of 100, 200 and 400 N corresponding to maximum compressive pressures of 0.57, 1.14 and 2.28 MPa were applied at a loading rate of 3.4 $MPa.min^{-1}$ to evaluate the optimal electrical responses. Due to better electromechanical responses, the pressure of 2.28 MPa was selected to test all samples. The tests were firstly performed applying 2.28 MPa of compressive pressure at a rate of 3.4 $MPa.min^{-1}$ and then the pressure was released at the same rate during five loading-unloading cycles. The resistivity ρ (Ωcm) of the specimens was calculated according to Equation 8:

$$\rho = R\frac{\pi.d^2}{4w} \quad (8)$$

where R is the electrical resistance (Ω), d is the diameter (cm) and w is the thickness (cm) of the samples. Moreover, the samples that presented good electromechanical responses and reproducibility of the results were further tested under 100 loading-unloading cycles under the same conditions. The analysis was carried out for three samples of each composition.

(a) (b)

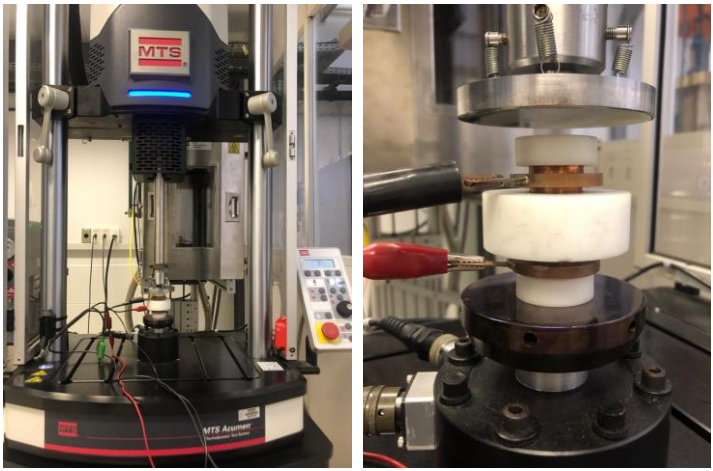

(c)

Figure 3-11: (a) MTS universal testing machine, (b) device composed of two electrodes used to measure the samples resistance and (c) Keithley electrometer.

3.6.11 Piezoelectric d33 constant

The piezoelectric properties of samples were assessed by measuring the d_{33} constant using a piezolelectric d_{33} meter OKD3-2000-F10N purchased from PolyK Technologies. The samples were placed between the reading electrodes and subjected to a static clamping force and an oscillating one. The static force was tuned

manually with a knob in 1N, 2N and 4N to evaluate the effect of the clamping force. The oscillating force of 0.25 N was applied to the samples with a fixed frequency of 110 Hz by the instrument and the d_{33} constant (pC/N) was measured by reading the surface charge on the electrodes.

Three tests were performed on each specimen in three different spots resulting in nine measurements per sample. The samples were analysed in the film format.

3.6.12 Electromagnetic interference shielding effectiveness (EMI-SE)

The electromagnetic interference shielding effectiveness (EMI-SE) measurements were carried out in the X-band frequency range from 8.2 to 12.4 GHz by a N5230C Agilent Technology PNA series analyzer connected to a rectangular waveguide with a cross-section of 23×10 mm used as the sample holder. Square samples of 2 mm were analyzed. The incident electromagnetic wave is applied to the sample and the transmitted and reflected waves are collected. The EMI-SE is the ability of the material in attenuating the electromagnetic waves, which is expressed in decibels (dB). The total EMI-SE of electrically conductive polymer composites, Equation 11, is composed of the shielding effectiveness by reflection (SE_R) and the shielding effectiveness by absorption (SE_A), which are described as Equations 9 and 10, respectively:

$$SE_R = 10 \log \frac{I}{I-R} \quad (9)$$

$$SE_A = 10 \log \frac{I-R}{T} \quad (10)$$

$$EMI\ SE = SE_R + SE_A = 10 \log \frac{I}{T} \quad (11)$$

where I is the incident wave, R is the reflected wave and T the transmitted wave.

Results and discussion

Chapter IV

4. Preparation and characterization of poly(vinylidene fluoride)/thermoplastic polyurethane composites comprising carbon black-polypyrrole

Part of this chapter has been published in:

Mayara C. Bertolini, Sithiprumnea Dul, Guilherme M. O. Barra, Alessandro Pegoretti

"Poly(vinylinede fluoride)/thermoplastic polyurethane flexible and 3D printable conductive composites",
Journal of Applied Polymer Science, No. 138 (2020) 50305.

Mayara C. Bertolini, Sithiprumnea Dul, Elaine C. Lopes Pereira, Bluma G. Soares, Guilherme M. O. Barra, Alessandro Pegoretti

"Fabrication and Characterization of piezoresistive flexible pressure sensors based on poly(vinylidene fluoride)/thermoplastic polyurethane filled with carbon black-polypyrrole"
Polymer Composites, No. 12 (2021) 6621-6634.

4.1 Introduction

This chapter is focused on the development of filaments composed of co-continuous blends of poly(vinylidene fluoride)/thermoplastic polyurethane containing a conductive filler carbon black-polypyrrole as a strategy to prepare structural and highly conductive 3D printed parts via fused filament fabrication (FFF) technique.

Although the addition of conductive fillers into PVDF/TPU co-continuous blends is an interesting strategy to combine the good mechanical properties of polymeric blends to electrical properties of conductive filler, only one study has been found in the open literature [28]. Also, to our best knowledge, the production of co-continuous insulating polymeric blends to control morphology and properties have been already proposed, however, only a few studies are reported on its use in FFF and none of them concern to the development of filaments comprising co-continuous polymer blends of PVDF/TPU and a conductive filler.

To overcome the above mentioned limitations and the lack of studies on the production of flexible and highly electrical conductive filaments for fused filament fabrication, this study proposes the preparation of a polymeric blend composed of PVDF and TPU as matrix comprising different fractions of carbon black doped with polypyrrole as conductive filler.

4.2 PVDF/TPU blends produced by compression molding

In this section, blends with different fractions of PVDF and TPU were investigated, see Table 4-1. The blends were compounded by melt mixing and then compression molded. The mechanical, chemical and optical properties and microstructure of the final samples were evaluated by quasi static tensile test, dynamic mechanical thermal analysis (DMTA), scanning electron microscopy (SEM) and energy dispersive X-ray spectroscopy (EDS).

Table 4-1: Composition of compression molded PVDF/TPU blends.

Material composition	
PVDF (vol%)	**TPU (vol%)**
100	0
0	100
59	41
50	50
48	52
38	62

4.2.1 Quasi static tensile test

Tensile tests were carried out in order to investigate the mechanical properties of the PVDF/TPU blends and the tensile stress versus tensile strain curves obtained from the fracture test are shown in Figure 4-1. It is possible to observe in the graphic that the tensile strength decreases proportionally to the amount of TPU in the blends. The highest strength of 56.9 MPa is achieved for neat PVDF, and it significantly drops to 5.5 MPa (i.e., 90%) as the TPU content is increased to 62 vol %. Moreover, the breaking strain of the blends increases with the addition of TPU. For neat PVDF the breaking strain is 0.18 $mm.mm^{-1}$ and it goes up to 1.5 $mm.mm^{-1}$ when 62 vol% of TPU is added to the blend. The sample composed of neat TPU did not break in tension due to the high elasticity of TPU and the travel limitations of crosshead of the equipment.

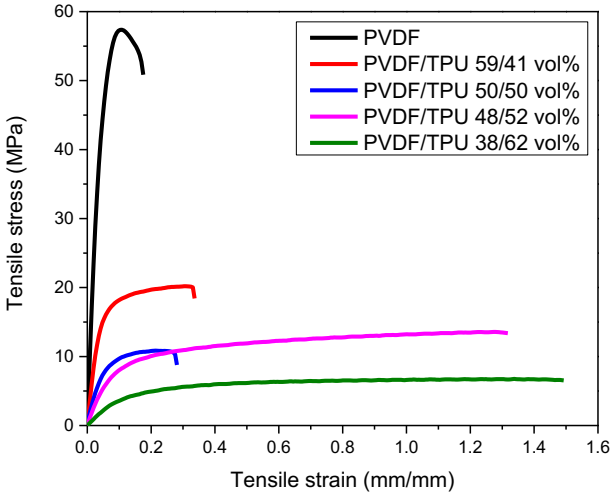

Figure 4-1: Tensile stress-strain curves for PVDF/TPU compression molded blends with various compositions.

In addition, the tensile properties, which are summarized in Table 4-2, show that increasing the TPU content in the PVDF/TPU blends a reduction of the elastic modulus and an increase of the elongation at break can be observed. The most flexible blend was found to be the one with 38/62 vol% of each component and it was one of the compositions selected to be used as matrix for the conductive composites. However, some studies claim that to achieve a co-continuous phase, which assists in the reduction of the percolation threshold in conductive composites, a concentration of 50 vol% of each polymer is necessary [42]. For this reason, the blend PVDF/TPU 50/50 vol% was also selected as matrix to prepare the conductive composites.

Table 4-2: Mechanical properties PVDF/TPU compression molded blends including average values and standard deviation.

PVDF/TPU (vol%/vol%)	Elastic modulus E (MPa)	Maximum tensile stress σ_{max} (MPa)	Elongation at break ε_b (%)
100/0	2424.7 ± 74.2	56.9 ± 1.2	21.4 ± 8.4
59/41	733.4 ± 70.6	19.8 ± 0.9	38.9 ± 26.1
50/50	287.8 ± 39.1	10.9 ± 0.9	27.5 ± 6.4
48/52	87.6 ± 19.9	13.1 ± 0.8	117 ± 22.2
38/62	41.2 ± 14.8	5.5 ± 1.1	153 ± 81.4
0/100	7.0 ± 0.4	n.m.	n.m.

n.m. = not measurable

4.2.2 Dynamic mechanical thermal analysis (DMTA)

The storage modulus (E') and loss tangent (tan δ) as measured from the dynamic mechanical thermal analysis (DMTA) are reported in Figure 4-2 and Figure 4-3, respectively. The storage modulus (E') as function of temperature is displayed in Figure 4-2. Neat PVDF shows storage modulus values higher than those found for the blends containing TPU and neat TPU. The storage modulus decreases with the increasing of TPU in the blends leading to a more flexible material, as expected, due to the elasticity of TPU. The trend of storage modulus is the same previously observed for the tensile Young's modulus.

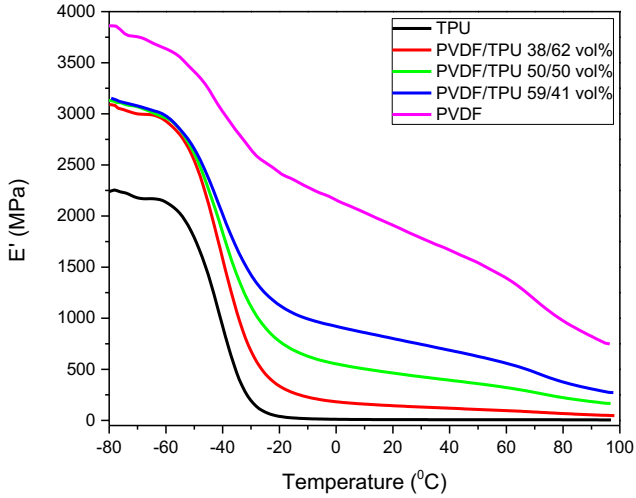

Figure 4-2: DMTA results of storage modulus as function of temperature for neat TPU, neat PVDF and blends compression molded with different compositions.

Moreover, the glass transition temperature (T_g) was determined as the peak of tan δ values and displayed in Table 4-3. For neat TPU and neat PVDF the T_g were found to be - 25 °C and – 39.2 °C, respectively. According to the literature, for immiscible polymer blends, two distinct T_g values are expected. However, the T_g of PVDF and TPU are in a narrow temperature range and the results show only one value between those observed for the neat polymers. The T_g of the blends are related to the amount of each polymer present in the blend. The blend composed of 38 vol% of PVDF shows a T_g value of -29.4 °C. When the PVDF percentage is increased to 50 vol% the Tg decreases down to -32.4 °C. Also, the blend containing higher amount of PVDF, 59 vol%, presents a lower T_g at -36.1 °C. This means that increasing the percentage of PVDF in the blends, which has a T_g lower than TPU, the glass transition temperature decreases proportionally in the blend.

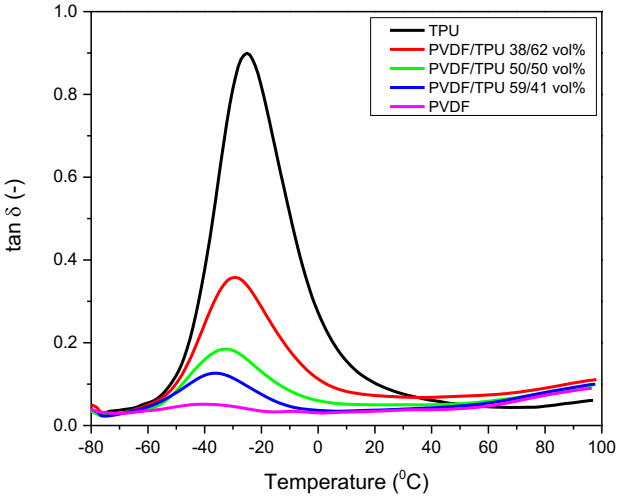

Figure 4-3: DMA results of loss tangent as function of temperature for neat TPU, neat PVDF and blends with different compositions.

Table 4-3: Tg values for neat TPU, neat PVDF and PVDF/TPU blends.

Sample	T_g Value
TPU	-25.0 °C
PVDF/TPU 38/62 vol%	-29.4 °C
PVDF/TPU 50/50 vol%	-32.4 °C
PVDF/TPU 59/41 vol%	-36.1 °C
PVDF	-39.2 °C

4.2.3 Scanning electron microscopy (SEM) and energy dispersive X-ray spectroscopy (EDS)

In order to investigate the formation of co-continuous phases, the microstructure of the compression molded blends was evaluated by scanning electron microscopy (SEM) observations of the cryogenically fractured surface. As reported in the SEM images of Figure 4-4, all blends present a gross phase-separated morphology, which is typical of heterogeneous incompatible blends. Distinguishable boundaries are observed at the interfaces and two phases with different structures can be seen. Usually, incompatible blends display a particle-dispersed-type morphology in which the component present in smaller fraction is dispersed in the major component or matrix [32]. The micrograph of the blend with 38 vol% of PVDF (Figure 4-4 (c)) shows that PVDF is in smaller volume amount and thus dispersed in the TPU phase. Nevertheless, when the PVDF content in the blend is raised to 50 vol% (Figure 4-4 (d)), it is possible to observe the presence of a co-continuous morphology as the two polymers are present in the blend in the same volume quantity. When PVDF becomes the prevalent phase in the blend (Figure 4-4 (e)) the microstructure becomes more homogeneous.

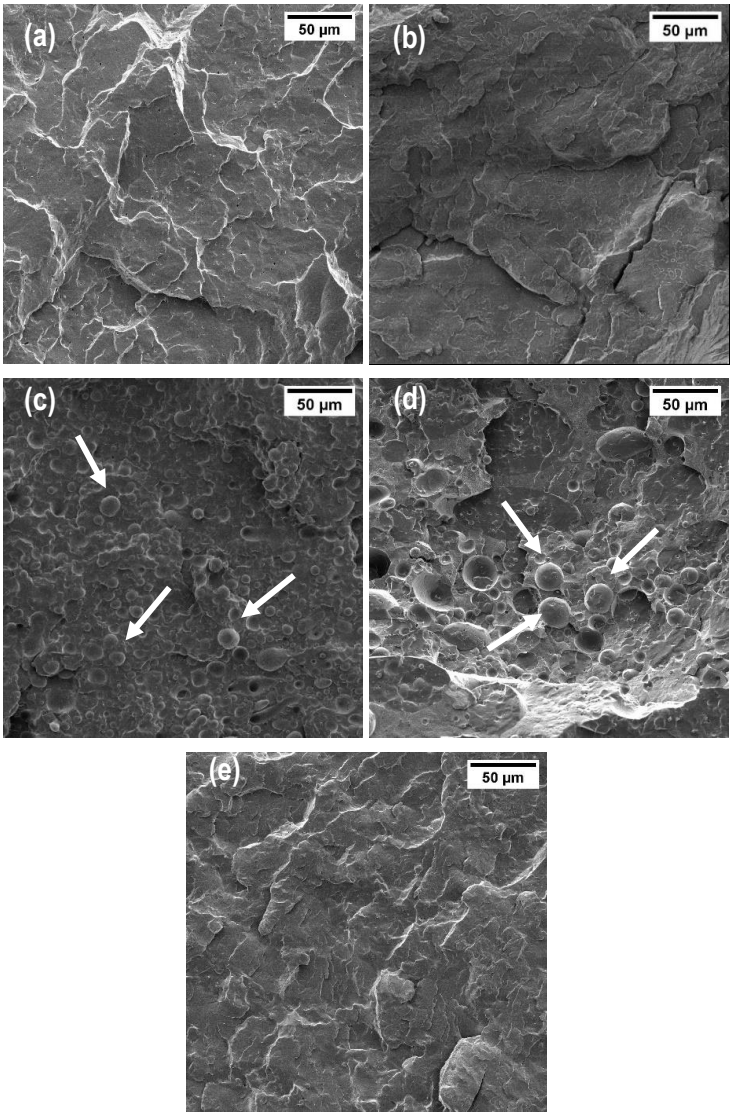

Figure 4-4: SEM images at 1000 x of magnification of (a) neat TPU; (b) neat PVDF; PVDF/TPU: (c) 38/62 vol%, (d) 50/50 vol% and (e) 59/41 vol% produced by compression molding. White arrows indicate the PVDF phase in the blends.

Moreover, the morphology of the blend PVDV/TPU comprising 50 vol% of each polymer was analysed by SEM coupled with energy dispersive X-ray spectroscopy (EDS) to investigate the composition of each phase. Figure 4-5 (a) shows the EDS mapping image of the blend, where the green colour represents regions containing fluorine (present in PVDF), while oxygen (present in TPU) is indicated in blue and nitrogen in pink. Also, the EDS spectrum for the blend is presented in Figure 4-5 (b). In addition, for a better observation of the microstructure, the TPU phase was removed from the blend by etching with tetrahydrofuran (THF). Figure 4-5 (c) and (d) show the SEM images for the etched blend supporting the claim of a blend with co-continuous morphology. Moreover, Figure 4-5 (e) displays the EDS mapping of the etched blend confirming that most part of TPU phase was removed and Figure 4-5 (f) shows the EDS spectrum for the etched blend illustrating the reduction in the amount of oxygen (related to the TPU phase) in the sample.

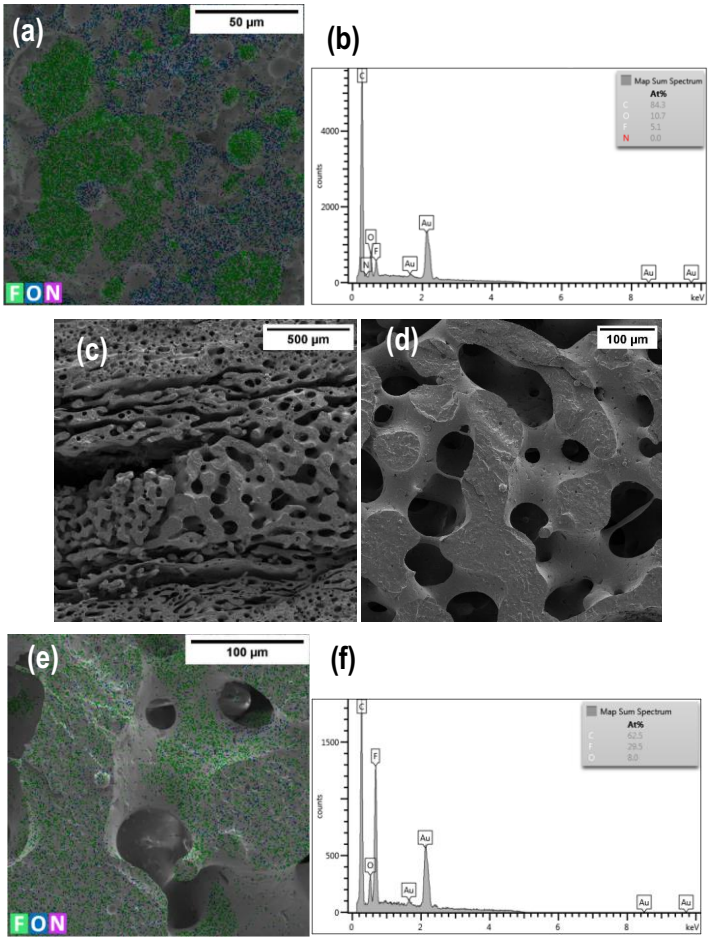

Figure 4-5: (a) EDS mapping and (b) EDS spectrum of compression molded PVDF/TPU 50/50 vol% at x1000 magnification; SEM images of the etched blend at magnifications of (c) x150 and (d) x500; and (e) EDS mapping and (f) EDS spectrum of the etched blend at x1000 magnification.

4.3 PVDF/TPU/CB-PPy composites produced by compression molding

This section is about the addition of the conductive filler carbon black-polypyrrole to the selected PVDF/TPU matrices. According to the results from section 4.2, the blends composed of PVDF/TPU 38/62 vol% and PVDF/TPU 50/50 vol% were selected to be used as matrices for the preparation of electrically conductive polymeric composites due to their high flexibility and potential achievement of co-continuous phases, respectively. In addition, composites comprising neat PVDF and neat TPU as matrix were prepare for further comparison. The compositions of the investigated composites are displayed in Table 4-4, they were prepared by melt compounding and then compression molded. Moreover, the samples were characterized by electrical conductivity measurements, quasi static tensile test, dynamic mechanical thermal analysis (DMTA), scanning electron microscopy (SEM) and energy dispersive X-ray spectroscopy (EDS) to evaluate their electrical and mechanical properties and their microstructure.

Table 4-4: Composition of the investigated compression molded PVDF/TPU/CB-PPy composites.

PVDF	TPU	PVDF/TPU 38/62 vol%	PVDF/TPU 50/50 vol%
% CB-PPy	% CB-PPy	% CB-PPy	% CB-PPy
0	0	0	0
1	-	-	1
2	-	-	2
3	3	3	3
5	5	5	5
6	6	6	6
7	7	7	10
10	10	10	-
-	-	15	-

4.3.1 Electrical conductivity

The electrical conductivity values of the investigated materials were determined as a function of the fraction of conductive filler. The curves of electrical conductivity versus content of filler for PVDF/CB-PPy, TPU/CB-PPy, PVDF/TPU/CB-PPy 38/62 vol% and 50/50 vol% composites are summarized in Figure 4-6 and the obtained electrical conductivity values are summarized in Table 4-5.

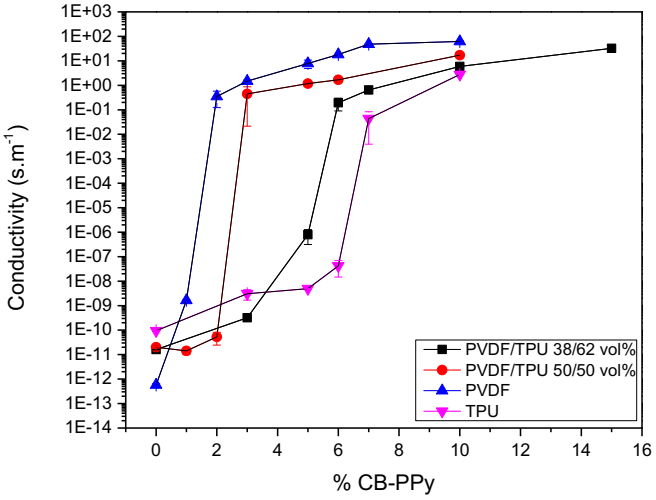

Figure 4-6: Electrical conductivity of compression molded PVDF/CB-PPy, TPU/CB-PPy, PVDF/TPU/CB-PPy 38/62 vol% and 50/50 vol% as function of CB-PPy percentage.

Table 4-5: Electrical conductivity as function of CB-PPy content for compression molded composites of PVDF/CB-PPy, TPU/CB-PPy, PVDF/TPU/CB-PPy 38/62 vol% and 50/50 vol%.

PVDF		TPU	
% CB-PPy	σ (s.m^{-1})	% CB-PPy	σ (s.m^{-1})
0	(5.73 ± 0.76) x 10^{-13}	0	(9.39 ± 0.42) x 10^{-11}
1	(1.65 ± 0.12) x 10^{-9}	3	(3.07 ± 1.40) x 10^{-9}
2	(3.49 ± 2.26) x 10^{-1}	5	(4.94 ± 0.02) x 10^{-9}
3	(1.48 ± 0.16) x 10^{0}	6	(4.21 ± 2.74) x 10^{-8}
5	(7.82 ± 2.92) x 10^{0}	7	(4.35 ± 3.96) x 10^{-2}
6	(1.82 ± 0.03) x 10^{1}	10	(2.77 ± 0.02) x 10^{0}
7	(4.81 ± 0.26) x 10^{1}		
10	(6.16 ± 0.49) x 10^{1}		

PVDF/TPU 38/62 vol%		PVDF/TPU 50/50 vol%	
% CB-PPy	σ (s.m^{-1})	% CB-PPy	σ (s.m^{-1})
0	(1.60 ± 0.03) x 10^{-11}	0	(1.99 ± 0.10) x 10^{-11}
3	(3.19 ± 0.03) x 10^{-10}	1	(1.42 ± 0.43) x 10^{-11}
5	(7.95 ± 4.82) x 10^{-7}	2	(5.30 ± 2.85) x 10^{-11}
6	(1.94 ± 1.04) x 10^{-1}	3	(4.49 ± 4.27) x 10^{-1}
7	(6.44 ± 0.64) x 10^{-1}	5	(1.18 ± 0.29) x 10^{0}
10	(5.90 ± 0.52) x 10^{0}	6	(1.69 ± 0.26) x 10^{0}
15	(3.23 ± 0.17) x 10^{1}	10	(1.70 ± 0.24) x 10^{1}

As reported in Figure 4-6, the electrical conductivity of the composites increases with the content of CB-PPy. For instance, PVDF/TPU/CB-PPy 38/62 vol% and 50/50 vol% composites with 15% and 10 % of CB-PPy display an electrical conductivity of 3.23 × 10^{1} S•m^{-1} and 1.70 10^{1} S•m^{-1} , respectively, which means an increase in the electrical conductivity of 10^{12} orders of magnitude when compared to the neat PVDF/TPU blends (1.60 × 10^{-11} S•m^{-1} and 1.99 × 10^{-11} S•m^{-1}, respectively).

Furthermore, according to the classical percolation theory, the dependence of the electrical conductivity (σ) of composites on the electrically conductive filler concentration (f) above the percolation concentration threshold (f_p) can be described by a scaling law of in the form of the following a power law equation [108]:

$$\sigma = c(f - f_p)^t \quad (12)$$

where c is a fitting constant and t a critical exponent. The values of these parameters are presented in Table 4-6. The theoretical predictions of *t* are related to the system dimension and the calculated *t* values are in agreement with the classical theory for tridimensional systems, with values ranging from 2 to 4 [4, 25].

Table 4-6: Values of c, f_p, t and R^2 for compression molded PVDF/CB-PPy, TPU/CB-PPy, PVDF/TPU/CB-PPy 38/62 vol% and 50/50 vol%.

Sample	*C*	f_p	*t*	R^2
PVDF/CB-PPy	0.44	1	3.86	0.99
TPU/CB-PPy	0.47	6	2.21	0.99
PVDF/TPU/CB-PPy 38/62 vol%	0.73	5	2.19	0.99
PVDF/TPU/CB-PPy 50/50 vol%	0.45	2	3.10	0.99

The percolation threshold for PVDF/CB-PPy and TPU/CB-PPy composites resulted to be 1% and 6%, respectively. This means that in the composites with a CB-PPy content lower than these values the creation of a conductive path does not occur due to the insufficient amount of conductive filler. In this case the obtained mixtures display electrical conductivities similar to those of the neat PVDF and TPU matrices. When the content of CB-PPy is higher than 1% and 6% for PVDF/CB-PPy and TPU/CB-PPy, respectively, there is a significant increase in the electrical conductivity of the composites due to the increase in the contact between the conductive particles that creates a conductive network in the polymeric matrix. On the other hand, the electrical percolation threshold for CB-PPy in the PVDF/TPU 38/62 vol% matrix and in the PVDF/TPU 50/50 vol% matrix were 5% and 2%, respectively. The electrical conductivity results show that blending PVDF and TPU can improve the percolation threshold of the mixtures when both components are present in 50 vol% in the composite that leads to the formation of a co-continuous structure. According to Bizhani et al. [40], a co-continuous immiscible polymer blend decreases the electrical percolation threshold due to the selective localization of the filler in one of the phases or at the interface of phases of the blend.

4.3.2 Quasi static tensile test

According to the results obtained from the electrical conductivity measurements, some composites were selected for additional characterizations.

Tensile stress-strain curves for composites with 38/62 vol% and 50/50 vol% of PVDF/TPU as matrix are represented in Figure 4-7 and mechanical properties of the samples are shown in Table 4-7. As expected, the curves indicate that increasing the amount of conductive filler in the blends leads to higher tensile strength values. For instance, the tensile strength for blend PVDF/TPU 38/62 vol% without any filler is 5.5 MPa, however, for the same blend comprising 6% of CB-PPy the tensile stress is 7.0 MPa and when the content of filler is increased to 10% the tensile strength rises to 8.0 MPa (i.e., a 27 and 45 % increase, respectively). Although the same behavior is observed for the PVDF/TPU/CB-PPy 50/50 vol% composites, the tensile strength of the blend without filler was already very high and the addition of conductive filler lead to a small increase in the tensile strength of the composites.

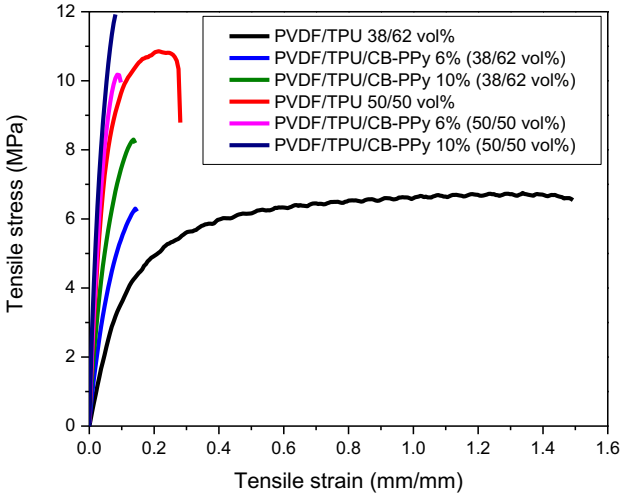

Figure 4-7: Tensile curves for compression molded PVDF/TPU/CB-PPy composites with different proportions of each component.

Moreover, considering the composites with the same amount of filler but different blends as matrix, the composite with the blend PVDF/TPU 50/50 vol%

(containing higher amount of PVDF than PVDF/TPU 38/62 vol%) present higher tensile strength. Furthermore, the results indicate that the incorporation of the filler into the blends rises the rigidity of the mixtures, increasing the elastic modulus and reducing the elongation at break. The same occurs when comparing the composites comprising the different matrices: 38/62 vol% and 50/50 vol%. The blends comprising higher amount of PVDF (50 vol%), at the same filler concentration, show higher elastic modulus and lower elongation at break due to the presence of less quantity of the elastomeric component (TPU).

Table 4-7: Mechanical properties of compression molded PVDF/TPU blends and composites including average values and standard deviation.

PVDF/TPU 38/62 vol%			
% CB-PPy	**Elastic modulus E (MPa)**	**Maximum tensile stress σ_{max} (MPa)**	**Elongation at break ε_b (%)**
0	41.2 ± 14.8	5.5 ± 1.1	153 ± 81
6	125.9 ± 7.2	7.0 ± 0.7	22.0 ± 9.1
10	210.0 ± 18.4	8.0 ± 0.4	16.0 ± 3.8
PVDF/TPU 50/50 vol%			
% CB-PPy	**Elastic modulus E (MPa)**	**Maximum tensile stress σ (MPa)**	**Elongation at break ε (%)**
0	287.8 ± 39.1	10.9 ± 0.9	27.5 ± 6.4
6	259.1 ± 34.6	9.0 ± 1.5	10.3 ± 3.9
10	369.4 ± 29.3	12.0 ± 1.6	9.5 ± 3.8

4.3.3 Dynamic mechanical thermal analysis

DMTA analysis was carried out on compression molded PVDF/CB-PPy and TPU/CB-PPy composites with 6% of conductive filler and PVDF/TPU/CB-PPy 38/62 vol% and 50/50 vol% composites with 3%, 6% and 10% of conductive filler in order to evaluate the influence of the composition on the viscoelastic parameters, storage

modulus (E') and loss tangent (tan δ), and the glass transition temperature (T_g) of the composites.

Figure 4-8 and Figure 4-9 show a comparison of the DMTA curves of storage modulus and loss tangent, respectively, as function of temperature for compression molded PVDF/CB-PPy, TPU/CB-PPy, PVDF/TPU/CB-PPy 38/62 and 50/50 vol% composites comprising 6% of the conductive filler CB-PPy. It is possible to observe in Figure 4-8 that the composites comprising neat PVDF and neat TPU as matrix report the highest and lowest storage modulus, respectively. In fact, when TPU is added to the blend the storage modulus of the final mixture decreases contributing to reach more flexible materials.

Moreover, Figure 4-9 represents the curves of tan δ versus temperature and the peak of the curves were used to measure the T_g values of the composites, which are displayed in Table 4-8.

The glass transition temperature for PVDF/CB-PPy containing 6% of conductive filler is -38.4 °C and it is increased to -33.4 °C and -34.3 °C with the addition of 62 and 50 vol% of TPU, respectively. This occurs because the composite composed of TPU/CB-PPy with same filler amount presents a higher T_g value of -32.3 °C, thus increasing the final T_g value of the mixtures. In addition, the T_g of the composites with PVDF/TPU blends as matrix present a T_g value between the two T_g values of the composite with neat PVDF and TPU as matrix and proportional to the amount of each polymer present in the composition. For instance, the composite of PVDF/TPU/CB-PPy 38/62 vol% with 6% of CB-PPy has a T_g value of -33.4 °C, while the composite of PVDF/TPU/CB-PPy 50/50 vol% with same amount of filler show a T_g value of -34.3 °C due to the lower amount of the component with higher T_g (TPU). It is important to notice that two distinct T_g values are expected for immiscible polymer blends, however, only one is observed in the PVDF/TPU composites due to the narrow distance between the T_g of the two neat polymers. It is also possible to observe that adding the conductive filler reduces the T_g value of the composites. Table 4-8 shows that adding 6% of the conductive filler CB-PPy to the PVDF/TPU 38/62 and 50/50 vol% blends the T_g values decrease from -29.4 and -32.4 °C to -33.4 and -34.3 °C, respectively. This fact could be attributed to the reduction of the mobility of the

polymeric chains with the addition of the conductive filler that also rises the rigidity of the mixture.

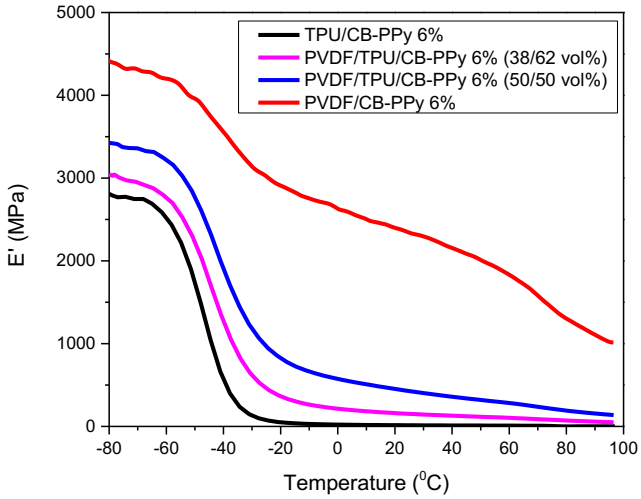

Figure 4-8: Storage modulus (E') as function of temperature for compression molded PVDF/CB-PPy, TPU/CB-PPy, PVDF/TPU/CB-PPy 38/62 vol% and 50/50 vol% composites with 6% of conductive filler.

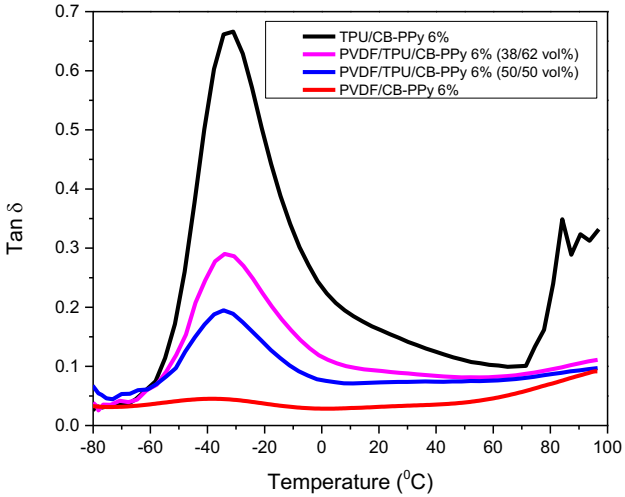

Figure 4-9: Loss tangent (tan δ) as function of temperature for compression molded PVDF/CB-PPy, TPU/CB-PPy, PVDF/TPU/CB-PPy 38/62 vol% and 50/50 vol% with 6% of conductive filler.

Table 4-8: Glass transition temperature (T_g) for compression molded PVDF/CB-PPy, TPU/CB-PPy, PVDF/TPU/CB-PPy 38/62 vol% and 50/50 vol% with various amount of conductive filler.

Sample	T_g (°C)
PVDF	-39.2
PVDF/CB-PPy 6%	-38.4
PVDF/TPU 38/62 vol%	-29.4
PVDF/TPU/CB-PPy 3% (38/62 vol%)	-28.9
PVDF/TPU/CB-PPy 6% (38/62 vol%)	-33.4
PVDF/TPU/CB-PPy 10% (38/62 vol%)	-35.2
PVDF/TPU 50/50 vol%	-32.4
PVDF/TPU/CB-PPy 3% (50/50 vol%)	-34.5
PVDF/TPU/CB-PPy 6% (50/50 vol%)	-34.3
PVDF/TPU/CB-PPy 10% (50/50 vol%)	-34.3
TPU	-25
TPU/CB-PPy 6%	-32.3

Moreover, Figure 4-10 and Figure 4-12 report the storage modulus as function of temperature for compression molded PVDF/TPU/CB-PPy 38/62 vol% and 50/50 vol% composites with different amount of conductive filler. When CB-PPy is added to PVDF/TPU, the storage modulus of the mixture increases, increasing the rigidity of the final material due to the formation of a three-dimensional network. Samples with higher amount of CB-PPy present higher storage modulus, for instance, for both matrices (PVDF/TPU 38/62 vol% and 50/50 vol%) the composites with the highest E' are those with 10% of conductive filler.

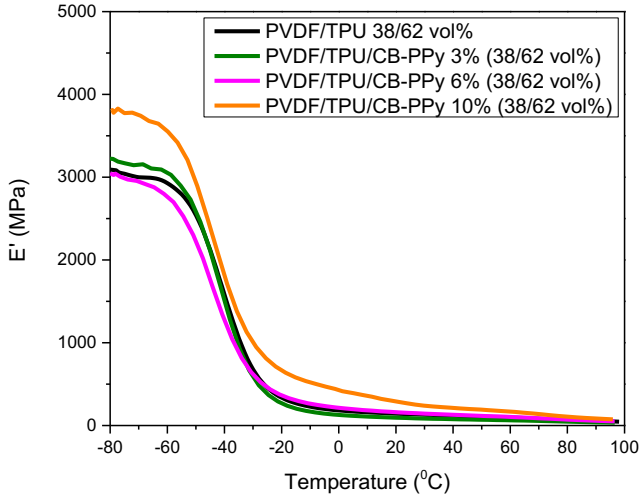

Figure 4-10: Storage modulus (E') as function of temperature for compression molded PVDF/TPU/CB-PPy 38/62 vol% composites with various amount of conductive filler.

In addition, Figure 4-11 and Figure 4-13 show the curves of tan δ as function of temperature for PVDF/TPU/CB-PPy 38/62 vol% and 50/50 vol% composites with various amount of conductive filler and their T_g values are reported Table 4-8. When comparing PVDF/TPU/CB-PPy 38/62 vol% composites with different filler content, the T_g values decrease as the filler concentration increases. In fact, the composite of PVDF/TPU/CB-PPy 38/62 vol% with 3% of CB-PPy has a T_g of -28.9 °C, while the composites with 6% and 10% of CB-PPy present Tg values of -33.4 and -35.2 °C, respectively. The observed behavior could be attributed to the higher restriction on the mobility of the polymeric chains with higher amount of the conductive filler present in the mixture. The same behavior is observed for the composites of PVDF/TPU/CB-PPy 50/50 vol%, the T_g value decreases as the conductive filler is added to the blend.

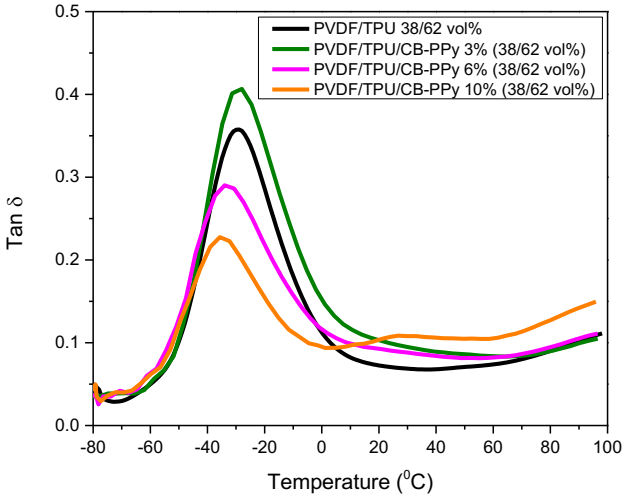

Figure 4-11: Loss tangent (tan δ) as function of temperature for compression molded PVDF/TPU/CB-PPy 38/62 vol% with various amount of conductive filler.

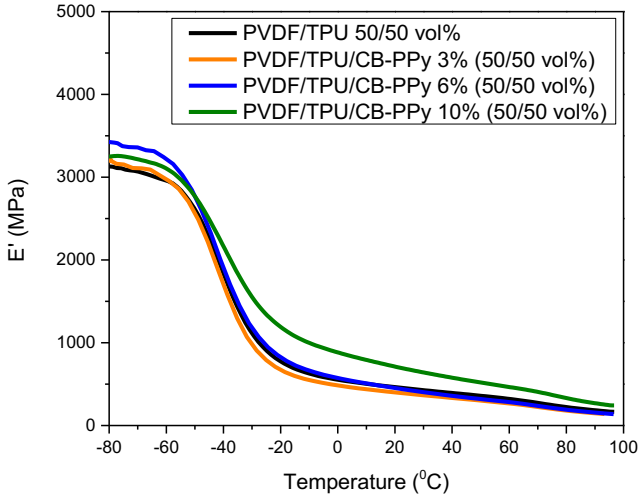

Figure 4-12: Storage modulus (E') as function of temperature for compression molded PVDF/TPU/CB-PPy 50/50 vol% composites with various amount of conductive filler.

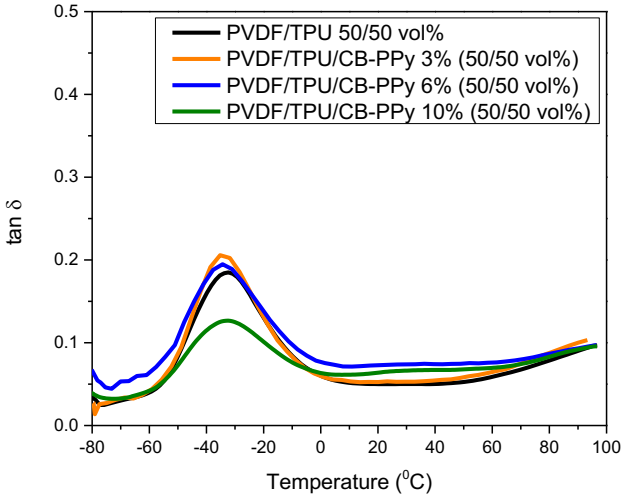

Figure 4-13: Loss tangent (tan δ) as function of temperature for compression molded PVDF/TPU/CB-PPy 38/62 vol% with various amount of conductive filler.

4.3.4 Scanning electron microscopy (SEM) and energy dispersive X-ray spectroscopy (EDS)

Scanning electron microscopy (SEM) images of cryogenically fractured surfaces of compression molded PVDF/CB-PPy, TPU/CB-PPy, PVDF/TPU/CB-PPy 38/62 vol% and 50/50 vol% conductive composites are displayed in Figure 4-14. Figure 4-14 (a) and (b) show the morphology of PVDF comprising 6% of CB-PPy and Figure 4-14 (c) and (d) of TPU comprising 6% of the filler at 5000 and 10000 times of magnification, respectively. It is possible to notice some white points that corresponds to the spherical morphology of CB-PPy dispersed in the polymeric matrices. Moreover, the images of PVDF/TPU/CB-PPy 38/62 vol% with 10% of filler are displayed in Figure 4-14Figure 4-14: SEM images of compression molded: (a) and (b) PVDF/CB-PPy 6%; (c) and (d) TPU/CB-PPy 6%; (e) and (f) PVDF/TPU/CB-PPy 10% (38/62 vol%) and (g) and (f) PVDF/TPU/CB-PPy 6% (50/50 vol%) at different magnifications (a, c, e, g:

x5000; f: x20000 and b, d, h: x10000).Figure 4-14 (c) and (d) showing the expected morphology for immiscible polymer blends also with white points of filler. In addition, the images (g) and (h) display the co-continuous morphology of the matrix PVDF/TPU 50/50 vol%. The SEM pictures reveal that the microstructure of the investigated materials is not substantially affected by the introduction of the CB-PPy conductive filler.

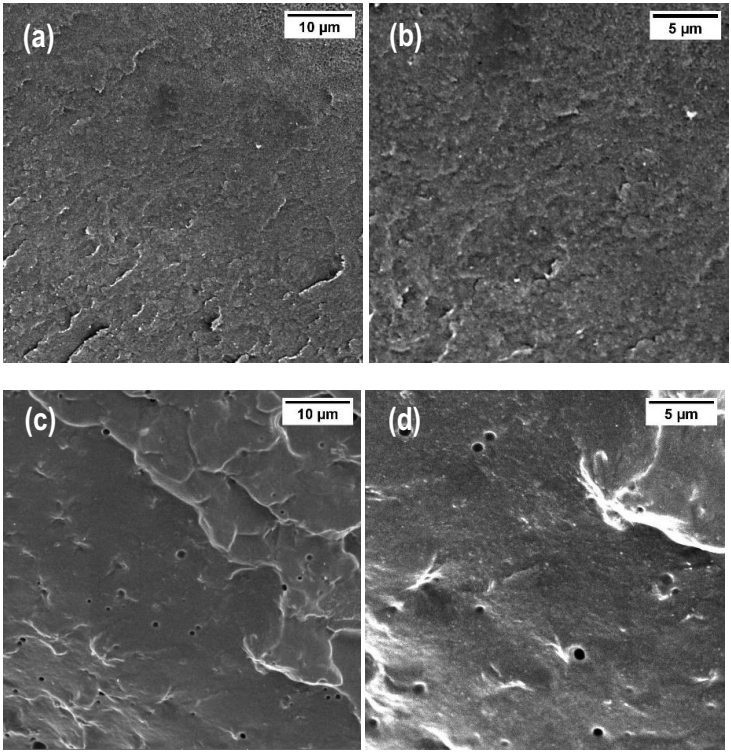

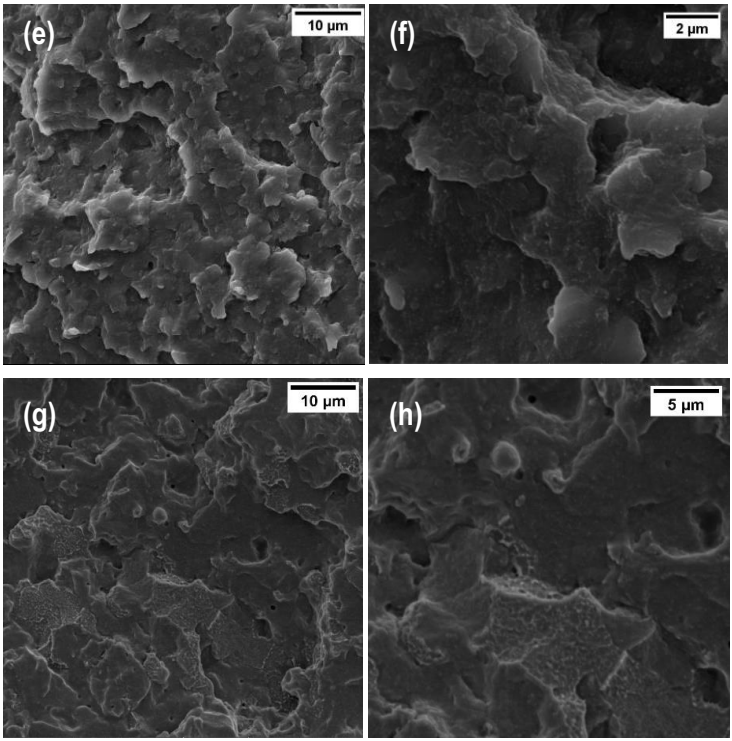

Figure 4-14: SEM images of compression molded: (a) and (b) PVDF/CB-PPy 6%; (c) and (d) TPU/CB-PPy 6%; (e) and (f) PVDF/TPU/CB-PPy 10% (38/62 vol%) and (g) and (f) PVDF/TPU/CB-PPy 6% (50/50 vol%) at different magnifications (a, c, e, g: x5000; f: x20000 and b, d, h: x10000).

Moreover, energy dispersive X-ray spectroscopy (EDS) was performed to better understand the morphology of the composites comprising the co-continuous blend as matrix. Figure 4-15 (a), (b) and (c) display the SEM image, EDS mapping and EDS spectrum of the composite PVDF/TPU/CB-PPy 6% (50/50 vol%). The EDS mapping image shows the co-continuous morphology of blend and the composition of each phase, where the green color represents the atoms of fluorine present in PVDF and the blue and pink color the atoms of oxygen and nitrogen, respectively, present in TPU. Since the conductive filler is composed of carbon black-polypyrrole, it is not possible to observe where the filler is localized using this technique.

Furthermore, the TPU phase of PVDF/TPU/CB-PPy 38/62 vol% with 6% of CB-PPy was removed with the immersion of the composite in THF. The SEM image of the etched composite is presented in Figure 4-15 (d) showing the remaining PVDF continuous phase. The composition of the remaining phase can be confirmed by the EDS spectra displayed in Figure 4-15 (e).

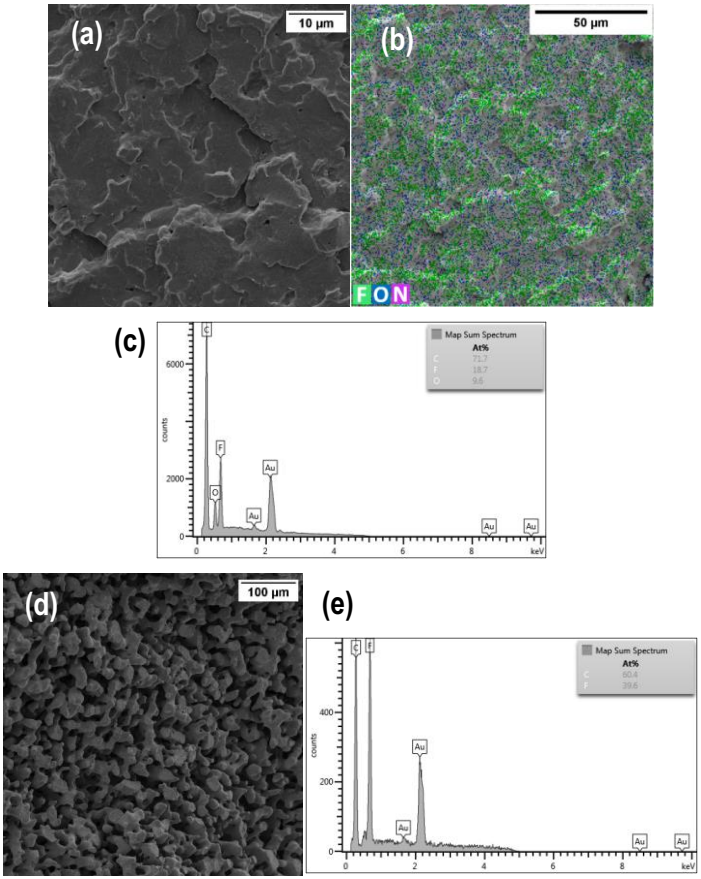

Figure 4-15: (a) SEM image at x5000 of magnification; (b) EDS mapping and (c) spectrum at x1000 of magnification of PVDF/TPU/CB-PPy 6% (50/50 vol%); (d) SEM image and (e) EDS spectrum of PVDF/TPU/CB-PPy 6% (50/50 vol%) etched with THF to remove TPU phase at x500 magnification showing the presence of PVDF in the unetched phase.

4.4 Fused filament fabrication

In this section, composites were selected based on their electrical conductivity and mechanical behavior and tested for a possible application in the fused filament fabrication (FFF) process. After melt compounding, the selected composites were grinded and extruded into filaments and subsequently 3D printed using a FFF commercial machine.

Firstly, PVDF/TPU/CB-PPy 38/62 vol% with 5% and 6% of conductive filler were selected due to their electrical conductivity near the electrical percolation threshold of the material where there is enough amount of filler to create a conductive network in the polymeric matrix. These compositions were selected because they achieved good electrical conductivity values at lowest filler concentration in the preliminary tests on compression molded samples. However, after the printing process the electrical conductivity of the specimens decreased significantly. In order to prepare highly conductive printed parts, the composite comprising 10% of CB-PPy was also selected for the 3D printing process.

Moreover, the mechanical and electrical properties and microstructure of 3D printed parts were investigated by quasi static tensile test, scanning electron microscopy, density measurement, percentage of voids and electrical conductivity measurements.

Table 4-9: Composition of 3D printed PVDF/TPU/CB-PPy composites.

PVDF/TPU 38/62 vol%	PVDF/TPU 50/50 vol%
% CB-PPy	% CB-PPy
0	-
5	-
6	-
-	10

4.4.1 Quasi static tensile test

The mechanical properties of 3D printed parts were evaluated by tensile tests and the main results are presented in Table 4-10. The tensile stress-strain curves obtained from the fracture test are presented in Figure 4-16. As expected, the addition of a conductive filler into the blends increases the elastic modulus (rising the rigidity of the material) and reduces the elongation at break of the composites. The tensile strength of the composites increases proportionally to the amount of filler added to the blends. In fact, composites with higher amount of filler, i.e. 6% and 10%, showed the highest tensile strength of 8.6 and 10.0 MPa, respectively, and it drops down to 3.1 MPa when no filler is added to the blend PVDF/TPU 38/62 vol%.

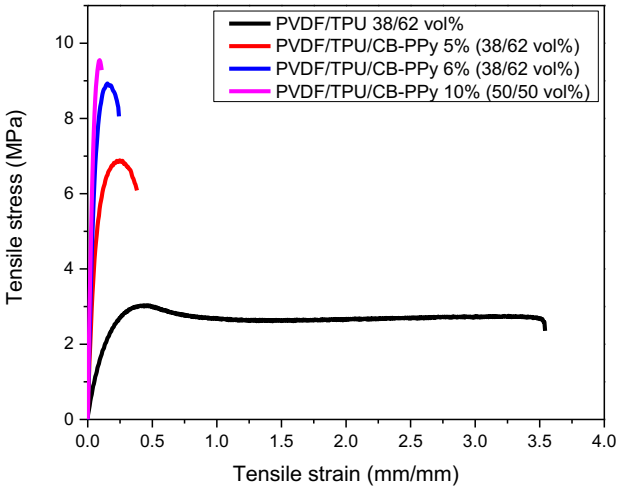

Figure 4-16: Tensile curves of composites 3D printed via FFF for PVDF/TPU comprising different amounts of conductive filler.

Table 4-10: Mechanical properties of selected compositions of 3D printed parts via FFF including average values and standard deviation.

PVDF/TPU 38/62 vol%			
% CB-PPy	**Elastic modulus E (MPa)**	**Maximum tensile stress σ_{max} (MPa)**	**Elongation at break ε_b (%)**
0	35.8 ± 0.1	3.1 ± 0.2	261 ± 89.4
5	179.9 ± 46.6	6.7 ± 0.3	38.6 ± 9.8
6	301.3 ± 32.7	8.6 ± 0.8	35.5 ± 17.1
PVDF/TPU 50/50 vol%			
% CB-PPy	**Elastic modulus E (MPa)**	**Maximum tensile stress σ_{max} (MPa)**	**Elongation at break ε_b (%)**
10	430.6 ± 13.0	10.0 ± 2.2	10.3 ± 1.5

Furthermore, a comparison between the mechanical properties of compression molded and 3D printed samples are summarized in Table 4-11. The tensile curves obtained from fracture test of compression molded and 3D printed specimens are displayed in Figure 4-17 and Figure 4-18. The results show that for samples with same composition, the maximum tensile stress is higher in compression molded than in 3D printed samples due to the lower amount of defects in the compression molded final parts. It is well known that FFF printed parts often show lower mechanical performance when compared to compression or injection molded specimens because of porosity and poor interlayer bonding [26].

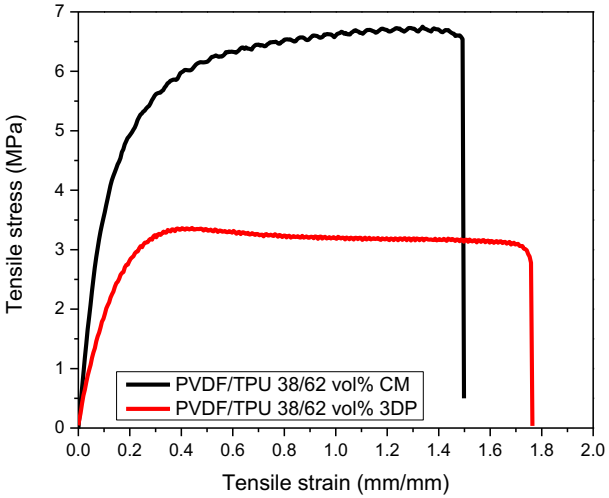

Figure 4-17: Comparison of tensile curves of compression molded and 3D printed PVDF/TPU 38/62 vol% blends.

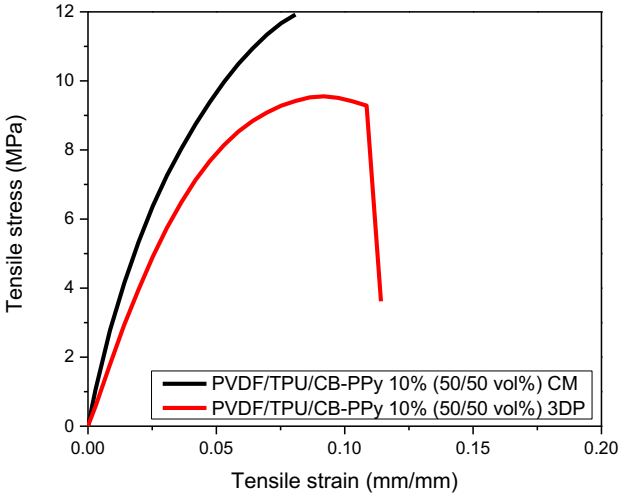

Figure 4-18: Comparison of tensile curves of compression molded and 3D printed PVDF/TPU/CB-PPy 50/50 vol% composite with 10% of conductive filler.

Table 4-11: Comparison of mechanical properties of selected compositions of compression molded and 3D printed samples including average values and standard deviation.

Sample	Elastic modulus E (MPa)	Maximum tensile stress σ_{max} (MPa)	Elongation at break ε_b (%)
PVDF/TPU 38/62 vol% CM	41.2 ± 14.8	5.5 ± 1.1	153 ± 81
PVDF/TPU 38/62 vol% 3DP	35.8 ± 0.1	3.1 ± 0.2	261 ± 89.4
PVDF/TPU/CB-PPy 10% (50/50 vol%) CM	369.4 ± 29.3	12.0 ± 1.6	9.5 ± 3.8
PVDF/TPU/CB-PPy 10% (50/50 vol%) 3DP	430.6 ± 13.0	10.0 ± 2.2	10.3 ± 1.5

4.4.2 Scanning electron microscopy, density measurement and percentage of voids

The micrographs of the cross-sections of cryogenically fractured 3D printed PVDF/TPU and PVDF/TPU/CB-PPy composites are presented in Figure 4-19. The 3D printed specimens are composed of ten layers of 0.2 mm each deposited during the fused filament fabrication process. The images exhibit the boundaries between the layers deposited during the FFF process with good adhesion between the layers for all samples. It is also possible to see the presence of voids between the layers and defects, mainly in Figure 4-19 (a) and (b). Moreover, with the increase in the filler content there is an increase in the layer adhesion and a decrease in the quantity of voids leading to a better compacted material. However, the percentage of voids (V%) obtained from the density measurements (see Table 4-12) indicates that the increase in the filler content leads to higher quantity of voids. That is because the cross-section fractures show only the morphology between the layers and they do not show the voids present between the deposited filaments on a single layer. As the addition of conductive filler rises the viscosity of the composite filaments causing a reduction in the filament flow through the extruding nozzle, less amount of material is deposited in the printing process leading to higher porosity in a single layer.

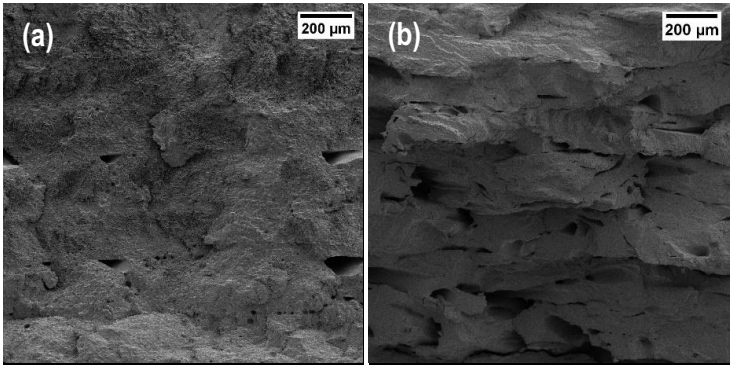

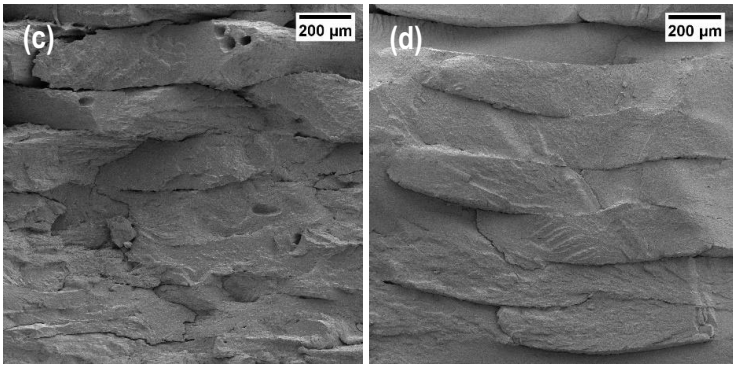

Figure 4-19: SEM images at 200x of magnification of 3D printed specimens of: (a) PVDF/TPU 38/62 vol%, (b) PVDF/TPU/CB-PPy 5% (38/62 vol%), (c) PVDF/TPU/CB-PPy 6% (38/62 vol%) and (d) PVDF/TPU/CB-PPy 10% (50/50 vol%).

Table 4-12: Experimental and theoretical density and percentage of voids (V%) for 3D printed PVDF/TPU/CB-PPy composites with different amount of conductive filler.

PVDF/TPU 38/62 vol%			
% CB-PPy	**Experimental density ($g.cm^{-3}$)**	**Theoretical density ($g.cm^{-3}$)**	**V %**
5%	1.18	1.38	15
6%	1.09	1.38	21
PVDF/TPU 50/50 vol%			
% CB-PPy	**Experimental density ($g.cm^{-3}$)**	**Theoretical density ($g.cm^{-3}$)**	**V %**
10%	1.13	1.49	24

4.4.3 Electrical conductivity

The electrical conductivity was measured for 3D printed samples of PVDF/TPU 38/62 vol%, PVDF/TPU/CB-PPy 38/62 vol% with 5% and 6% of filler and

PVDF/TPU/CB-PPy 50/50 vol% with 10% of conductive filler. For all samples, the 3D specimens presented lower values of electrical conductivity when compared to the compression molded samples with the same composition. The significant drop in the electrical conductivity of 3D printed samples can be attributed to the presence of voids and defects in 3D printed parts. This behavior was already reported in the literature [18, 23, 27, 109]. A comparison between the electrical conductivity values of compression molded and 3D printed specimens are reported in Table 4-13.

It is possible to observe that, although the compression molded samples containing 6% of CB-PPy showed a high value electrical conductivity of 1.94 x 10^{-1} S•m^{-1}, the 3D printed part with the same composition presented a significant lower value of electrical conductivity of 6.01 x 10^{-8} S•m^{-1}. On the other hand, for the composite containing 10% of CB-PPy and the co-continuous PVDF/TPU 50/50 vol% matrix, even after the 3D-printing process the electrical conductivity of the sample was 4.14 10^{0} S•m^{-1}, only one order of magnitude lower than the compression molded counterparts, 1.70 x 10^{1} S•m^{-1}, indicating a promising use of this filament for technological applications requiring electrical conductivity.

Table 4-13: Comparison of the electrical conductivity of compression molded and 3D printed samples including average values and standard deviation.

PVDF/TPU 38/62 vol%		
% CB-PPy	**σ compression molded (S•m^{-1})**	**σ 3D printed (S•m^{-1})**
0	(1.60 ± 0.03) x 10^{-11}	(5.90 ± 0.30) x 10^{-12}
5	(7.95 ± 4.82) x 10^{-7}	(9.74 ± 7.78) x 10^{-8}
6	(1.94 ± 1.04) x 10^{-1}	(6.01 ± 3.72) x 10^{-8}
PVDF/TPU 50/50 vol%		
% CB-PPy	**σ compression molded (S•m^{-1})**	**σ 3D printed (S•m^{-1})**
10	(1.70 ± 0.24) x 10^{1}	(4.14 ± 0.08) x 10^{0}

Furthermore, Table 4-14 displays a comparison of the electrical conductivity values of 3D printed nanocomposites containing different polymers with

carbon nanofillers from various studies of different authors. Most of the works that present values of electrical conductivity as high as the values obtained in this research report the addition of at least 3 vol% of carbon nanotubes (CNT). Although carbon nanotubes have shown to be more effective in creating a conductive network in polymeric matrices due to its higher aspect ratio, the addition of carbon nanotubes filler leads to a significant increase in the polymer viscosity, thus the material becomes more difficult to be processed at the same filler concentration than CB-PPy composites [6].

Table 4-14: Comparison of electrical conductivity values for nanocomposites produced via fused filament fabrication from different authors.

Matrix	Type of nanofiller	Nanofiller content	σ (S•m^{-1})	References
ABS	CB	3 wt%	10^{-12}	[11]
ABS	CNT	3 wt%	10^{-7}	[11]
ABS	MWCNT	6 wt%	10^{-2}	[18]
ABS	MWCNT	10 wt%	10^{0}	[51]
ABS	GNP	6 wt%	10^{-13}	[18]
ABS	GNP/CNT	6 wt% (50:50)	10^{-3}	[23]
ABS	GO	3.8 wt%	10^{-7}	[110]
PBT	CNT	3.5 vol%	10^{1}	[111]
PLA	CNT	3 vol%	10^{0}	[49]
PLA	r-GO	6 wt%	10^{2}	[112]
TPU	MWCNT	3 wt%	10^{-1}	[15]
TPU	CNT	3 wt%	10^{-4}	[9]

4.5 Conclusions

Flexible, electrically conductive and 3D printable composites of PVDF/TPU/CB-PPy were successfully produced using PVDF/TPU blends as polymeric matrix and carbon black-polypyrrole as conductive filler. In order to achieve an optimal compromise between electrical conductivity, mechanical properties and printability, composites with different compositions were prepared.

The flexibility aimed for the final material was improved with the addition of TPU to PVDF composites. Furthermore, the achievement of a co-continuous blend comprising 50/50 vol% of PVDF/TPU improved not only the mechanical properties but also electrical conductivity of the composites resulting in a flexible and highly conductive material. In fact, the electrical percolation threshold of the conductive composite comprised of the co-continuous blend was 2%, while the electrical percolation threshold of the composite with the blend 38/62 vol% was 5%, confirming that the co-continuous phase assists in the reduction of the percolation threshold while improves the flexibility and printability of PVDF composites.

Moreover, compression molded composites showed higher electrical conductivity when compared to the 3D printed parts with same composition due to the presence of void, defects and overlapping layers in 3D parts that can hinder the flow of electrons. However, the 3D printed composite PVDF/TPU/CB-PPy 10% (50/50 vol%) presented a high value of electrical conductivity, 4.14×10^{0} $S \cdot m^{-1}$, even after the printing process indicating a potential use of this filament for electrically conductive applications.

Chapter V

5. Poly(vinylidene fluoride)/thermoplastic polyurethane composites comprising carbon black-polypyrrole for piezoresistive sensors application

Part of this chapter has been published in:

Mayara C. Bertolini, Sithiprumnea Dul, Elaine C. Lopes Pereira, Bluma G. Soares, Guilherme M. O. Barra, Alessandro Pegoretti

"Fabrication and Characterization of piezoresistive flexible pressure sensors based on poly(vinylidene fluoride)/thermoplastic polyurethane filled with carbon black-polypyrrole"
Polymer Composites, (2021) 42(12) 6621-6634.

5.1 Introduction

In this chapter the fabrication and characterization of piezoresistive flexible materials for pressure sensors composed of poly(vinylidene fluoride)/thermoplastic polyurethane blends as matrix filled with various fractions of carbon black doped with polypyrrole prepared by compression molding and fused filament fabrication is presented.

The main challenge in the preparation of piezoresistive materials composed of conductive polymeric composites is achieving good responses at minimum filler content to preserve the mechanical properties and processability of the matrix [4]. One of the reported strategies to reduce the percolation threshold in CPCs is based on the usage of matrices composed of polymeric blends [28, 32-38, 40, 42]. Moreover, fused filament fabrication is a promising technology for the fabrication of flexible pressure sensors [7, 10, 58]. Combining this technique with conductive polymeric composites is an efficient way to fabricate materials with conductive, structural and sensing functionalities [2, 5, 15, 69]. In this framework, only a few studies report on the use of polymeric blends to control properties and improve printability of composites filaments for FFF [33].

Although some researches confirm that PVDF/TPU blends are an efficient way to prepare materials with excellent combination of mechanical and pyroelectric/piezoelectric properties and flexibility [32, 75, 76], to our best knowledge, there are no studies concerning the development of such materials in filament form comprising a conductive filler and suitable for 3D printing.

In the next sections the fabrication and characterization of composites of PVDF/TPU 38/62 vol% and PVDF/TPU 50/50 vol% with different fractions of CB-PPy are investigated. The composites were prepared by melt mixing followed by compression molding, then selected composites were extruded into filament format and subsequently 3D printed using the FFF technique.

5.2 PVDF/TPU/CB-PPy composites prepared by compression molding

PVDF/TPU/CB-PPy 38/62 vol% and 50/50 vol% comprising various amount of CB-PPy were produced by melting compounding followed by compression molding. The compositions of the prepared composites are displayed in Table 5-1. The materials rheological and mechanical properties, as the interactions between the components of the polymeric blend, the dispersion and formation a tridimensional network of the filler in the polymeric matrix were evaluated by rheological measurements and the piezoresistive behavior of the samples was investigated by electromechanical analysis.

Table 5-1: Composition of compression molded PVDF/TPU/CB-PPy 38/62 vol% and 50/50 vol% composites.

PVDF/TPU 38/62 vol%	PVDF/TPU 50/50 vol%
% CB-PPy	% CB-PPy
0	0
-	1
-	2
3	3
5	5
6	6
7	10
10	-
15	-

5.2.1 Rheological analysis

Rheology measurements were carried out in order to investigate the polymer composites to better understand the interactions between the components of

the polymeric blend and the formation of a tridimensional network of the filler in the polymeric matrix [36, 38, 113]. The rheological analysis was performed in the molten state for neat PVDF, neat TPU, PVDF/TPU 38/62 vol% and PDF/TPU 50/50 vol% blends and composites comprising various amounts of CB-PPy to evaluate structural changes in the polymeric composites.

Figure 5-1 (a) and (b) shows the curves of storage modulus (G') and complex viscosity (η*) as a function of frequency for neat PVDF, neat TPU and PVDF/TPU 38/62 vol% and PDF/TPU 50/50 vol% blends and Table 5-2 summarizes the main rheological properties of the composites.

It is possible to observe that the storage modulus of TPU is higher than the storage modulus of PVDF, while the blends display an intermediate value of storage modulus between the two neat components. The same behavior can be observed for the complex viscosity of the materials. TPU has the highest viscosity while PVDF the lowest, while the PVDF/TPU blends have an intermediate viscosity between the pure components.

(a)

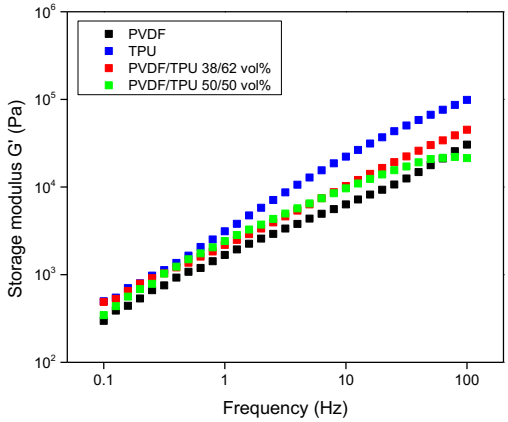

(b)

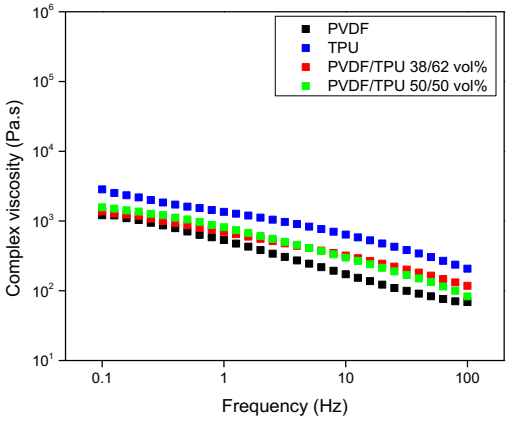

Figure 5-1: (a) Storage modulus and (b) complex viscosity as function of frequency at 180 °C for neat PVDF, neat TPU, PVDF/TPU 38/62 vol% and PVDF/TPU 50/50 vol%.

Table 5-2: Summary of main rheological properties at 180 °C of PVDF/TPU and PVDF/TPU/CB-PPy composites with different filler content.

PVDF/TPU 38/62 vol%			
% CB-PPy	**Viscosity at 10^{-1} Hz (Pa.s)**	**G' at 10^{-1} Hz (Pa)**	**G" at 10^{-1} Hz (Pa)**
0	700	2184	3816
3	1022	4114	4927
5	2647	12556	10910
6	4931	25979	16886
10	37962	226762	73971
PVDF/TPU 50/50 vol%			
% CB-PPy	**Viscosity at 10^{-1} Hz (Pa.s)**	**G' at 10^{-1} Hz (Pa)**	**G" at 10^{-1} Hz (Pa)**
0	815	2421	4515
1	1357	4283	7372
3	1934	7431	9612
5	5694	28557	21556
10	98279	601647	139059

In addition, a comparison of the storage (G') and loss (G") modulus as function of frequency for neat PVDF, neat TPU, PVDF/TPU 38/62 vol% and PDF/TPU 50/50 vol% blends are present in Figure 5-2. For neat PVDF and TPU the loss modulus (G") is higher than the storage modulus (G') at low frequencies indicating a liquid-like behavior. However, at a specific frequency, the G' and G" curves cross and G' becomes higher than G" describing a solid-like behavior. Moreover, for the PVDF/TPU 38/62 vol% and 50/50 vol% blends G" is higher than G' indicating a good interaction between PVDF and TPU.

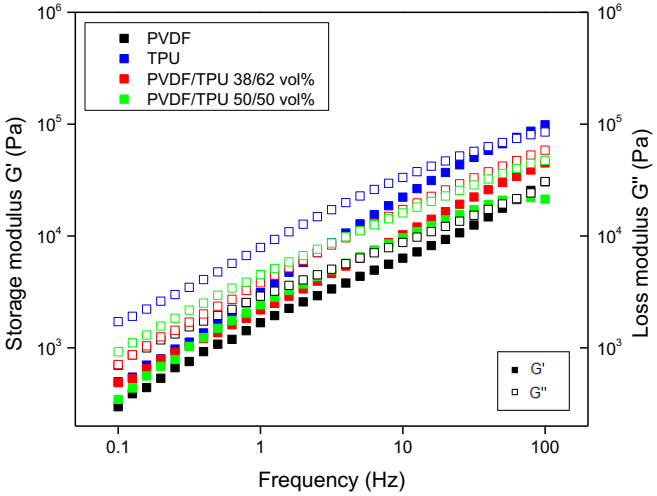

Figure 5-2: Dependence of storage and loss modulus with frequency at 180 °C for PVDF, neat TPU and PVDF/TPU 38/62 vol% and PVDF/TPU 50/50 vol%.

Additionally, the curves of storage modulus and complex viscosity as a function of frequency for PVDF/TPU/CB-PPy 38/62 vol% are show in Figure 5-3 (a) and (b), while the same curves for PVDF/TPU/CB-PPy 50/50 vol% are displayed in Figure 5-4 (a) and (b). For all composites, the addition of the conductive filler CB-PPy significantly increases the storage modulus (G') and complex viscosity of the composites (η*). This behavior can be explained by a reduction in the mobility of the polymeric chains and an increase in the viscosity of the mixtures with the addition of the filler due to the creation of a tridimensional network. Moreover, the addition of an elevated amount of filler (i.e. 5% and 10%) leads to an abrupt drop in the storage modulus and complex viscosity with increasing the frequency thus indicating a shear thinning behavior characteristic of the pseudo-plastic behavior. In fact, composites comprising 10% of CB-PPy present higher G' and η* values in comparison to the composites with less amount of filler or the PVDF/TPU blends. For instance, the PVDF/TPU 38/62 vol% blend presents a G' of 2184 Pa and η* of 700 Pa.s at 1Hz

frequency and 180 °C, while its composite with 10% of filler shows very higher G' and η* of 226762 Pa and 37962 Pa.s, respectively (see Table 5-2). The same behavior is observed for the PVDF/TPU/CB-PPy 50/50 vol% composites. The values of G' and η* for the blend without any amount of filler are 2421 Pa and 815 Pa.s, respectively, while for its composite with 10% of CB-PPy the G' and η* are 601647 Pa and 98279 Pa.s.

(a)

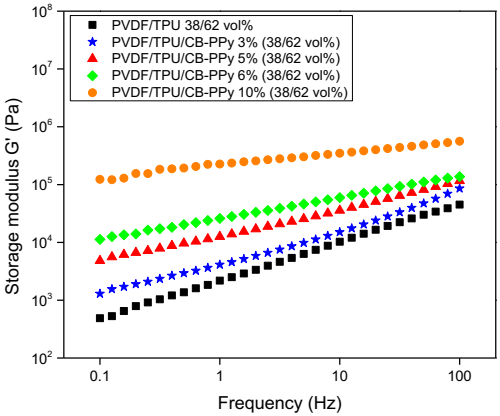

(b)

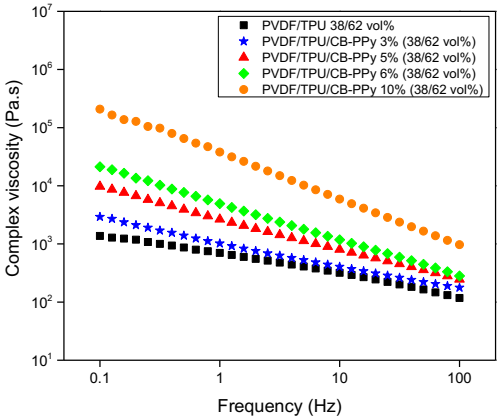

Figure 5-3: (a) Storage and (b) complex viscosity as function of frequency at 180 °C for PVDF/TPU/CB-PPy 38/62 vol% conductive composites with different amounts of filler.

(a)

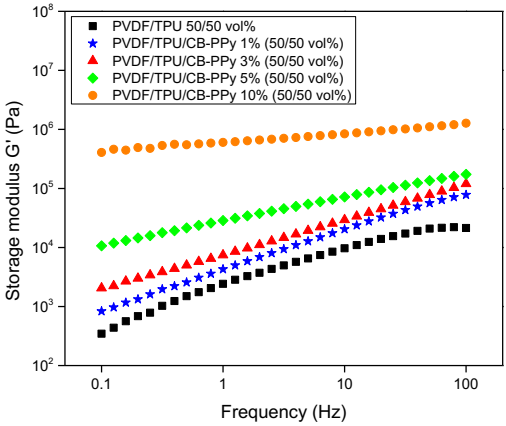

(b)

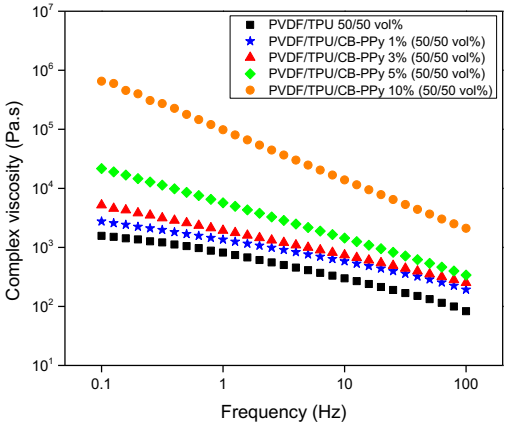

Figure 5-4: (a) Storage and (b) complex viscosity as function of frequency at 180 °C for PVDF/TPU/CB-PPy 50/50 vol% conductive composites with different amounts of filler.

Moreover, a comparison between the storage modulus and loss modulus as function of frequency is displayed in Figure 5-5 for (a) PVDF/TPU/CB-PPy 38/62 vol% and (b) PVDF/TPU/CB-PPy 50/50 vol% comprising different quantity of filler and their main rheological properties of those composites are summarized in Table 5-2. It is possible to observe that the values of G' and G" increase with frequency for all samples and the addition of conductive filler affects significantly the rheological behavior of the composites.

In fact, PVDF/TPU/CB-PPy 38/62 vol% and 50/50 vol% composites with CB-PPy content lower than 3% present higher values of G" than G', indicating a liquid-like behavior. When 3% of CB-PPy is added, similar values of G' and G" are reported over the entire frequency range indicating both solid-like and liquid-like behaviors. On the other hand, when more than 5% of CB-PPy is added to the composites, G' becomes higher than G" thus indicating a solid-like behavior related to the creation of a tridimensional network. Although G' is slightly higher than G" when 5% and 6% of filler is added, the composites containing 10% of CB-PPy displays a storage modulus significantly higher than the loss modulus in the whole frequency range thus confirming that the material behavior becomes less viscous and more elastic with the addition of conductive filler.

(a)

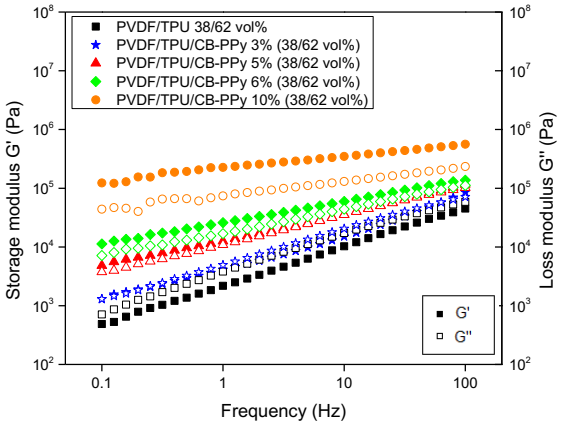

(b)

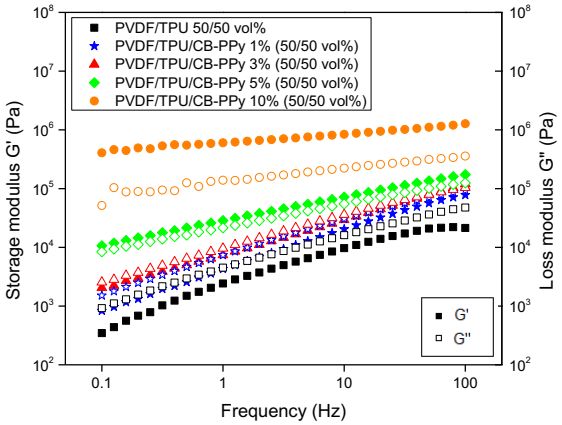

Figure 5-5: Dependence of storage and loss modulus with frequency at 180 °C for (a) PVDF/TPU/CB-PPy 38/62 vol% and (b) PVDF/TPU/CB-PPy 50/50 vol% conductive composites with different amounts of filler.

Furthermore, the rheological percolation threshold of the composites at the frequency of 10^{-1} Hz can be calculated by the power law equation (Equation 13) using the classical percolation theory:

$$G' = (f - f_p)^t \quad (13)$$

where G' is the storage modulus (Pa), f is the filler fraction (%), f_p is the filler fraction at the rheological percolation threshold (%) and t is a critical exponent.

The rheological percolation threshold of PVDF/TPU/CB-PPy 38/62 vol% and 50/50 vol% composites were found to be 3% and 1% (see Table 5-3), respectively, representing the critical filler concentration that leads to the formation of a tridimensional network that progressively hinders the movement of the polymeric chains causing a transition from liquid-like to solid-like behavior.

Table 5-3: Values of f_p, t and R^2 for PVDF/TPU/CB-PPy 38/62 vol% and 50/50 vol%.

Sample	f_p	t	R^2
PVDF/TPU/CB-PPy 38/62 vol%	3	2.35	0.99
PVDF/TPU/CB-PPy 50/50 vol%	1	2.94	0.97

A comparison of the electrical and rheological percolation threshold of the PVDF/TPU/CB-PPy 38/62 vol% and 50/50 vol% is reported in Table 5-4. For the composite PVDF/TPU/CB-PPy 38/62 vol%, the electrical and rheological percolation thresholds were found to be 5% and 3%, respectively, while for the composite PVDF/TPU/CB-PPy 50/50 vol% the electrical and rheological percolation thresholds were 2% and 1%. The differences between electrical and rheological percolation values are mainly attributed to the different phenomena required for inducing a conducting pathway in the polymer matrix or a transition in the rheological behavior. For electrical percolation threshold, the CB-PPy particles should be very close to each other in order to allow a conductive network, which increases abruptly the electrical

conductivity of the composite. On the other hand, in the rheological measurement, which is conducted at the processing temperature, the interaction between CB-PPy and the polymer matrices restricts the chain mobility changing the relaxation process. Thus, lower CB-PPy content is necessary to reach the rheological percolation threshold that it is related to the critical amount of conductive filler necessary to restrict the chain mobility of the polymeric matrix and the conductive particles are not necessarily in contact to each other. Therefore, the distance of CB-PPy particles necessary to achieve the rheological percolation is higher than that observed for electrical percolation.

Table 5-4: Comparison of the electrical and rheological percolation threshold of PVDF/TPU/CB-PPy 38/62 vol% and 50/50 vol% composites.

Sample	*Electrical percolation threshold*	*Rheological percolation threshold*
PVDF/TPU/CB-PPy 38/62 vol%	5	3
PVDF/TPU/CB-PPy 50/50 vol%	2	1

Another investigated parameter was the phase angle, which ranges from zero to ninety degrees. Low phase angles are related to materials that deform elastically as a solid, while high phase angles indicate that the material flows viscously as a liquid. Figure 5-6 presents the phase angle as a function of complex modulus for PVDF/TPU/CB-PPy 38/62 vol% and PVDF/TPU/CB-PPy 50/50 vol% conductive composites with various amounts of filler. It can be observed that for composites of both blends, the addition of the conductive filler reduces significantly the phase angle of the material indicating that the materials become more rheologically elastic with the addition of CB-PPy. In addition, the semi-circle format of the curves represents a good dispersion of the conductive filler in the polymer matrix.

(a)

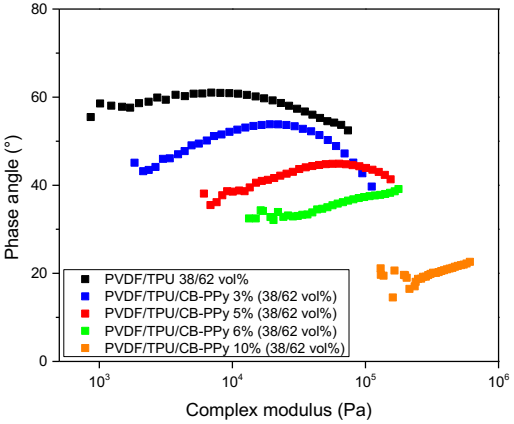

(b)

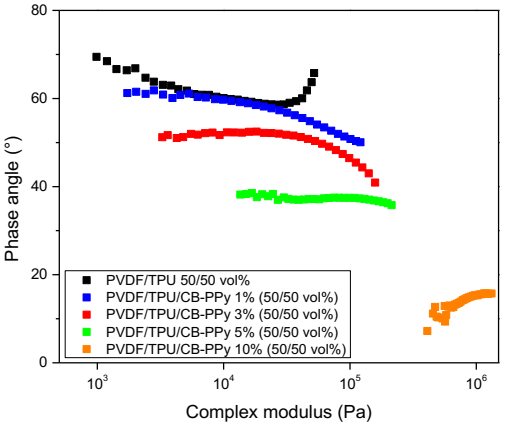

Figure 5-6: Phase angles vs. complex modulus for (a) PVDF/TPU/CB-PPy 38/62 vol% and (b) PVDF/TPU/CB-PPy 50/50 vol% conductive composites with different amounts of filler.

5.2.2 Piezoresistive behavior

The piezoresistive behavior of the compression molded PVDF/TPU/CB-PPy 38/62 vol% and 50/50 vol% composites comprising various amount of CB-PPy was evaluated by the electromechanical analysis where a compressive pressure was applied to the samples while their electrical conductivity was measured. Initially, a compressive pressure of 2.28 MPa at 3.4 $MPa.min^{-1}$ was applied to the samples and then the pressure was released at the same rate during five loading-unloading cycles.

For the composites with PVDF/TPU 38/62 vol% as matrix, the samples comprising 3%, 5%, 6%, 7%, 10% and 15% of CB-PPy were investigated. The results indicated that the polymer matrix PVDF/TPU and the composite with 3% of CB-PPy did not manifest a piezoresistive response because of the low amount of conductive filler that was not enough to increase the electrical conductivity of the material during the application of the compressive pressure. On the other hand, as expected, composites with CB-PPy content close to the electrical percolation threshold, i.e. 5% and 6%, displayed a better electromechanical responses. Figure 5-7 shows the curves of compression stress and relative electrical resistance ($\Delta R/R_0$) as a function of time for composites prepared by compression molding. It is possible to observe that the application of a compressive pressure has a significant effect on the samples electrical resistivity. When increasing the applied compressive stress, $\Delta R/R_0$ substantially decreases due to the reduction in the distance between the conductive particles in the polymer matrix during the application of the compressive stress, increasing the electrical conductivity of the composites probably because of the tunneling resistance mechanism and the creation of new conductive paths in the polymer matrix. Moreover, when the compressive pressure is released, the electrical resistivity of the materials returns to its initial value. This behavior demonstrate the sensitivity of the material to the applied pressure in terms of piezoresistive response.

Furthermore, the samples comprising 7%, 10% and 15% of conductive filler did not show a significant change in their electrical resistivity due to the high amount of filler that already have formed a conductive network in the PVDF/TPU 38/62 vol% matrix even before the application of the compressive stress.

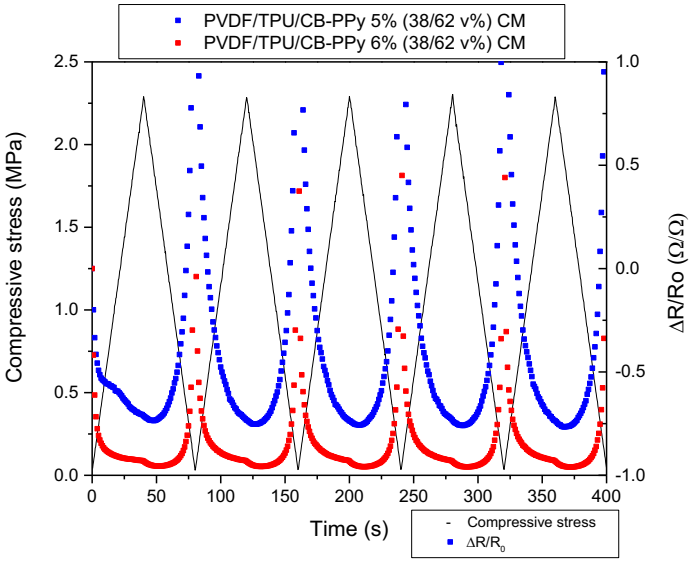

Figure 5-7: Piezoresistive response of compression molded PVDF/TPU/CB-PPy 38/62 vol% with 5% and 6% of conductive filler under five loading-unloading cycles.

The PVDF/TPU/CB-PPy 50/50 vol% composites with 1%, 2%, 3%, 5%, 6% and 10% of the conductive filler CB-PPy prepared by compression molding were also investigated. As expected, the matrix PVDF/TPU 50/50 vol% and the composites with 1% and 2% of CB-PPy did not show any piezoresistive response due to the low filler content that was not able to create a conductive path in the PVDF/TPU matrix even after the application of the compressive stress. On the other hand, composites with 3%, 5% and 6% of CB-PPy display a change in their electrical resistivity with the application of the compressive pressure and their electromechanical responses are reported in Figure 5-8. For all the three composites, the $\Delta R/R_0$ decreases when the compressive stress is increased, however, the composite with 3% presented an electromechanical response lower than that of the composite with 5% of CB-PPy. Moreover, the composite with 6% did not show a reproducible response during further tests.

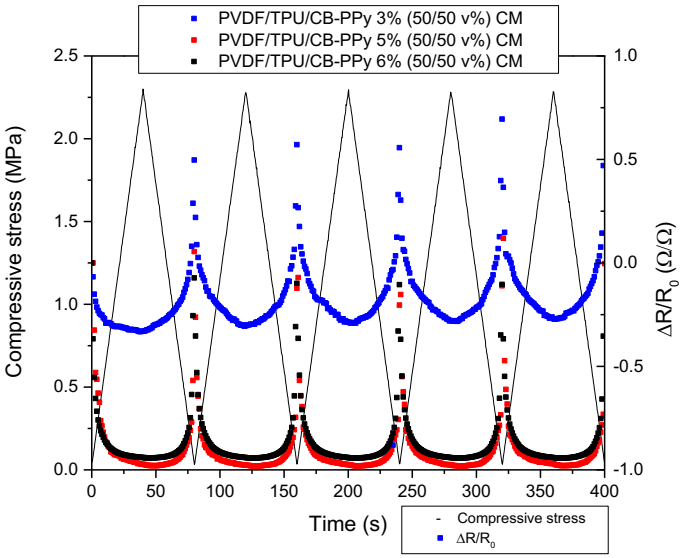

Figure 5-8: Piezoresistive response of compression molded PVDF/TPU/CB-PPy 50/50 vol% with 3%, 5% and 6% of conductive filler under five loading-unloading cycles.

Additionally, to investigate the reproducibility of the piezoresistive responses, 100 loading-unloading cycles were performed for PVDF/TPU/CB-PPy 38/62 vol% compression molded composites containing 5% and 6% of conductive filler and PVDF/TPU/CB-PPy 50/50 vol% composite with 5% of conductive filler.

For the PVDF/TPU/CB-PPy 38/62 vol% composites, the composite with 5% of CB-PPy displayed diminished piezoresistive response over the 100 cycles thus indicating that the piezoresistive response was not reproducible. On the other hand, the composite with 6% of CB-PPy show reproducible piezoresistive response along 100 loading-unloading cycles although some degree of hysteresis is present as shown in Figure 5-9 (a) that displays the compressive stress-strain curves for the cycles 1 to 10, 40 to 50 and 90 and 100 for the composite PVDF/TPU/CB-PPy 38/62 vol% with 6% of filler illustrating the hysteresis effect during 100 cycles. Although for the first 10 cycles the hysteresis effect is very small, when comparing to 40 to 50 and 90 to 100

cycles some variation of the hysteresis loops can be noticed. This behavior can be explained by the occurrence of an irreversible phenomena, such as plastic deformation in the PVDF/TPU polymer matrix. According to Zheng et. al (2020), the hysteresis effect in stretchable sensors is mainly assigned to the viscoelastic behavior of polymers and the interactions between them and nanofillers [54]. In fact, during the first 10 cycles the piezoresistive response is not significantly affect by increasing the number of cycles due to a reversible organization of the conductive path formed by the conductive filler. In addition, Figure 5-9 (c) shows that the piezoresistive response slightly change for the 90 to 100 loading-unloading cycles indicating some degree of plastic deformation of the PVDF/TPU 38/62 vol% matrix.

(a)

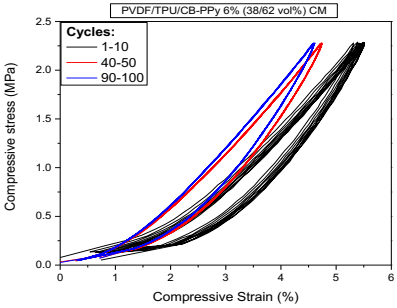

(b)

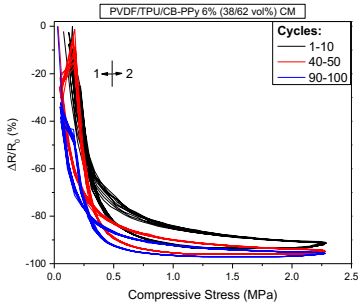

(c)

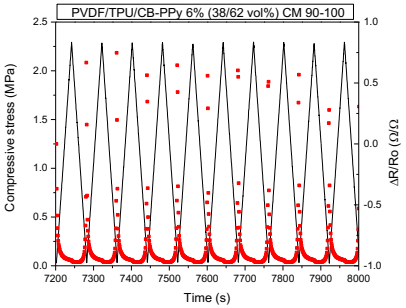

Figure 5-9: (a) Compressive stress-strain curves, (b) relative electrical resistance ($\Delta R/R_0$) as a function of compressive stress and (c) compressive stress and relative electrical resistance ($\Delta R/R_0$) as a function of time for 90 to 100 cycles for PVDF/TPU/CB-PPy 6% (38/62 vol%) compression molded.

Furthermore, the reproducibility of the composite PVDF/TPU/CB-PPy 50/50 vol% comprising 5% of CB-PPy was also investigated under 100 loading-unloading cycles. The composite presented a reproducible response, however, a hysteresis effect can be also observed under the 100 cycles. Figure 5-10 (a) presents the compressive stress as function of compressive strain for the cycles 1 to 10, 40 to 50 and 90 and 100 for the composite PVDF/TPU/CB-PPy 50/50 vol% with 5% of CB-PPy where is possible to notice that the hysteresis effect is not very pronounced for the first 50 cycles, however, when comparing to the 90 to 100 cycles, the hysteresis effect increases significantly. As explained before, this behavior can be assigned to the viscoelasticity and plastic deformation of the polymer matrix and its interaction with the conductive filler. Although some hysteresis is present, Figure 5-10 (c) shows that the piezoresistive response is constant.

(a)

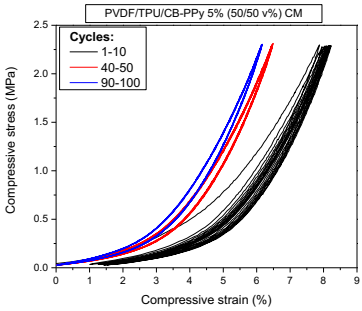

(b)

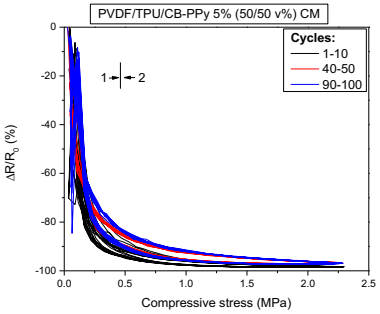

(c)

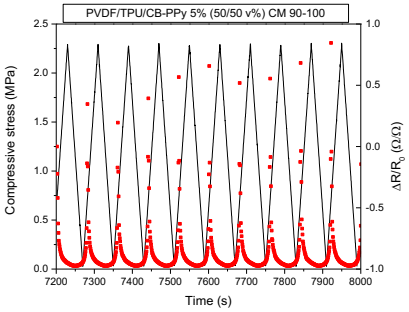

Figure 5-10: (a) Compressive stress-strain curves, (b) relative electrical resistance ($\Delta R/R_0$) as a function of compressive stress and (c) compressive stress and relative electrical resistance ($\Delta R/R_0$) as a function of time for 90 to 100 cycles for PVDF/TPU/CB-PPy 5% (50/50 vol%) compression molded.

Furthermore, the pressure sensitivity, which is the ability of sensor to convert the external applied pressure into electrical signals, was calculated for the composites PVDF/TPU/CB-PPy 6% (38/62 vol%) and PVDF/TPU/CB-PPy 5% (50/50 vol%). It was calculated as the slope of the curve of the relative electrical resistance ($\Delta R/R_0$) as a function of compressive stress represented in Figure 5-9 (b) and Figure 5-10 (b), where the two regions corresponding to different sensitivities are identified [64-66, 68, 114].

For the composite PVDF/TPU/CB-PPy 6% (38/62 vol%), the pressure sensitivity of the first region, from 0 to 0.5 MPa, and of the second region, from 0.5 to 2 MPa, were 1.71 MPa^{-1} and 0.083 MPa^{-1}, respectively, as shown in Figure 5-11. On the other hand, the sensitivity of the first region for the composite PVDF/TPU/CB-PPy 5% (50/50 vol%) was 1.74 MPa^{-1} and of the second region was 0.042 MPa^{-1}, as shown in Figure 5-12.

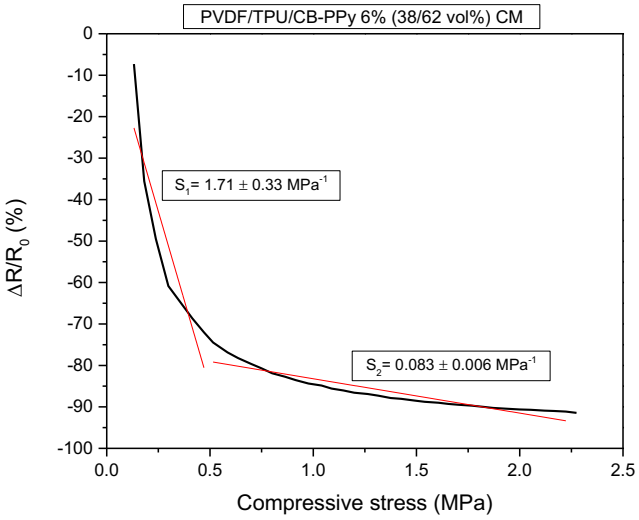

Figure 5-11: Representation of the sensitivity calculation from the curve of relative electrical resistance ($\Delta R/R_0$) as a function of compressive stress for the compression molded composite PVDF/TPU/CB-PPy 6% (38/62 vol%).

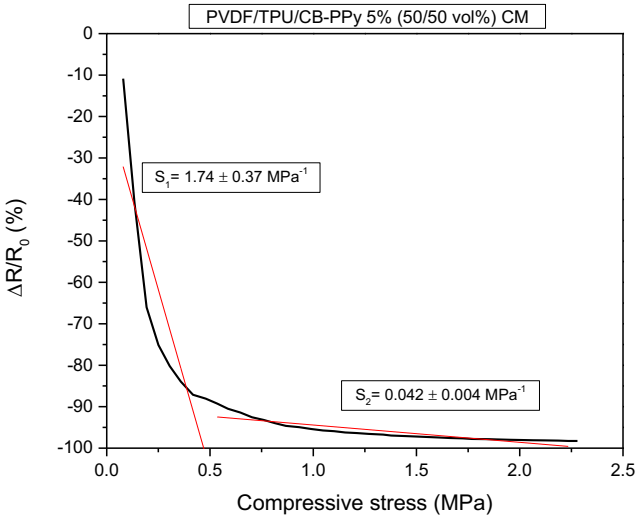

Figure 5-12: Representation of the sensitivity calculation from the curve of relative electrical resistance ($\Delta R/R_0$) as a function of compressive stress for the compression molded composite PVDF/TPU/CB-PPy 5% (50/50 vol%).

Another parameter used to evaluate the performance of piezoresistive pressure sensors is the gauge factor (GF). The GF assesses the materials response in relation to its deformation and ca be calculated by the slope of the curves of the relative electrical resistance ($\Delta R/R_0$) as function of the strain [1, 2, 7, 9, 15, 54, 64-68]. Two regions corresponding to different values of GF were identified, which were found to be 35.92 and 4.55 for PVDF/TPU/CB-PPy 6% (38/62 vol%) compression molded composites, see Figure 5-13, and 28.34 and 2.90 for the composite PVDF/TPU/CB-PPy 5% (50/50 vol%), see Figure 5-14. A large range of GF, varying from 0.35 to hundreds, are mentioned in the literature for stretchable polymer-based sensors and its depends on the matrices and fillers [2]. In this work, the calculated values of sensitivity and gauge factor were comparable to others piezoresistive sensors already studied [64-68].

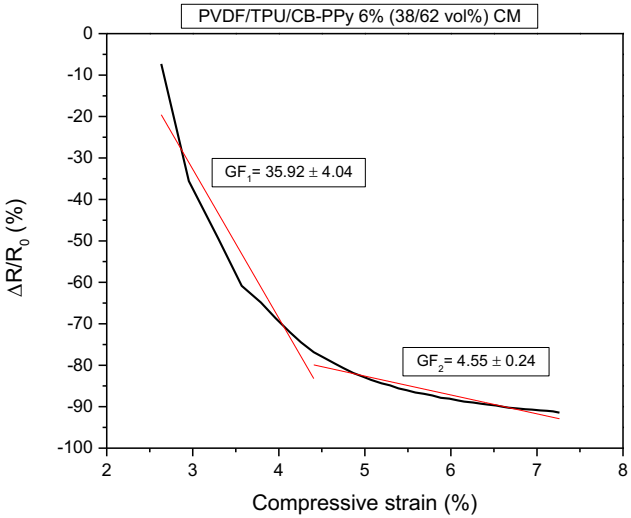

Figure 5-13: Representation of gauge factor calculation from the curve of relative electrical resistance ($\Delta R/R_0$) as a function of compressive strain for the compression molded composite PVDF/TPU/CB-PPy 6% (38/62 vol%).

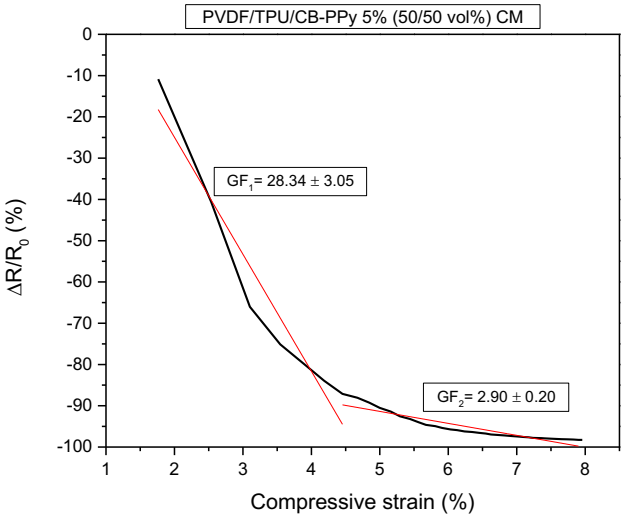

Figure 5-14: Representation of gauge factor calculation from the curve of relative electrical resistance ($\Delta R/R_0$) as a function of compressive strain for the compression molded composite PVDF/TPU/CB-PPy 5% (50/50 vol%).

5.2 PVDF/TPU/CB-PPy composites prepared by fused filament fabrication (FFF)

Some composites selected in Chapter IV, on the basis of their electrical conductivity and mechanical behavior, were prepared by fused filament fabrication (FFF) and their electromechanical response is presented in this section. The composition of the investigated 3D printed samples is described in Table 5-5.

Table 5-5: Composition of 3D printed PVDF/TPU/CB-PPy 38/62 vol% and 50/50 vol% composites.

PVDF/TPU 38/62 vol%	PVDF/TPU 50/50 vol%
% CB-PPy	% CB-Ppy
0	-
5	-
6	-
-	10

5.2.2 Piezoresistive behavior

The electromechanical behavior of the composites mentioned above was initially investigated applying a compressive stress of 2.28 MPa at 3.4 MPa.min^{-1} under five loading-unloading cycles. As expected, the matrix PVDF/TPU 38/62 vol% did not show a piezoresistive response under the application of the compressive stress. On the other hand, the composites of PVDF/TPU 38/62 vol% with 5% and 6% of CB-PPy have their curves of the relative electrical resistance ($\Delta R/R_0$) as a function of compressive stress and time displayed in Figure 5-15. Both composites presented a change in their electrical resistivity when the compressive pressure is applied. The application of the compressive pressure leads to the reduction of the electrical resistivity, in other words, an increase in the electrical conductivity of the composite probably related to the creation of new electrically conductive paths in the PVDF/TPU matrix as the distance between the CB-PPy is smaller. Then, when the compressive stress is release, the electrical resistivity of the samples returns to its initial value. Moreover, it can be noticed the piezoresistive responses of the 3D printed PVDF/TPU/CB-PPy 38/62 vol% samples comprising 5% and 6 wt% of CB-PPy were similar to the responses of the same materials prepared by compression molding.

For the samples composed of PVDF/TPU/CB-PPy 50/50 vol% with 10% of conductive filler, non-significant piezoresistive responses were observed due to the

fact that the high amount of filler, that were already close enough to create the electrical conductive paths even before the application of the compressive pressure, was not able to increase de electrical conductivity of the material.

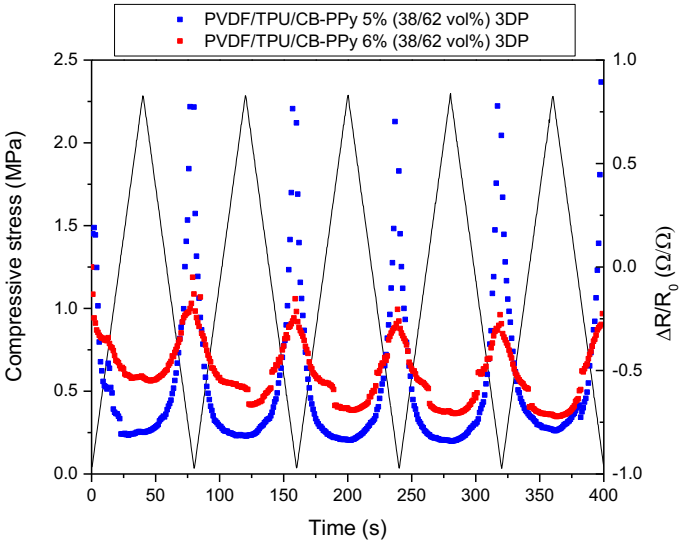

Figure 5-15: Piezoresistive response of 3D printed PVDF/TPU/CB-PPy 38/62 vol% with 5% and 6 % of conductive filler under five loading-unloading cycles.

In addition, the 3D printed samples composed of PVDF/TPU/CB-PPy 38/62 vol% with 5% and 6% of CB-PPy were further investigated under 100 loading-unloading cycles to evaluate the reproducibility of the piezoresistive responses.

The composite comprising 5% of CB-PPy did not show reproducible responses during the 100 applied cycles. On the other hand, the samples composed of PVDF/TPU/CB-PPy 38/62 vol% with 6% of conductive filler presented a reproducible piezoresistive response under the 100 loading-unloading cycles although some degree of hysteresis can be observed. Figure 5-16 (a) shows the curves of compressive stress as a function of compressive strain for the cycles 1 to 10, 40 to 50

and 90 to 100 and Figure 5-16 (c) displays the variation of the relative electrical resistance ($\Delta R/R_0$) with the of compressive stress and time for the last 10 cycles (90 to 100).

(a)

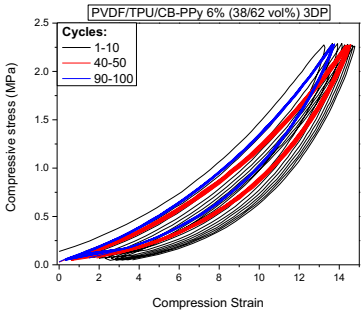

(b)

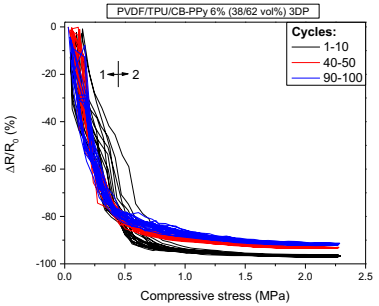

(c)

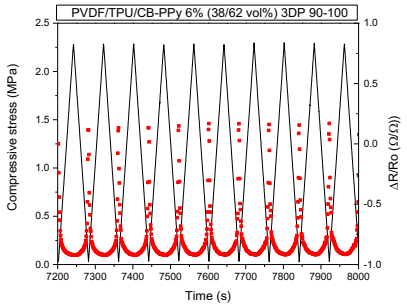

Figure 5-16: (a) Compressive stress-strain curves, (b) relative electrical resistance ($\Delta R/R_0$) as a function of compressive strain and (c) compressive stress and relative electrical resistance ($\Delta R/R_0$) as a function of time for 90 to 100 cycles for PVDF/TPU/CB-PPy 6% (38/62 vol%) 3D printed.

Moreover, the pressure sensitivity was also calculated for the composite PVDF/TPU/CB-PPy 6% (38/62 vol%) prepared by FFF and two regions corresponding to different sensitivities are observed as shown in Figure 5-16 (b). The first region from 0 to 0.5 MPa displays a pressure sensitivity of 1.50 MPa^{-1}, while the second region from 0.5 to 2 MPa shows a pressure sensitivity of 0.048 MPa^{-1} as presented in Figure 5-17.

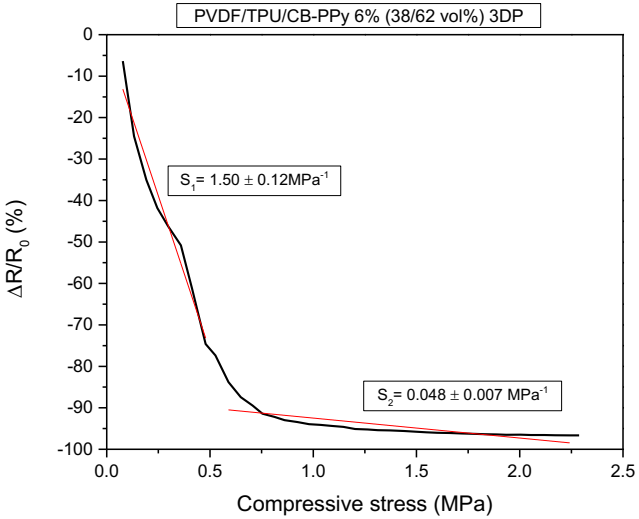

Figure 5-17: Representation of the sensitivity calculation from the curve of relative electrical resistance ($\Delta R/R_0$) as a function of compressive stress for the 3D printed composite PVDF/TPU/CB-PPy 6% (38/62 vol%).

Two regions with different gauge factors were also detected for the composite PVDF/TPU/CB-PPy 6% (38/62 vol%) prepared by FFF. The GF calculated from the slope of the curve of relative electrical resistance ($\Delta R/R_0$) as a function of compressive strain, see Figure 5-18, was found to be 13.81 for the first region and 0.80 for the second region. The sensitivity and gauge factor calculated for the composites PVDF/TPU/CB-PPy 38/62 vol% with 6% of CB-PPy prepared for both

manufacturing methods, compression molding and fused filament fabrication, are comparable to many other piezoresistive sensors [64-68]. Overall, the flexible polymer composites prepared by both methods demonstrate high sensitivity and gauge factor, large pressure range and stable behavior.

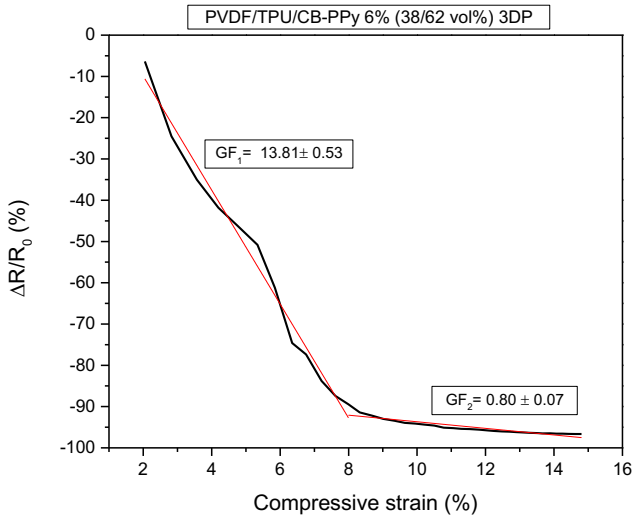

Figure 5-18: Representation of gauge factor calculation from the curve of relative electrical resistance ($\Delta R/R_0$) as a function of compressive strain for the 3D printed composite PVDF/TPU/CB-PPy 6% (38/62 vol%).

5.3 Conclusions

In this chapter, the main results on piezoresistive flexible pressure sensors composed of PVDF/TPU/CB-PPy obtained by compression molding and fused filament fabrication are presented. The rheological measurements show that the storage modulus (G') and the complex viscosity (η*) of the composites increase while the phase angle decreases with the addition of CB-PPy, thus indicating that the

material is becoming more rigid with the addition of filler due to the creation of a 3D network. The rheological percolation threshold was found to be 3% and 1% for PVDF/TPU/CB-PPy 38/62 vol% and 50/50 vol% composites, respectively. This means that the composites with higher content of conductive filler display G' higher than G" presenting a solid-like behavior and suggesting that the addition of higher amount of conductive filler could compromise the processability of the composites. On the other hand, PVDF/TPU/CB-PPy 38/62 vol% and 50/50 vol% composites presented electrical percolation thresholds of 5% and 2%, respectively. The rheological percolation threshold is lower than the electrical percolation threshold indicates that the critical amount of filler to restrict the chain mobility of the polymeric matrix is lower than the content of filler necessary to create a conductive network since the particles has to become closer to create electrical conductive paths.

Moreover, the compression molded and 3D printed composites of PVDF/TPU/CB-PPy 38/62 vol% with 5% and 6% of CB-PPy exhibited good piezoresistive response. On the other hand, the compression molded composites of PVDF/TPU/CB-PPy 50/50 vol% with 3%, 5% and 6% show piezoresistive response. However, the response were better for the samples with 5% and 6% of CB-PPy. In fact, composites with conductive filler content close to the electrical percolation threshold are expected to have a better electromechanical response. However, only the compression molded and 3D printed composites PVDF/TPU/CB-PPy 38/62 vol% with 6% of CB-PPy and the compression molded PVDF/TPU/CB-PPy 50/50 vol% with 5% of CB-PPy showed high sensitivity and gauge factor values, large pressure range and reproducible piezoresistive responses under 100 cycles. In summary, the results suggest that the compression molding and fused filament fabrication are promising techniques for the fabrication of piezoresistive flexible sensors based on PVDF/TPU/CB-PPy composites.

Chapter VI

6. Investigation of piezoelectric properties of poly(vinylidene fluoride)/thermoplastic polyurethane composites comprising carbon black-polypyrrole

Part of this chapter has been published in:

Mayara C. Bertolini, Nico Zamperlin, Guilherme M. O. Barra, Alessandro Pegoretti

"Development of poly(vinylidene fluoride)/thermoplastic polyurethane/carbon black-polypyrrole composites with enhanced piezoelectric properties". In preparation.

6.1 Introduction

This chapter proposes the piezoelectric properties investigation of the previously produced composites of poly(vinylidene fluoride)/thermoplastic polyurethane filled with carbon black doped with polypyrrole.

Piezoelectric responses are based on the production of electrical potential variations as response to an external stress. With the application of a force, the electric dipole moments are separated and the two surfaces of the material became charged positively and negatively creating a piezopotential leading to the flow of the free electrons through the external circuit to reach a balanced state again [7, 53, 55, 57].

In this framework, piezoelectric polymers have getting attention for developing piezoelectric sensors due to its physical and chemical properties and higher flexibility than the commonly used ceramics [7, 72]. PVDF is well known for its piezoelectric properties. Combining the piezoelectric properties of PVDF and elastomeric properties of TPU is an interesting strategy to prepare high flexible polymer composites that can be used as piezoelectric pressure sensors [57, 76].

The main challenge in achieving high piezoelectric responses for PVDF is the achievement of the β phase, which is the polar phase responsible for its piezoelectric properties. Some of the studied strategies for improving the β phase content are the addition of nanofilers [53, 79, 93], polymer blending [91, 92], hot pressing [83] and 3D printing [95].

As mentioned in the previous chapters, studies show that PVDF/TPU blends are an efficient way to prepare materials with excellent combination of mechanical and pyroelectric/piezoelectric properties and flexibility [32, 75, 76], however, to our best knowledge, there is no studies concerning the development of materials filaments comprising polymer blends of PVDF/TPU and conductive filler.

In this chapter, the previous fabricated and characterized composites of PVDF/TPU 38/62 vol% and PVDF/TPU 50/50 vol% with different fractions of CB-PPy are further tested to evaluate the PVDF phase transformation and the PVDF piezoelectric responses are investigated.

6.2 Fourier transform infrared (FTIR)

Fourier transform infrared (FTIR) was employed to investigate the chemical structure and interactions between PVDF and TPU. Also, to evaluate the crystalline phases of PVDF and the influence of processing and materials composition in PVDF β phase.

FTIR spectra of neat PVDF, neat TPU and blends composed of PVDF/TPU 38/62 vol% and PVDF/TPU 50/50 vol% prepared by compression molding are shown in Figure 6-1 (a) and a zoom at the region 1750-650 cm^{-1} of the FTIR spectra is show in Figure 6-1(b).

In the FTIR spectrum of neat TPU the band at 3301 cm^{-1} is correlated to the hydrogen-bonded N-H stretching while those at 2971 and 2915 cm^{-1} are related to symmetric and asymmetric axial deformation of aliphatic CH_2. The bands at 1728 and 1702 cm^{-1} correspond to the free carbonyl stretching vibration and hydrogen bonded carbonyl groups, respectively [2, 25, 32]. Besides, the peak at 1529 cm^{-1} is associated to C-N stretching, at 1309 cm^{-1} to N-H bending, while the bands at 1222 and 1978 cm^{-1} are assigned to aliphatic C-O stretching and C-O-C bond [32].

Regarding to the PVDF spectrum, the bands at 870 and 1402 cm^{-1} are related to C-F stretching vibration and the band at 1177 cm^{-1} is attributed to C-C bond [69, 76]. The peak at 762 cm^{-1} corresponds to the CH_2 in-plane bending and the peaks at 795 and 974 cm^{-1} are attributed to CH_2 rocking and CH_2 twisting, respectively [2]. Furthermore, the peaks appearing at 762, 795, 854, 974 and 1424 cm^{-1} are characteristic of the PVDF α phase [2, 32, 73, 81, 84-86], while the peaks at 840, 1073 and 1278 cm^{-1} are associated to the β phase [69, 73, 76, 83-85].

The FTIR spectra for the blends PVDF/TPU 38/62 vol% and 50/50 vol% display the main band absorptions for both components since the phases of the blend are not mutually soluble or chemically bonded.

(a)

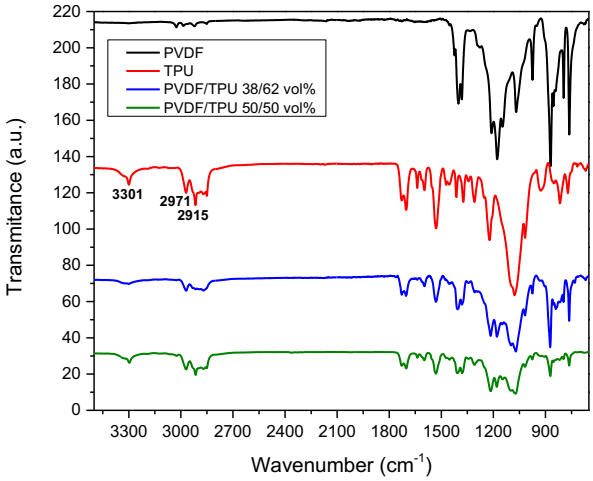

(b)

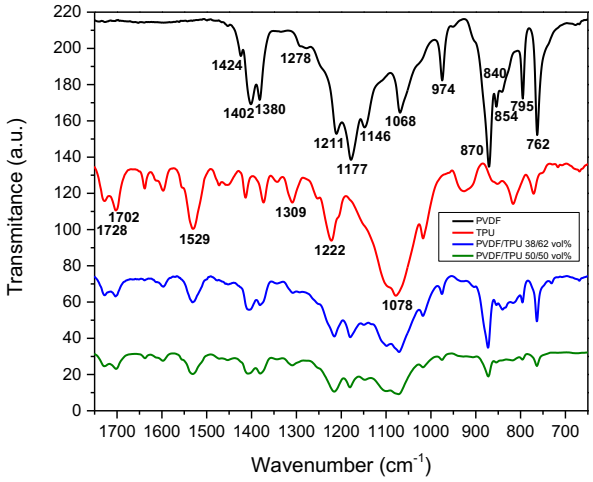

Figure 6-1: (a) FTIR spectra of PVDF, TPU, PVDF/TPU 38/62 vol% and PVDF/TPU 50/50 vol% and (b) zoom in the FTIR spectra at the region of 1750-650 cm^{-1}.

In addition, Equation 14 is used to quantify the content of PVDF β phase in the analyzed samples considering the absorption intensity at 762 and 840 cm^{-1} characteristics of α and β phases, respectively [73, 76, 81, 84]:

$$F(\beta) = \frac{A_\beta}{(K_\beta/K_\alpha)A_\alpha + A_\beta} \times 100 \quad (14)$$

where F(β) is the β phase content, A_α and A_β are the absorbance intensities and K_α and K_β are the absorption coefficients at 762 cm^{-1} and 840 cm^{-1}, respectively, with values of $6.1x10^4$ $cm^2.mol^{-1}$ and $7x10^4$ $cm^2.mol^{-1}$ [73, 84]. The wavenumbers, absorbance values for the mentioned peaks and β phase content in neat PVDF and in the blends 38/62 vol% and 50/50 vol% are displayed in Table 6-1. According to the calculations, the β phase content for neat PVDF is 31%, while for the blend composed of PVDF/TPU 38/62 vol% the β phase quantity increases to 41% and for the blend of PVDF/TPU 50/50 vol% it increases to 33% supporting the idea that the polymer blending can assist the PVDF phase transformation as stated by some authors [91, 92, 115].

Table 6-1: Values of λ, A and F(β) for neat PVDF and the blends composed of PVDF/TPU 38/62 vol% and 50/50 vol%.

Sample	λ_α (cm^{-1})	λ_β (cm^{-1})	A_α	A_β	F(β)	F(β) %
PVDF	762	840	0.403	0.204	0.31	31
PVDF/TPU 38/62 vol%	762	840	0.115	0.092	0.41	41
PVDF/TPU 50/50 vol%	762	840	0.017	0.009	0.33	33

Furthermore, another investigated parameter was the influence of the processing technique in PVDF β phase transformation. Figure 6-2 shows the FTIR spectra for neat PVDF in the form of pellet, compression molded, extruded into

filament format and 3D printed. The F(β) % for the samples were also calculated from Equation 14 and the results are presented in Table 6-2. The band at 840 cm^{-1} appeared strongly for PVDF in the form of pellet, which shows a slight higher content of β phase (i.e. 42%) than the polymer after being submitted to the processing techniques. Moreover, there is no difference between compression molding and fused filament fabrication on the β phase content of PVDF, which was found to be 31% for compression molded samples and 32% for 3D printed specimens. Kim et al state that the β phase content can be diminished with heating processing techniques due to the thermal effect that can repolarize the crystalline phase of PVDF [85].

(a)

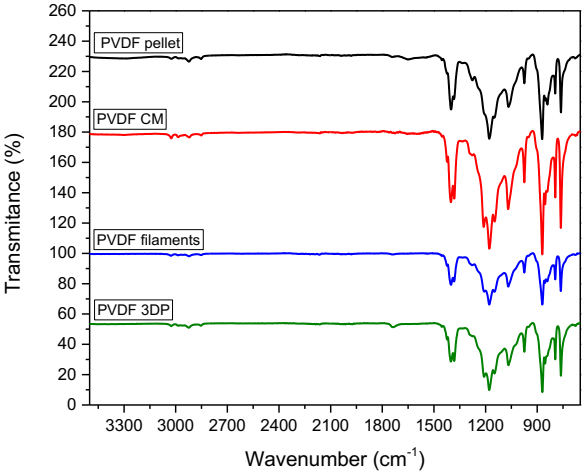

(b)

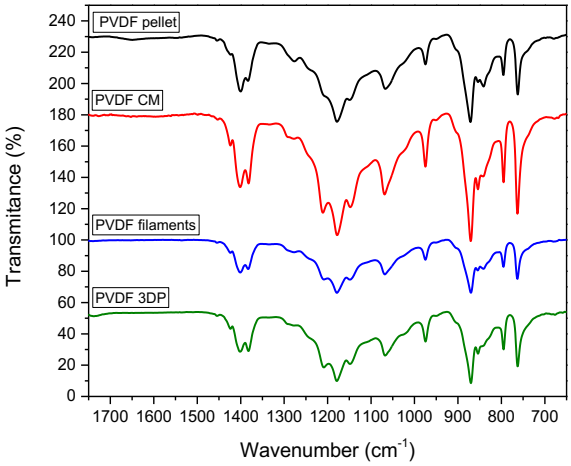

Figure 6-2: (a) FTIR spectra of neat PVDF in the form of pellet, compression molded, extruded into filament format and 3D printed and (b) zoom in the FTIR spectra at the region of 1750-650 cm^{-1}.

Table 6-2: Values of λ, A and F(β) for neat PVDF prepared by different processing techniques.

Sample	λ_α (cm^{-1})	λ_β (cm^{-1})	A_α	A_β	F(β)	F(β) %
PVDF pellet	762	840	0.200	0.165	0.42	42
PVDF CM	762	840	0.403	0.204	0.31	31
PVDF filament	763	841	0.101	0.072	0.38	38
PVDF 3DP	762	840	0.174	0.095	0.58	32

Additionally, FTIR measurements were carried out for PVDF/TPU/CB-PPy 38/62 vol% and 50/50 vol% composites comprising different amounts of CB-PPy to investigate the influence of the addition of filler in PVDF phase transformation. According to previous studies, one of the methods developed to improve the formation of PVDF β phase is the addition of fillers to PVDF composites [53, 77-79, 81, 82, 90, 94]. Wu et al. [90] claim that the addition of carbon black in PVDF composites assisted the formation of β phase due to the action of CB as nucleating agent.

Figure 6-3 and Figure 6-4 show the FTIR spectra of PVDF/TPU/CB-PPy 38/62 vol% and PVDF/TPU/CB-PPy 50/50 vol%, respectively, comprising various amount of CB-PPy. In addition, Table 6-3 and Table 6-4 present the content of β phase for the samples. It can be noticed from the spectra that the addition of high amount of CB-PPy induces an increase in the band at 840 cm^{-1} related to PVDF β phase that can be confirmed by the calculated F(β) %. Generally, the percentage of β phase increases with the addition CB-PPy, however, this effect is stronger in samples containing high concentration of filler (i.e. 6% or more). In fact, samples with 6% and 10% of CB-PPy show higher β phase content for both composites varying from 50% up to 61% of β phase endorsing the idea that the addition of the filler can assist the β phase transformation of PVDF.

(a)

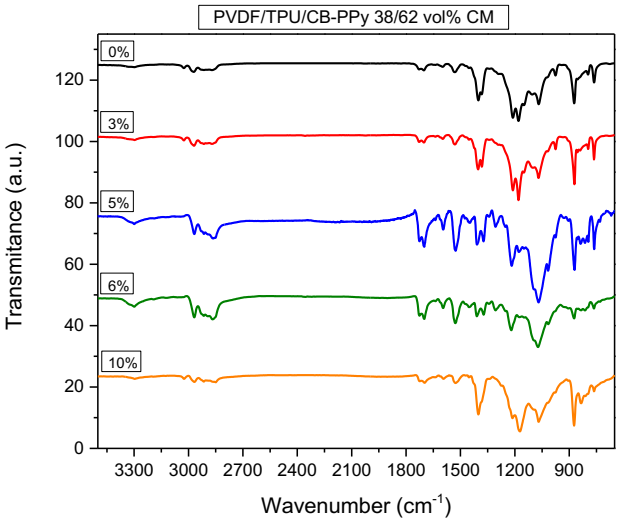

(b)

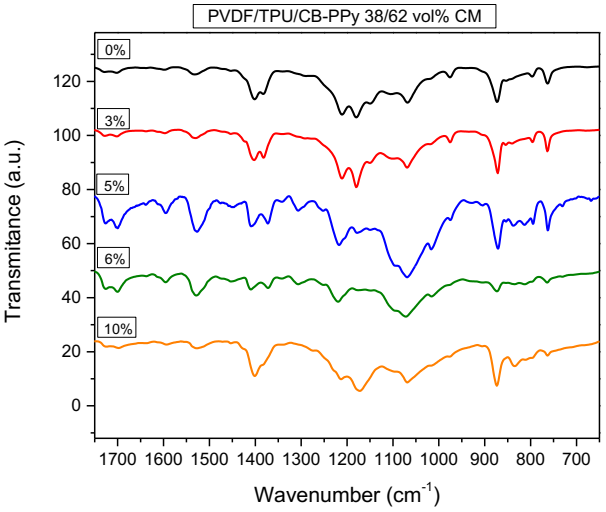

Figure 6-3: (a) FTIR spectra of PVDF/TPU/CB-PPy 38/62 vol% with different fractions of CB-PPy and (b) zoom in the FTIR spectra at the region of 1750-650 cm^{-1}.

(a)

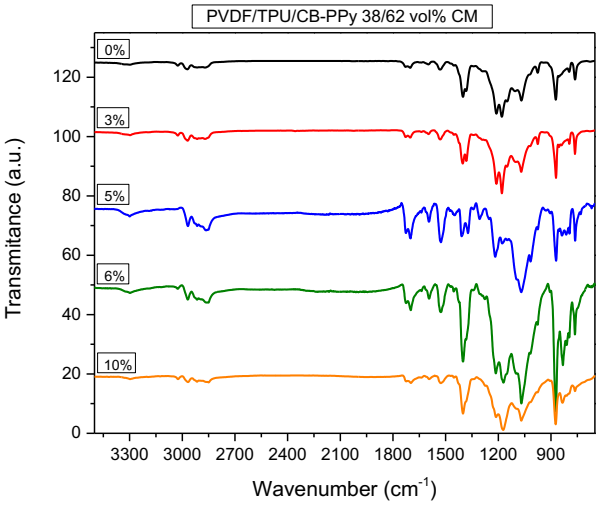

(b)

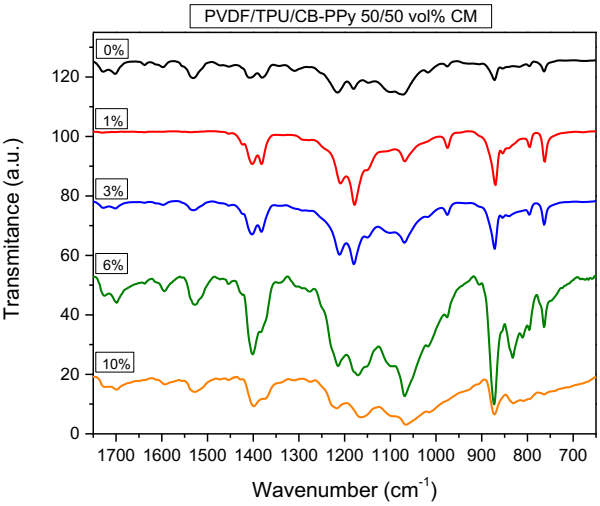

Figure 6-4: (a) FTIR spectra of PVDF/TPU/CB-PPy 50/50 vol% with different fractions of CB-PPy and (b) zoom in the FTIR spectra at the region of 1750-650 cm^{-1}.

Table 6-3: Values of λ, A and F(β) for PVDF/TPU/CB-PPy 38/62 vol% composites with different content of CB-PPy prepared by compression molding.

PVDF/TPU 38/62 vol%						
% CB-PPy	λ_α (cm^{-1})	λ_β (cm^{-1})	A_α	A_β	F(β)	F(β) %
0	762	840	0.115	0.092	0.41	41
3	763	840	0.029	0.023	0.41	41
5	762	837	0.163	0.152	0.45	45
6	764	835	0.018	0.021	0.50	50
10	763	835	0.023	0.042	0.61	61

Table 6-4: Values of λ, A and F(β) for PVDF/TPU/CB-PPy 50/50 vol% composites with different content of CB-PPy prepared by compression molding.

PVDF/TPU/ 50/50 vol%						
% CB-PPy	λ_α (cm^{-1})	λ_β (cm^{-1})	A_α	A_β	F(β)	F(β) %
0	763	840	0.017	0.010	0.33	33
1	762	841	0.047	0.026	0.32	32
3	763	840	0.023	0.013	0.32	32
6	764	840	0.237	0.289	0.52	52
10	764	833	0.027	0.040	0.57	57

Moreover, a comparison between the F(β)% values for samples prepared by compression molding and fused filament fabrication is displayed in Table 6-5. The results show that β phase content is lower for all samples prepared by FFF when compared to the compression molded composites with same composition. As explained before, it is related to the fact that the heating process can affect the polarization of the crystalline phase of PVDF reducing the content of β phase.

Table 6-5: Comparison of F(β)% values between PVDF/TPU/CB-PPy composites prepared by compression molding and fused filament fabrication.

PVDF/TPU 38/62 vol%		
% CB-PPy	F(β) % CM	F(β) % 3DP
0	41	37
5	45	43
6	50	43
PVDF/TPU 50/50 vol%		
% CB-PPy	F(β) % CM	F(β) % 3DP
10	57	49

6.3 X-ray diffraction (XRD)

The x-ray diffraction (XRD) measurements were performed on PVDF, TPU, PVDF/TPU 38/62 vol% and 50/50 vol% blends and PVDF/TPU/CB-PPy composites to evaluate the influence of the addition of TPU and CB-PPy to PVDF and the printing process on the PVDF crystalline phases. The XRD patterns for neat PVDF, neat TPU and their blends are shown in Figure 6-5. For neat TPU, the broad and diffuse peak at 20.5° is characteristic of a completely amorphous material and it is related to both hard and soft domains of TPU. On the other hand, neat PVDF displays a significant degree of crystallinity. The diffraction peaks at 17.7°, 18.4°, 20.0° and 26.6° corresponding to the (100), (020), (110) and (021) diffraction planes are generally associated to the nonpolar α phase of PVDF [8, 79, 81, 85]. The diffraction peak at 36.0 (200) corresponds to the β phase of PVDF [79, 85]. Studies show that the main characteristic peak of PVDF β phase is at 20.6° [76, 85], however, α, β and γ phases have an intense diffraction peak around 20° making it difficult to identify each other only by XRD patterns [77].

Moreover, as expected, the XRD pattern of PVDF/TPU 38/62 vol% and 50/50 vol% blends are a combination of the diffraction patterns of the two neat polymers. It seems that the diffraction peak at 18.4° corresponding to the α phase was

diminished for the PVDF/TPU blends while the peak at 36.0 related to β phase was slightly increased, which is in agreement to the FTIR results.

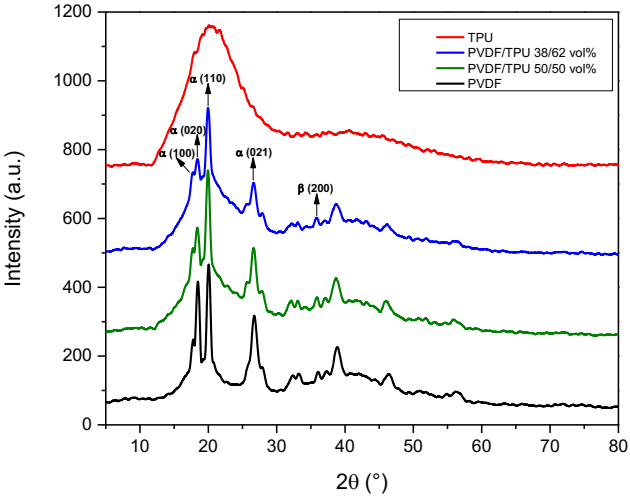

Figure 6-5: XRD patterns of neat PVDF, neat TPU and PVDF/TPU 38/62 vol% and 50/50 vol% blends.

Figure 6-6 and Figure 6-7 present the x-ray diffraction patterns for PVDF/TPU/CB-PPy 38/62 vol% and 50/50 vol% composites, respectively, prepared by compression molding. The XRD patterns are in agreement to the FTIR spectra for those composites where it is possible to observe that the addition of 3% and 5% of conductive filler slightly change the XRD patterns of the composites indicating that content of PVDF β is similar in those composites. However, when 6% and 10% of CB-PPy are added to the composites, more substantial changes can be observed on the XRD patterns demonstrating that the crystalline phases of PVDF are modified. For instance, by adding 6% and 10% of CB-PPy the peak at 17.7° related to α phase disappears for 38/62 and 50/50 vol% composites and the peak at 18.4° strongly decreases for PVDF/TPU/CB-PPy 50/50 vol% composites. Also, for PVDF/TPU/CB-

PPy 38/62 vol% the peak at 26.6° decreases for 6% composition and nearly disappear for 10% composition, while for PVDF/TPU/CB-PPy 50/50 vol% these peaks practically disappear for 6% and 10% compositions.

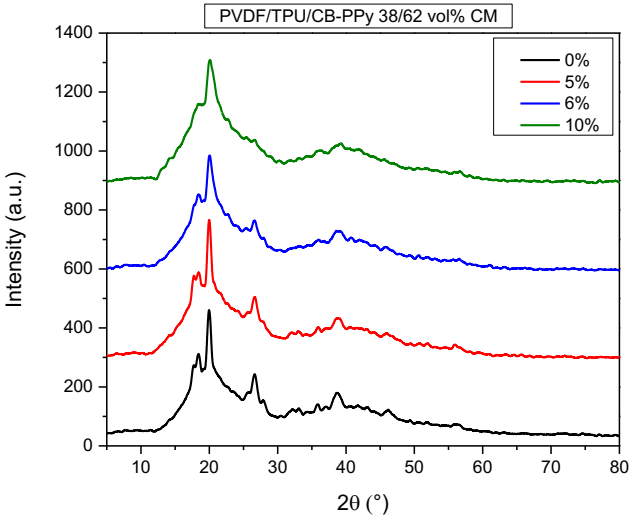

Figure 6-6: XRD patterns of PVDF/TPU/CB-PPy 38/62 vol% composites prepared by compression molding comprising different amount of filler.

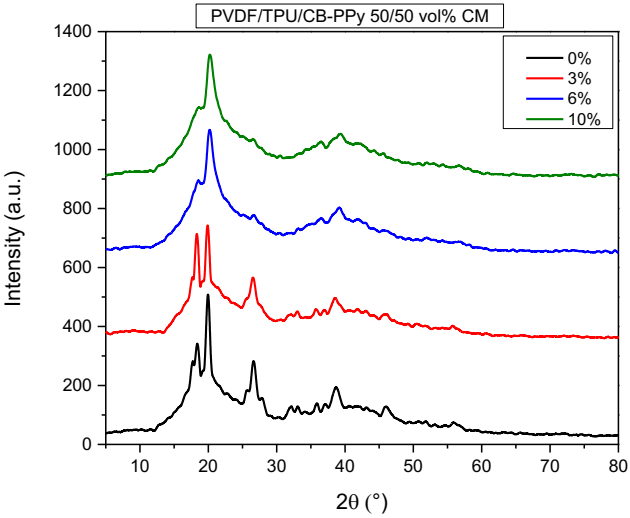

Figure 6-7: XRD patterns of PVDF/TPU/CB-PPy 50/50 vol% composites prepared by compression molding comprising different amount of filler.

The x-ray diffraction measurements were also carried out for the 3D printed specimens. Small changes in the XRD patterns can be observed for the 3D printed samples indicating that the crystalline phases of PVFD may be affected by the printing process.

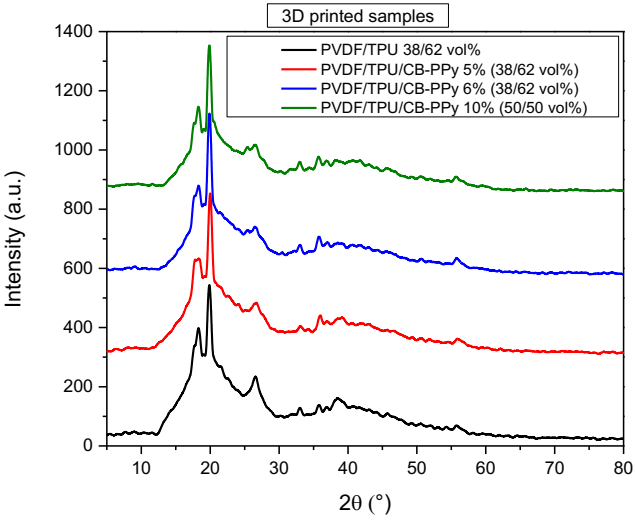

Figure 6-8: XRD patterns of PVDF/TPU 3D printed composites comprising different filler content prepared by fused filament fabrication.

6.4 Differential scanning calorimetry (DSC)

Differential scanning calorimetry (DSC) was performed to assess the melting temperature, T_m, of the specimens, the crystallinity of PVDF, the impact of blending it with TPU and the addition of the conductive filler CB-PPy on the PVDF crystallinity. The DSC results can be used to calculate the samples crystalline percentage (X_c) according to Equation 15:

$$X_c = \frac{\Delta H_m}{\Delta H_m^* \emptyset} \times 100\% \quad (15)$$

where ΔH_m is the melting enthalpy of the material obtained by the DSC analysis, ΔH_m^* is the melting enthalpy of the pure crystalline PVDF (104.5 $J.g^{-1}$ [32, 73, 86]) and Ø is the weight fraction of PVDF. The results are shown in Table 6-6.

Initially, the curves of heat flow as function of temperature for PVDF and the blends PVDF/TPU 38/62 vol% and 50/50 vol% are presented in Figure 6-9 and the calculation of ΔH_m from the crystalline peak and T_m values for the blends are presented in Figure 6-10. It is interesting to notice that blending PVDF with TPU increases the degree of crystallinity of the samples, thus indicating that adding TPU to the blends can assist the crystallization of PVDF chains corroborating with the results found in the FTIR analysis.

Moreover, the addition of TPU slightly decreases the melting temperature (T_m) of the mixtures because of the incompatibility between PVDF and TPU. In fact, the decrease in T_m is more noticeable in compatible blends or blends with increased compatibility. For instance, Bera et al claim that the melting temperature of PVDF reduces 27 °C in PVDF/PMMA 70/30 compatible blends, which is significantly greater than for PVDF/TPU 70/30 mixtures [32]. These results confirm the incompatibility between PVDF and TPU phases already described in Chapter IV.

Table 6-6: Values of melting temperature, melting enthalpy, PVDF weigh fraction and crystalline percentage of materials.

Sample	T_m (°C)	ΔH_m (J.g^{-1})	Ø	X_C (%)
PVDF	172.65	51.89	1	49.6
PVDF/TPU 38/62 vol%				
% CB-PPy	**T_m (°C)**	**ΔH_m (J.g^{-1})**	**Ø**	**X_C (%)**
0	170.18	35.00	0.5	67.0
3	168.57	29.96	0.485	59.1
5	169.22	30.61	0.475	61.7
10	166.61/172.26	28.58	0.45	60.8
PVDF/TPU 50/50 vol%				
% CB-PPy	**T_m (°C)**	**ΔH_m (J.g^{-1})**	**Ø**	**X_C (%)**
0	171.34	48.22	0.620	74.4
1	167.92	36.46	0.614	56.8
5	165.75/170.89	35.23	0.589	57.2
10	175.04	34.01	0.558	58.3

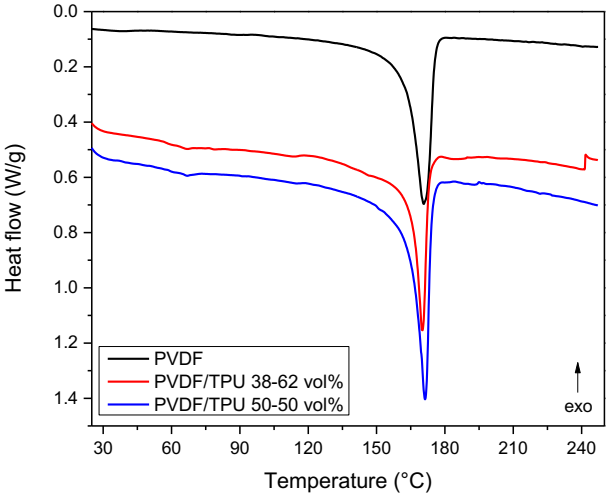

Figure 6-9: Heat flow as function of temperature for neat PVDF and PVDF/TPU 38/62 vol% and 50/50 vol% blends.

(a)

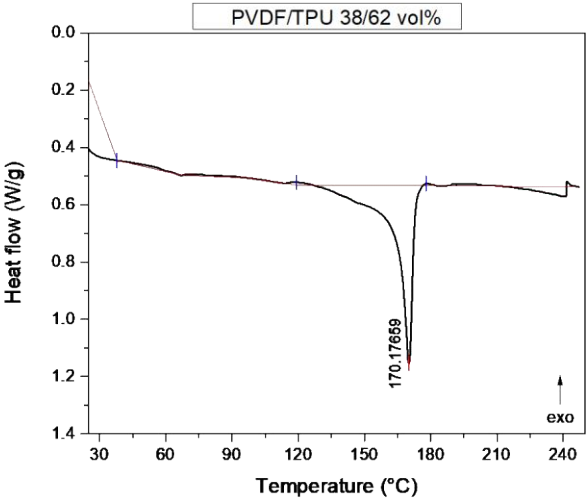

(b)

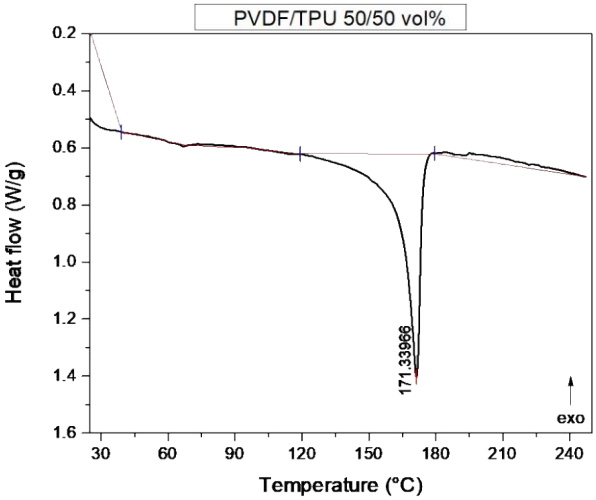

Figure 6-10: DSC curves showing the calculation of ΔH_m from the crystalline peak and T_m values for (a) PVDF/TPU 38/62 vol% and (b) PVDF/TPU 50/50 vol%.

Furthermore, DSC results for the PVDF/TPU/CB-PPy 38/62 vol% and 50/50 vol% composites are also presented in Table 6-6. The curves of heat flow as function of temperature for both composites comprising different amount of filler are shown in Figure 6-11 and Figure 6-13. In addition, the calculation of ΔH_m from the crystalline peak and T_m values for the blends are presented in Figure 6-12 and Figure 6-14.

Generally, the melting temperature and the degree of crystallinity of the specimens decrease with the addition of the conductive filler CB-PPy indicating that the conductive particles can hinder the crystallization of PVDF chains. Although the results from FTIR show that usually the percentage of β phase increases with the addition CB-PPy, the overall crystallinity of the samples decreases.

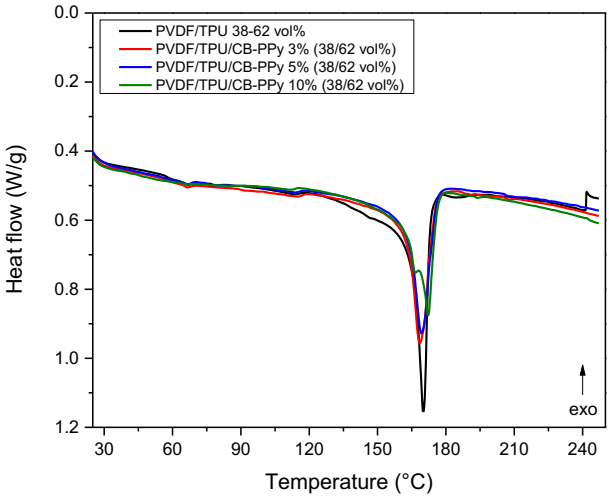

Figure 6-11: Heat flow as function of temperature for PVDF/TPU/CB-PPy 38/62 vol% composites with different filler content.

Additionally, the samples composed of PVDF/TPU/CB-PPy 38/62 vol% with 10% of CB-PPy and PVDF/TPU/CB-PPy 50/50 vol% with 5% of CB-PPy display

a double melting peak. It can be related to the formation of two distinct types of crystals, imperfect crystallites or melt recrystallization [116]. The samples with only a single melting peak can be associated to more homogeneous lamellae that melt simultaneously during the heating process.

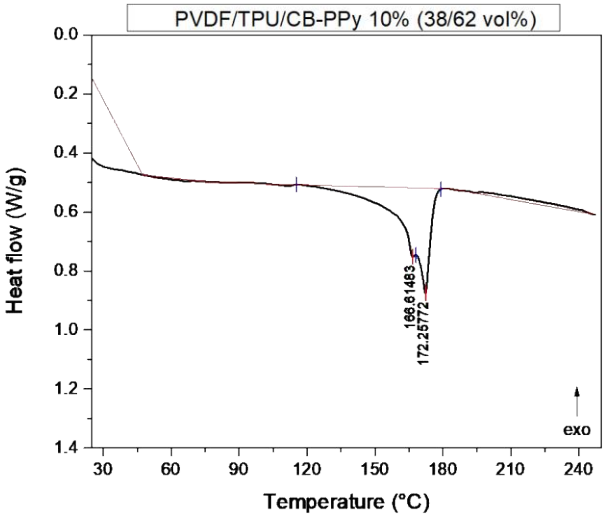

Figure 6-12: DSC curves showing the calculation of ΔH_m from the crystalline peak and T_m values for PVDF/TPU/CB-PPy 38/62 vol% with 10% of CB-PPy.

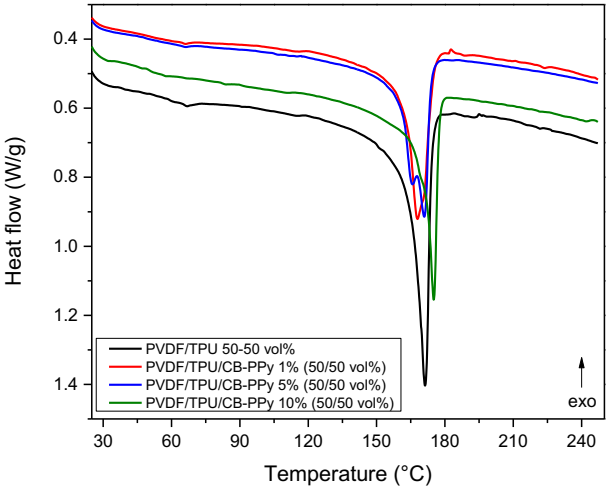

Figure 6-13: Heat flow as function of temperature for PVDF/TPU/CB-PPy 50/50 vol% composites with different filler content.

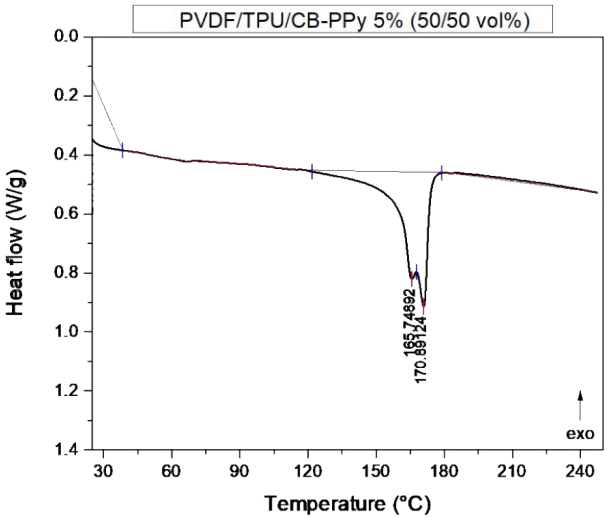

Figure 6-14: DSC curves showing the calculation of ΔH_m from the crystalline peak and T_m values for PVDF/TPU/CB-PPy 50/50 vol% with 5% of CB-PPy.

6.5 Piezoelectric d_{33} constant

The piezoelectric coefficient (d_{33}) is a measure of the electric response of the material to an applied force in units of charge per force [72, 86]. The piezoelectric coefficient was measured to evaluate the relationship between the β phase content in PVDF and its piezoelectricity. The measurements were performed for neat PVDF, neat TPU, PVDF/TPU 38/62 vol% and PVDF/TPU 50/50 vol% blends and PVDF/TPU/CB-PPy composites prepared by compression molding and fused filament fabrication. The samples were subjected to three different static forces: 1N, 2N and 4N to investigate the effect of the clamping force.

6.5.1 Samples prepared by compression molding

Figure 6-15 presents the d_{33} values for neat PVDF and neat TPU. As expected, PVDF shows better piezoelectric properties than TPU. In addition, the d_{33} values with the application of the static force of 1N, 2N and 4N are summarized in Table 6-7 for PVDF and PVDF/TPU/CB-PPy composites.

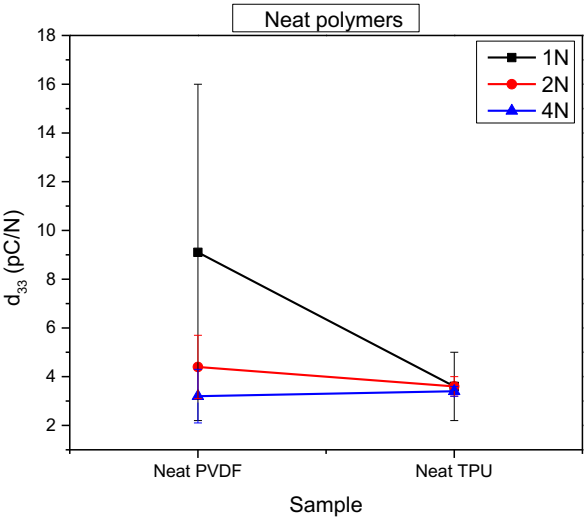

Figure 6-15: Piezoelectric coefficient (d_{33}) for neat polymers PVDF and TPU with applied static forces of 1N, 2N and 4N.

Table 6-7: Summary of the piezoelectric coefficient (d_{33}) for PVDF and PVDF/TPU/CB-PPy composites prepared by compression molding with applied static forces of 1N, 2N and 4N.

Sample	d_{33} (pC/N)		
	1N	2N	4N
PVDF	9.1 ± 6.9	4.4 ± 1.3	3.2 ± 1.1
PVDF/TPU 38/62 vol%			
% CB-PPy	**1N**	**2N**	**4N**
0	2.8 ± 0.7	2.7 ± 0.6	2.8 ± 0.5
3	3.5 ± 0.3	3.2 ± 0.1	3.2 ± 0.1
5	4.9 ± 2.2	3.3 ± 1.3	3 ± 0.7
6	3.5 ± 1.7	3.5 ± 0.6	3.7 ± 0.2
7	7.6 ± 2.9	4.8 ± 1.5	3.7 ± 0.6
10	16.9 ± 7.6	7.5 ± 2.4	5.1 ± 1.1
15	20.2 ± 3.4	10.7 ± 2	6.4 ± 0.7
PVDF/TPU 50/50 vol%			
% CB-PPy	**1N**	**2N**	**4N**
0	3 ± 0.8	3.1 ±0.3	3.1 ± 0.1
1	5.3 ± 2.1	3.9 ± 0.9	3.3 ± 0.3
2	3.7 ± 0.6	3.2 ± 0.1	3.1 ± 0.1
3	3.4 ± 0.6	3.3 ± 0.3	3.2 ± 0.1
5	3 ± 1.1	3.7 ± 1.4	3.3 ± 0.3
6	6 ± 2.9	3.7 ± 1.2	3.5 ± 0.4
10	12.2 ± 4.3	7 ± 1.9	5.1 ± 1.2

Figure 6-16 and Figure 6-17 display the d_{33} values for PVDF/TPU/CB-PPy 38/62 vol% and PVDF/TPU/CB-PPy 50/50 vol% composites, respectively. The results show that when the content of CB-PPy added to the PVDF/TPU matrices in higher amount than 6% for PVDF/TPU/CB-PPy 38/62 vol% and 5% for PVDF/TPU/CB-PPy 50/50 vol% some effect on the piezoelectric properties can be noticed. Although the piezoelectric response is commonly poor for the analyzed samples, when high

quantities of the conductive filler are added to the composites a visible improvement in the piezoelectric properties can be observed. In fact, the piezoelectric coefficient significantly increases when filler concentration overpasses the piezoelectric threshold value of 6% and 7% for PVDF/TPU/CB-PPy 38/62 vol% and 50/50 vol%, respectively. The highest values of d_{33} are achieved with the addition of 15 % of CB-PPy in 38/62 vol% composite and 10% of CB-Py in 50/50 vol% composite.

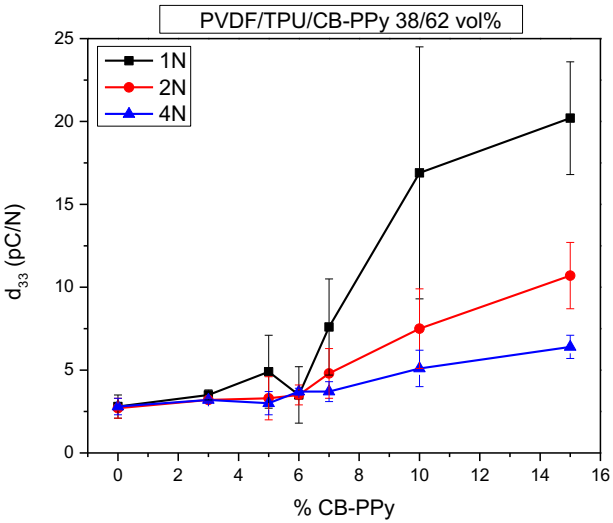

Figure 6-16: Piezoelectric coefficient (d_{33}) for PVDF/TPU/CB-PPy 38/62 vol% composites prepared by compression molding with applied static forces of 1N, 2N and 4N.

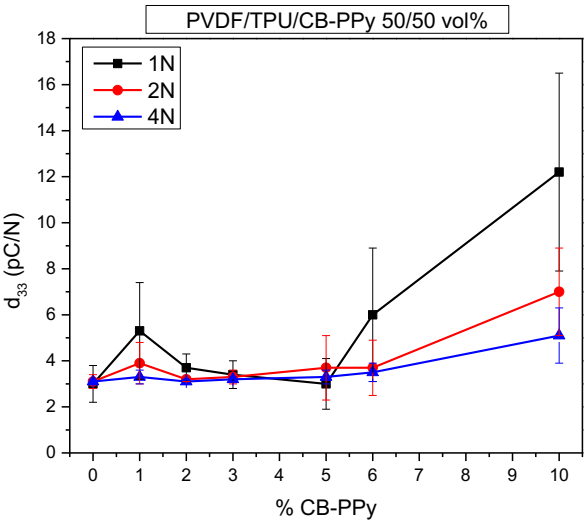

Figure 6-17: Piezoelectric coefficient (d_{33}) for PVDF/TPU/CB-PPy 50/50 vol% composites prepared by compression molding with applied static forces of 1N, 2N and 4N.

Additionally, it is interesting to notice that when the static clamping force is 1N the error bars are significantly large, which can be related to non-homogeneity of samples or to non-optimal clamping causing imprecisions during the measurements. When the clamping force is raised to 2N and 4N, the error bars are greatly reduced, however, when the static force is raised to 4N a flattening can be observed in the d_{33} curves. This can occur because the clamping force may be too high for soft polymers and thin samples causing high deformation. In order to reduce the error bars and to have stable measurements avoiding sample deformation in soft polymeric composites, the static clamping force should probably be between 1N and 2N.

Moreover, Table 6-8 shows a comparison between the F(β)% and the piezoelectric coefficient to evaluate the relationship between the β phase content in PVDF and its piezoelectricity. In general, the piezoelectric coefficient increased with the F(β)% for both composites, as expected. In fact, samples with more than 6% show

higher values of d_{33} and higher β phase content, indicating that the addition of high amount of conductive filler was capable of inducing the PVDF phase transformation.

Table 6-8: F(β)% and the piezoelectric coefficient d_{33} with 1N of static force for PVDF/TPU/CB-PPy composites prepared by compression molding.

PVDF/TPU 38/62 vol%		
% CB-PPy	**F(β) %**	**d_{33} (pC/N)**
0	41	2.8
3	41	3.5
6	50	3.5
10	61	16.9
PVDF/TPU 50/50 vol%		
% CB-PPy	**F(β) %**	**d_{33} (pC/N)**
0	33	3
3	32	3.4
6	52	6
10	57	12.2

6.5.2 Samples prepared by fused filament fabrication

The piezoelectric coefficient d_{33} was also measured for the samples prepared by fused filament fabrication (FFF) under 1N, 2N and 4N of static clamping force. The d_{33} values for PVDF and PVDF/TPU/CB-PPy composites are displayed in Figure 6-18 and summarized in Table 6-9. Overall, very low piezoelectric response was found for the 3D printed materials.

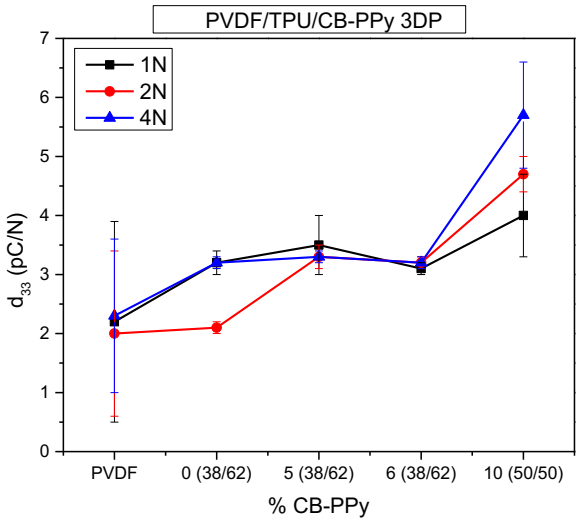

Figure 6-18: Piezoelectric coefficient (d_{33}) for PVDF and PVDF/TPU/CB-PPy composites prepared by fused filament fabrication with applied static forces of 1N, 2N and 4N.

Table 6-9: Summary of the piezoelectric coefficient (d_{33}) for PVDF and PVDF/TPU/CB-PPy composites prepared by fused filament fabrication with applied static forces of 1N, 2N and 4N.

3D printed samples	d_{33} (pC/N)		
	1N	2N	4N
PVDF	2.2 ± 1.7	2.0 ± 1.4	2.3 ± 1.3
PVDF/TPU 38/62 vol%			
% CB-PPy	1N	2N	4N
0	3.2 ± 0.2	3.2 ± 0.1	3.2 ± 0.1
5	3.5 ± 0.5	3.3 ± 0.2	3.3 ± 0.1
6	3.1 ± 0.1	3.2 ± 0.1	3.2 ± 0.1
PVDF/TPU 50/50 vol%			
% CB-PPy	1N	2N	4N
10	4 ± 0.7	4.7 ± 0.3	5.7 ± 0.9

Furthermore, a comparison between F(β)% and d_{33} values of compression molded and 3D printed samples is shown in Table 6-10. It can be seen that the fused filament fabrication process induces a reduction in β phase content and in the piezoelectric response of the materials when compared to compression molding samples. In addition, the content of conductive filler in 3D printed composites does not significantly affect the piezoelectric response of the materials. In fact, even samples with high amount of conductive filer (i.e. 6% and 10%) have not displayed an improvement in the d_{33} values.

The results confirm that the PVDF piezoelectric properties is related to its β phase. Also, the process of 3D printing affect directly the phase transformation of PVDF. In fact, the samples prepared by compression molding have presented higher amount of β phase and better piezoelectric responses.

Table 6-10: Comparison between F(β)% and the piezoelectric coefficient (d_{33}) of compression molded and 3D printed samples with static forces of 1N.

Sample	CM		3DP	
	F(β) %	d_{33} (pC/N)	F(β) %	d_{33} (pC/N)
PVDF	31	9.1 ± 6.9	32	2.2 ± 1.7
PVDF/TPU 38/62 vol%				
% CB-PPy	**F(β) %**	**d_{33} (pC/N)**	**F(β) %**	**d_{33} (pC/N)**
0	41	2.8 ± 0.7	37	3.2 ± 0.2
5	45	4.9 ± 2.2	43	3.5 ± 0.5
6	50	3.5 ± 1.7	43	3.1 ± 0.1
PVDF/TPU 50/50 vol%				
% CB-PPy	**F(β) %**	**d_{33} (pC/N)**	**F(β) %**	**d_{33} (pC/N)**
10	57	12.2 ± 4.3	49	4 ± 0.7

6.6 Conclusions

Piezoelectric responses of compression molded and 3D printed PVDF/TPU/CB-PPy composites were evaluated in this chapter. Also, the crystallinity and phase transformation of PVDF in PVDF/TPU/CB-PPy composites were investigated.

In general, the percentage of PVDF β phase increases with the addition CB-PPy, however, this effect is more pronounced in samples containing high concentration of filler (i.e. 6% or more). In addition, the results show that the β phase content in PVDF is lower for samples prepared by FFF when compared to the compression molded specimens with the same composition.

Moreover, the addition of CB-PPy in the composites seems to have a significant effect on the piezoelectric coefficient (d_{33}) of the composites when the filler concentration is higher than 6-7%. In addition, samples prepared by fused filament fabrication showed lower piezoelectric responses when compared to compression molded composites.

Overall, the piezoelectric coefficient increased with the F(β) value for all composites and the 3D printing process affect directly the phase transformation of PVDF and piezoelectric coefficient of the materials.

Chapter VII

7. Composites based on poly(vinylidene fluoride), thermoplastic polyurethane and carbon black-polypyrrole for electromagnetic shielding application

Part of this chapter has been published in:

Mayara C. Bertolini, Silvia D. A. S. Ramoa, Bluma G. Soares, Guilherme M. O. Barra, Alessandro Pegoretti

"Poly(vinylidene fluoride) and thermoplastic polyurethane composites filled with carbon black-polypyrrole for electromagnetic shielding applications". In preparation.

7.1 Introduction

Electrically conductive polymer composites, besides the already mentioned applications as piezoresistive sensors [1, 2, 41, 57, 69] and piezoelectric materials [7, 72], have a significant role on electromagnetic interference (EMI) shielding application as the particles of the conductive filler can interact with the electromagnetic wave [36].

In this framework, many investigations have been carried out aiming at reducing the percolation threshold of composites, achieving high electrical conductivity values with the lowest amount of conductive filler, in order to preserve the mechanical properties and processability of the polymeric matrices [4]. Among different strategies, using polymeric matrices composed of immiscible polymer blends to selectively localize a conductive filler in one of the polymer phases or at the interface between them is an interesting way to reduce the composite percolation threshold [28, 32-38, 40, 42]. Moreover, blends with a co-continuous phase structure have been reported to reduce the electrical percolation threshold more efficiently due to double percolation [36].

For this reason, the electromagnetic shielding effectiveness of the prepared composites composed of the polymeric blends of poly(vinylidene fluoride) and thermoplastic polyurethane with carbon black-polypyrrole as conductive filler were evaluated. In addition, the composites based on poly(vinylidene fluoride)/CB-PPy and thermoplastic polyurethane/CB-PPy were also investigated for comparison. The electrical conductivity and electrical percolation threshold of those composites were already discussed in Chapter IV. The scanning electron microscopy and dynamic mechanical thermal analysis of the investigated materials were already discussed in the previous chapters.

In order to better characterize the materials, additional rheology measurements were performed for PVDF/CB-PPy and TPU/CB-PPy composites. The electromagnetic interference shielding effectiveness (EMI-SE) was evaluated for PVDF/CB-PPy, TPU/CB-PPy, PVDF/TPU/CB-PPy 38/62 vol% and PVDF/TPU/CB-PPy 50/50 vol% composites comprising various amount of CB-PPy and the results are discussed in this chapter.

7.2 Rheology measurements

Rheology measurements were carried out in the molten state for the composites comprising the neat matrices PVDF/CB-PPy and TPU/CB-PPy to evaluate the interaction between the conductive filler and the polymeric matrices [36, 38, 113]. The analysis was already performed for the composites comprising the blends as matrices and discussed in the previous chapters. The curves of storage modulus (G') and complex viscosity (η*) as function of frequency for PVDF/CB-PPy containing 0%, 3%, 5% and 10% of filler are shown in Figure 7-1 and for TPU/CB-PPy with 0%, 3%, 5% and 10% of filler are shown in Figure 7-2. The main rheological properties of the composites are summarized in Table 7-1.

The results show that the storage modulus (G') and complex viscosity (η*) for both composites generally increase with the addition of filler due to creation of a conductive network that reduces the mobility of the polymeric chains increasing the viscosity of the materials. In addition, it can be noticed that the effect of filler is much more pronounced in the PVDF composites. For instance, neat PVDF presents G' of 1678 Pa and η* of 533 Pa.s at 1 Hz frequency, while its composite with 10% of CB-PPy show G' of 579944 Pa and η* of 94265 Pa.s thus indicating an increase of almost 346 times in G' and 177 times in η*. On the other hand, the values of storage modulus and complex viscosity of neat TPU are 3122 Pa and 1352 Pa.s, respectively, (higher than for PVDF) but when 10% of CB-PPy is added to the mixture, they go up to 12409 Pa and 2421 Pa.s representing an increase of about 4 and 2 times, respectively. This behavior may be related to a poorer dispersion of the filler in the TPU matrix or some plasticizer effect of low concentrations of filler in the TPU matrix that leads to a low decrease in viscosity of the composites. When the filler is better dispersed and distributed in the polymer matrix, it results in a greater reduction on the mobility of the polymeric chains, thus increasing the storage modulus and viscosity of the material.

(a)

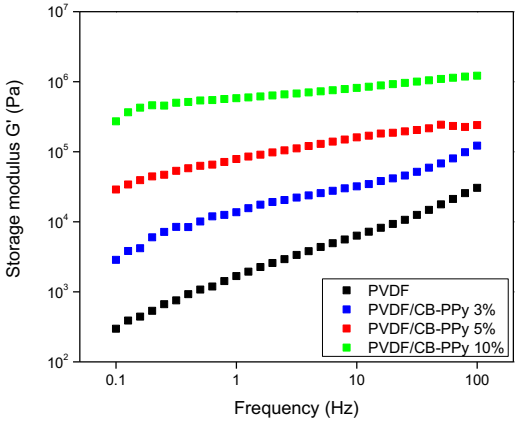

(b)

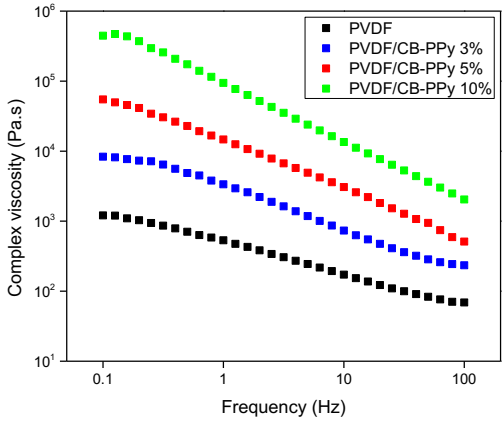

Figure 7-1: (a) Storage modulus and (b) complex viscosity as function of frequency for neat PVDF and PVDF/CB-PPy with 3%, 5% and 10% of CB-PPy.

Table 7-1: Summary of main rheological properties of PVDF/CB-PPy and TPU/CB-PPy composites with different filler content.

Sample	Viscosity at 10^{-1} Hz (Pa.s)	G' at 10^{-1} Hz (Pa)	G" at 10^{-1} Hz (Pa)
PVDF	533	1678	2896
PVDF/CB-PPy 3%	3360	13703	16058
PVDF/CB-PPy 5%	14690	78816	48035
PVDF/CB-PPy 10%	94265	579944	120271
Sample	**Viscosity at 10^{-1} Hz (Pa.s)**	**G' at 10^{-1} Hz (Pa)**	**G" at 10^{-1} Hz (Pa)**
TPU	1352	3122	7900
TPU/CB-PPy 3%	941	4953	3227
TPU/CB-PPy 5%	697	3743	2272
TPU/CB-PPy 10%	2421	12409	8794

(a)

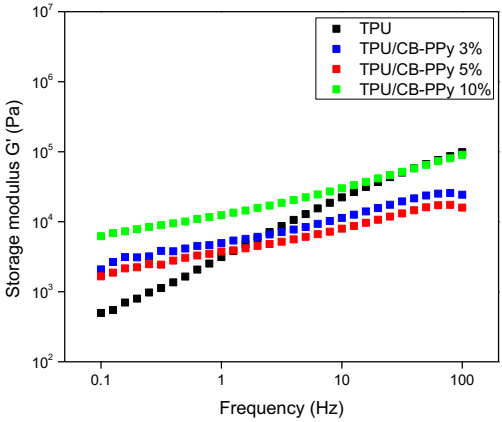

(b)

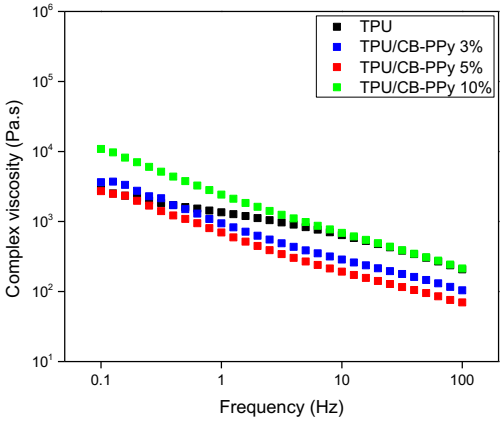

Figure 7-2: (a) Storage modulus and (b) complex viscosity as function of frequency for neat TPU and TPU/CB-PPy with 3%, 5% and 10% of CB-PPy.

Furthermore, Figure 7-3 displays a comparison between the storage (G') and loss (G") modulus as function of frequency for PVDF/CB-PPy and TPU/CB-PPy comprising 0%, 3%, 5% and 10% of CB-PPy. The results show that storage and loss modulus increase with frequency for all samples and the addition of conductive filler affects the rheological behavior of all studied composites. For PVDF composites, the loss modulus (G") is higher than the storage modulus (G') at low frequencies for neat PVDF indicating a liquid-like behavior. However, at a specific frequency, the G' and G" curves are intercepted and G' becomes higher than G" describing a solid-like behavior. When 3% of filler is added, similar values of G' and G" are displayed over the entire frequency range indicating both solid-like and liquid-like behaviors. On the other hand, PVDF composites with 5% and 10% of filler show G' higher than G" reporting a solid-like behavior for the whole frequency range that is associated to the creation of a tridimensional network in higher degree. Although G' is slightly higher than G" for PVDF with 5% of CB-PPy, when 10 % of filler is added to the composite, G' is significantly higher than the G" in the whole frequency range thus endorsing that idea that the material behavior becomes more solid with the addition of the conductive filler.

For the TPU-based composites, the loss modulus (G") is also higher than the storage modulus (G') at low frequencies only for the neat TPU. When the conductive filler is added G' becomes higher than G" at low frequencies representing a solid-like behavior, however, at a specific frequency G' and G" curves are intercepted and the loss modulus becomes higher than the storage modulus indicating a liquid-like behavior, however, this behavior is less pronounced with increasing the content of CB-PPy.

(a)

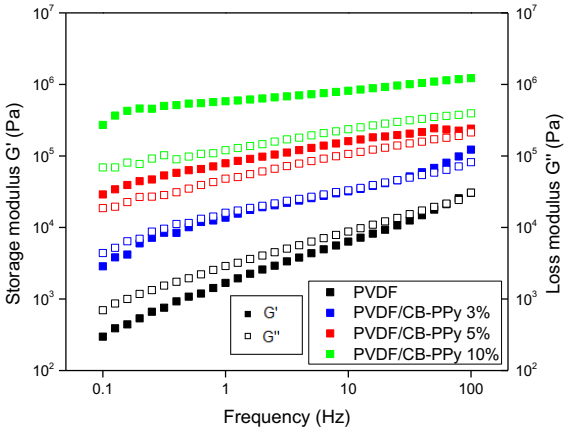

(b)

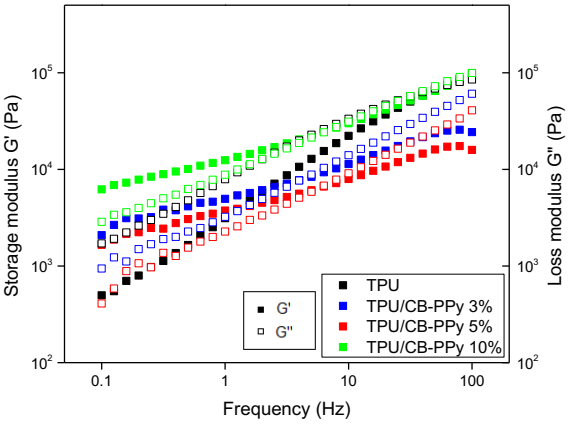

Figure 7-3: Dependence of storage and loss modulus with frequency for (a) PVDF/CB-PPy and (b) TPU/CB-PPy composites with 0%, 3%, 5% and 10% of filler.

Additionally, a comparison between the storage (G') and loss (G") modulus curves for the composites composed of PVDF/CB-PPy, TPU/CB-PPy, PVDF/TPU/CB-PPy 38/62 vol% and 50/50 vol% with 5% and 10% of conductive filler are displayed in Figure 7-4. For the composites comprising 5% of CB-PPy, the PVDF/TPU/CB-PPy 38/62 vol% composite reports an intermediate behavior between the two neat polymer composites with same amount of filler, as the amount of TPU is higher in the blend, the materials behavior is a bit more influenced by TPU rheology, while PVDF/TPU/CB-PPy 50/50 vol% presents G' and G" curves more related to the PVDF/CB-PPy. When 10% of filler is added to the blends, the PVDF influence on the materials rheology is more evident. In fact, the curves of PVDF/CB-PPy and PVDF/TPU/CB-PPy 50/50 vol% with 10% of CB-PPy overlap in the whole frequency range and the PVDF/TPU/CB-PPy 38/62 vol% curves are closer to PVDF/CB-PPy than to TPU/CB-PPy even if TPU content in the blend is higher than the PVDF content.

(a)

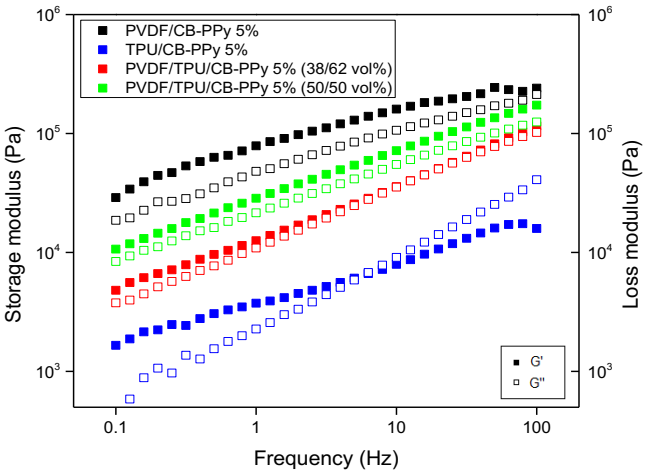

(b)

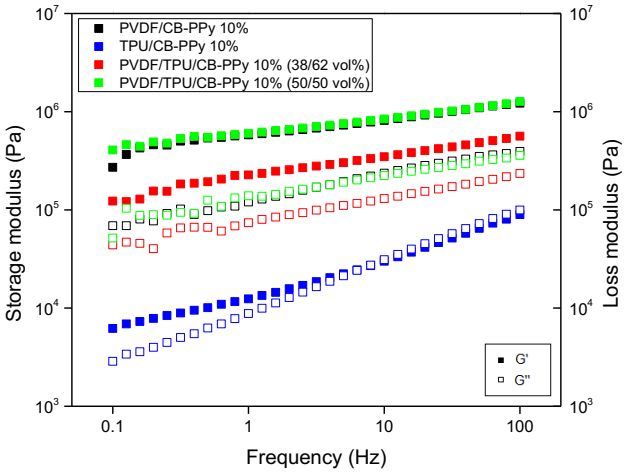

Figure 7-4: Dependence of storage and loss modulus with frequency for PVDF/CB-PPy, TPU/CB-PPy, PVDF/TPU/CB-PPy 38/62 vol% and 50/50 vol% with (a) 5% and (b) 10% of CB-PPy.

In addition, a comparison of the storage modulus as function of frequency between the composites based on the neat polymers and the polymer blends as matrices are shown in Figure 7-5. The curves are displayed for the composites containing 5% and 10% of CB-PPy. It is interesting to notice that the composites composed of the blends as matrices present a behavior intermediate between those of the composites composed of the two neat polymers. However, in the PVDF/TPU/CB-PPy composites, mainly in the 50/50 vol%, the effect of the conductive filler in the PVDF is more pronounced leading to a material with rheological behavior more similar to that of neat PVDF/CB-PPy composites. In fact, G' curves for PVDF/TPU/CB-PPy 50/50 vol% and PVDF/CB-PPy with 10% of filler overlap. This behavior demonstrates that the filler is more capable of restricting the movement of the polymeric chains in the PVDF polymer leading to higher storage modulus and complex viscosity. Moreover, Figure 7-6 reports that same pattern occurs to the complex viscosity.

(a)

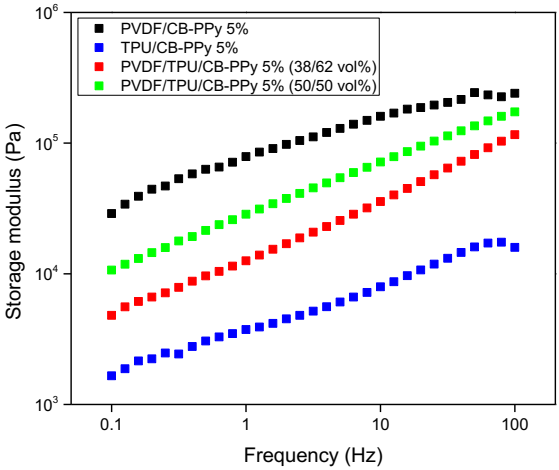

(b)

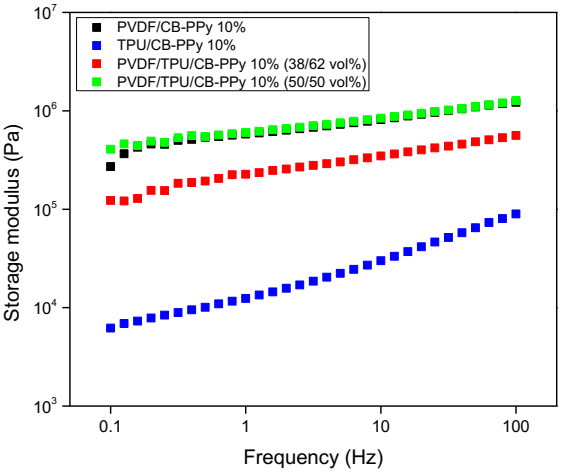

Figure 7-5: Storage modulus as function of frequency for PVDF/CB-PPy, TPU/CB-PPy, PVDF/TPU/CB-PPy 38/62 vol% and 50/50 vol% with (a) 5% and (b) 10% of CB-PPy.

(a)

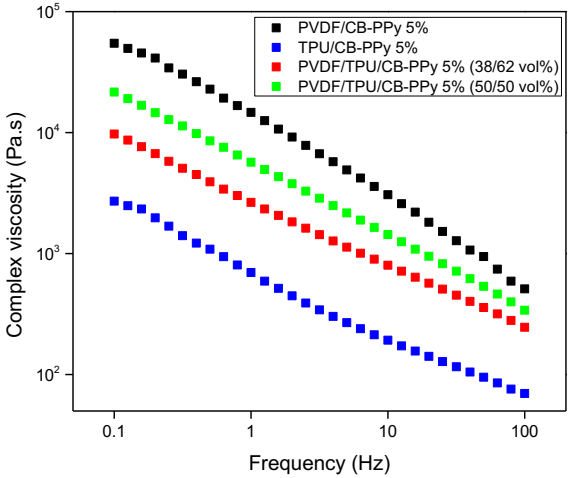

(b)

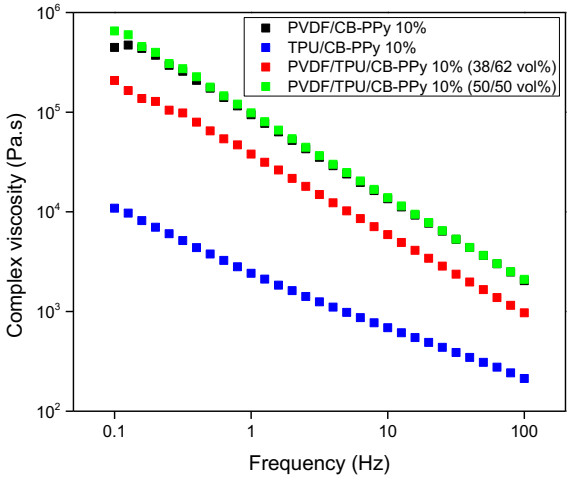

Figure 7-6: Complex viscosity as function of frequency for PVDF/CB-PPy, TPU/CB-PPy, PVDF/TPU/CB-PPy 38/62 vol% and 50/50 vol% with (a) 5% and (b) 10% of CB-PPy.

Furthermore, the phase angle for the PVDF/CB-PPy and TPU/CB-PPy composites was evaluated and compared to those found for the composites comprising the blends PVDF/TPU/CB-PPy 38/62 vol% and PVDF/TPU/CB-PPy 50/50 vol% as matrices. The curves of phase angle as a function of complex modulus for the composites comprising 10% of CB-PPy are presented in Figure 7-7. The phase angle goes from zero up to ninety degrees and it is related to the solid or liquid behavior of the materials. The results confirm that the TPU/CB-PPy 10% composite shows significantly higher phase angle that, related to the rheological behavior of the material that flows viscously as a liquid. On the other hand, the composites of PVDF/TPU/CB-PPy and PVDF/CB-PPy present lower phase angles indicating that the materials deform more elastically as a solid. The phase angles for the composites comprising the PVDF/TPU blends as matrices are between the phase angles found for the composites comprising the neat polymers as matrices, however, the composite composed of 50/50 vol% of PVDF/TPU show a very similar phase angle curve to the neat PVDF composite endorsing the claim that PVDF has a more significant effect on the composites rheology. Moreover, the curves format of semi-circles indicate a good dispersion of the conductive filler CB-PPy in the polymeric matrices.

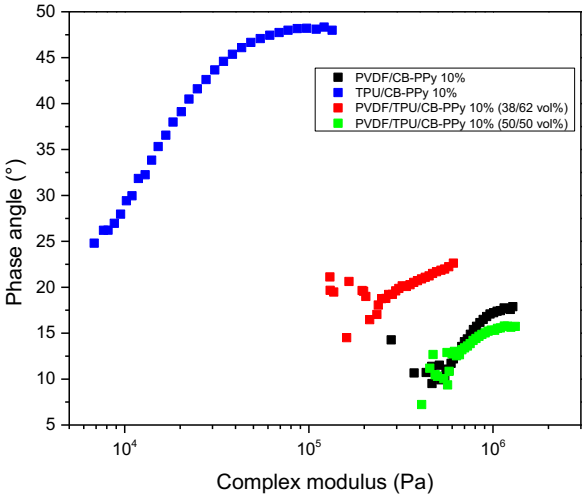

Figure 7-7: Phase angles vs. complex modulus for composites with 10% of conductive filler.

7.3 Electromagnetic interference shielding effectiveness (EMI-SE)

The effects of the content of conductive filler and type of polymeric matrix on the electromagnetic shielding effectiveness (EMI-SE) of PVDF/CB-PPy, TPU/CB-Py, PVDF/TPU/CB-PPy 38/62 vol% and 50/50 vol% composites were investigated in the X-band frequency ranging from 8 to 12 GHz. The electromagnetic interference shielding effectiveness depends on the conductivity of the material, the frequency and the thickness of the sample. The EMI-SE values as function of filler content for PVDF/CB-PPy and TPU/CB-PPy composites comprising various amount of CB-PPy are reported in Figure 7-8 and Figure 7-11, respectively.

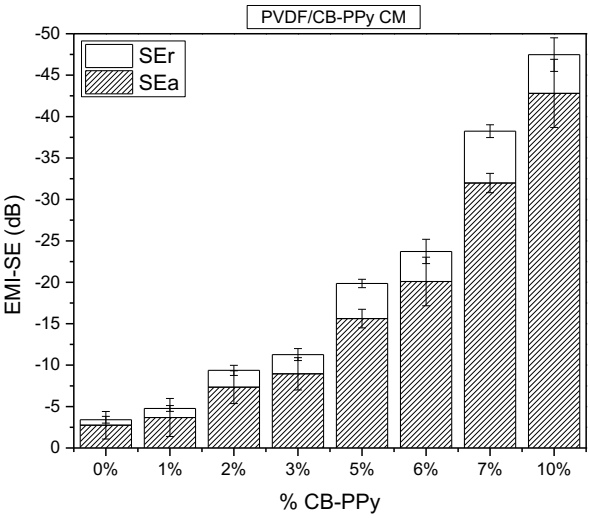

Figure 7-8: Total EMI-SE, SE_R and SE_A as function of CB-PPy content for PVDF/CB-PPy composites prepared by compression molding.

The results show that the addition of a conductive filler increases the attenuation of the electromagnetic radiation for both composites. These results are in agreement to the electrical conductivity values measured in Chapter IV, since the EMI-SE of electrically conductive polymer composites is enhanced as the electrical conductivity increase [18, 117].

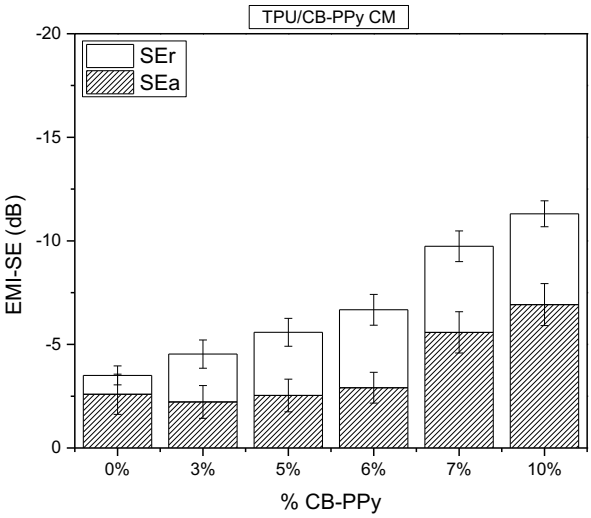

Figure 7-9: Total EMI-SE, SE_R and SE_A as function of CB-PPy content for TPU/CB-PPy composites prepared by compression molding.

In addition, the EMI-SE values of the composites comprising the polymeric blends of PVDF/TPU 38/62 vol% and 50/50 vol% as matrices with various amounts of CB-PPy are shown in Figure 7-10 and Figure 7-11, respectively. The same behavior was found for these composites, where increasing the filler content leads to higher attenuation of the electromagnetic radiation. It is possible to notice that the EMI-SE values for the composites comprising the blends are located between those found for the composites comprising the neat polymers, as expected. However, the composites comprising the co-continuous blend of PVDF/TPU 50/50 vol% as matrix displayed a better combination between electrical conductivity, EMI shielding efficiency and mechanical properties. In fact, PVDF/TPU/CB-PPy 50/50 vol% composites are capable to reach higher shielding of the electromagnetic radiation with lower amount of filler when compared to PVDF/TPU/CB-PPy 38/62 vol% composites. By adding lower amount of filler, the mechanical properties and processability of the polymeric matrix is well preserved. Besides this fact, co-continuous composites are showed in

previous chapters to have a better compromise between electrical and mechanical properties.

Moreover, the attenuation of the electromagnetic radiation of -20 dB corresponds to the shielding of more than 99% of the incident wave [11, 18, 117], which is enough for most EMI shielding applications. This value was obtained for PVDF/CB-PPy composites even with 5% of CB-PPy, nevertheless for TPU/CB-PPy composites the minimum EMI attenuation required for shielding applications is not achieved. For the composites comprising the blends as matrix, PVDF/TPU/CB-PPy 38/62 vol% reached the attenuation of at least -20 dB only with 15% of CB-PPy, while 10% of CB-PPy is enough to reach this value in co-continuous PVDF/TPU/CB-PPy 50/50 vol% composites.

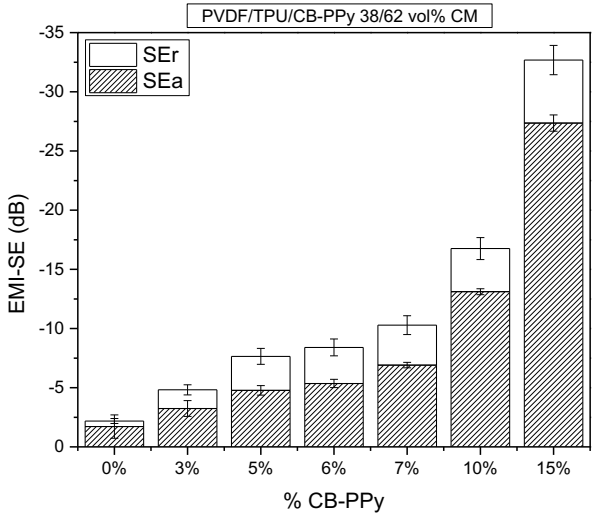

Figure 7-10: Total EMI-SE, SE_R and SE_A as function of CB-PPy content for PVDF/TPU/CB-PPy 38/62 vol% composites prepared by compression molding.

Furthermore, there are three mechanisms associated to the electromagnetic interference shielding: reflection (R), absorption (A) and multiple

reflection (MR). The multiple reflection mechanism represents the internal reflection within the shielding materials and it is commonly insignificant for frequencies in the GHz range [36, 117]. The shielding effectiveness by reflection (SE_R) is related to the interaction of the electromagnetic radiation with mobile charges carries, electrons or holes. On the other hand, the shielding effectiveness by absorption (SE_A) is associated to electrical and magnetic dipoles that interact with the electromagnetic wave converting the electromagnetic energy into heat [36, 117].

The stack plots for PVDF/CB-PPy, TPU/CB-PPy, PVDF/TPU/CB-PPy 38/62 vol% and 50/50 vol% present the total EMI-SE, the shielding effectiveness by absorption (SE_A) and the shielding effectiveness by reflection (SE_R). The overall EMI-SE of all composites is associated to the reflection and absorption mechanisms and both are increased by the increase in the CB-PPy content. Nevertheless, the contribution of the absorption mechanism is generally higher for the composites, which is important for some applications, for instance, military radar shielding materials. Usually the EMI-SE commanding mechanism for carbon-based composites is the absorption due to their electrical properties [11]. For TPU/CB-PPy composites, the incident electromagnetic radiation is shielded in similar amounts by reflection and absorption mechanisms.

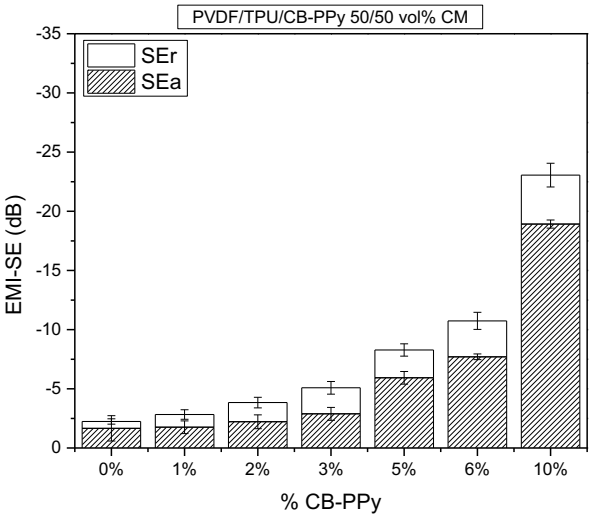

Figure 7-11: Total EMI-SE, SE_R and SE_A as function of CB-PPy content for PVDF/TPU/CB-PPy 50/50 vol% composites prepared by compression molding.

Moreover, a comparison of the composites with 10% of CB-PPy based on different matrices is shown in Figure 7-12. It can be observed that the PVDF/CB-PPy 10% composite presents much higher EMI-SE than the TPU/CB-PPy 10% composite. However, PVDF/CB-PPy 10% does not have the mechanical flexibility aimed for the intended applications. On the other hand, the PVDF/TPU/CB-PPy 50/50 vol% co-continuous composite with 10% of CB-PPy show a good balance between mechanical properties (as previous discussed in Chapter IV) and EMI-SE shielding properties displaying a total EMI-SE value of -23 dB that is higher than the minimum EMI attenuation required for shielding applications.

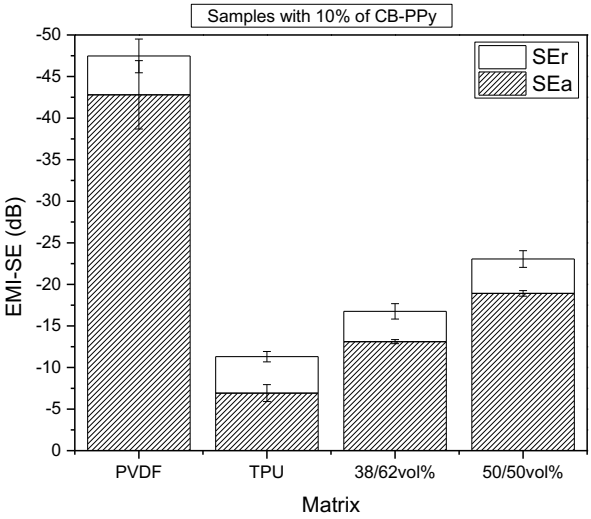

Figure 7-12: Comparison of total EMI-SE, SE_R and SE_A between PVDF/CB-PPy, TPU/CB-PPy and PVDF/TPU/CB-PPy composites comprising 10% of CB-PPy prepared by compression molding.

Furthermore, PVDF/TPU/CB-PPy samples prepared by fused filament fabrication were analyzed to investigate the influence of the printing technique on the EMI shielding effectiveness. Figure 7-13 shows the total EMI-SE, SER and SEA for the previous prepared composites of PVDF/TPU/CB-PPy 38/62 vol% with 5% and 6% of filler and PVDF/TPU/CB-PPy 50/50 vol% with 10% of CB-PPy. In addition, a comparison of total EMI-SE values between compression molded and 3D printed specimens is displayed in Table 7-2.

As explained before, the volume conductivity of the composites is related to their EMI-SE values. 3D printed specimens showed a substantial drop in the electrical conductivity when compared to CM samples with the same composition that can be attributed to the presence of voids and defects in 3D printed parts resulted from the layer-by-layer deposition. On the other hand, CM composites are more compacted thus presenting a much lower amount of voids and defects. Besides the porous

structure, the 3D printed specimens also present less material to interact with the incident electromagnetic radiation. In fact, the samples manufactured by via FFF presented an EMI shielding effectiveness lower than that of the samples processed via compression molding. For instance, the total EMI-SE for PVDF/TPU/CB-PPy 50/50 vol% with 10% of conductive filler processed by compression molding is -23 dB, whereas the sample with same composition prepared by FFF present an EMI attenuation around -15 dB.

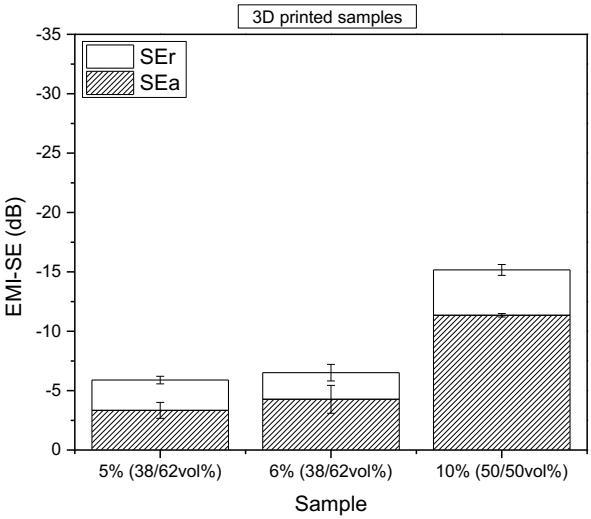

Figure 7-13: Total EMI-SE, SE_R and SE_A of PVDF/TPU/CB-PPy 38/62 vol% with 5% and 6% of CB-PPy and PVDF/TPU/CB-PPy 50/50 vol% with 10% of CB-PPy prepared by fused filament fabrication.

Table 7-2: Comparison of total EMI-SE values between compression molded and 3D printed specimens.

PVDF/TPU/CB-PPy	EMI-SE (dB)	
	CM	3DP
5% (38/62 vol%)	-7.6	-5.9
6% (38/62 vol%)	-8.4	-6.5
10% (50/50 vol%)	-23.0	-15.2

7.4 Conclusions

The electromagnetic interference shielding effectiveness of PVDF/TPU/CB-PPy samples prepared by compression molded and 3D printed was evaluated in this chapter. The EMI-SE of the composites resulted to be directly related to their electrical conductivity, i.e. to the content of the conductive CB-PPy additive. The results show that materials with higher electrical conductivity showed a better shielding of the electromagnetic radiation since the amount of particles that can interact with the electromagnetic wave is higher. In addition, the main mechanism of EMI shielding found for the composites was the absorption, which is required for some applications.

Moreover, the composites comprising the co-continuous blend as matrix showed a better combination between EMI shielding efficiency and mechanical properties. In fact, for PVDF/TPU/CB-PPy 38/62 vol% composites 15% of CB-PPy was necessary to reach the attenuation of at least -20 dB (which corresponds to a shielding efficiency of more than 99% of the incident wave), while the addition of 10% of CB-PPy is capable to induce the same level in PVDF/TPU/CB-PPy 50/50 vol% co-continuous composites. Furthermore, specimens prepared by fused filament fabrication presented a diminished EMI-SE response when compared to compression molded samples with the same composition due to the presence of voids and defect in 3D printed parts.

Chapter VIII

8. Conclusions and future perspectives

Flexible, high electrically conductive and 3D printable composites based on poly(vinylidene fluoride)/thermoplastic polyurethane blends as matrix and carbon black-polypyrrole as conductive filler were successfully prepared by both compression molding and fused filament fabrication techniques. Blends with different compositions were produced and the results show that the flexibility aimed for the final material was reached with the addition of TPU to PVDF. In order to achieve an optimal compromise between electrical conductivity, mechanical properties and printability, blends composed of PVDF/TPU 38/62 vol% and 50/50 vol% were selected for the addition of 0 to 15% of CB-PPy. SEM images show the achievement of a co-continuous blend comprising 50/50 vol% of PVDF/TPU. This microstructure was found to improve not only the mechanical properties but also electrical properties of the composites due to the preferable localization of CB-PPy in the PVDF phase resulting in a flexible and highly conductive material. In fact, the electrical percolation threshold of the conductive composite comprised of the co-continuous blend was 2%, while the electrical percolation threshold of the composite with the PVDF/TPU blend with 38/62 vol% was 5%, confirming that the co-continuous phase assists in the reduction of the percolation threshold while improves the flexibility and printability of PVDF.

The tensile stress-strain curves indicate that the incorporation of the filler into the blends increases the rigidity and the elastic modulus of the mixtures, and it reduces the elongation at break. The DMTA curves indicate that the storage modulus of the blends increases with the addition of CB-PPy, which is agreement to the rheological measurements that show that the viscosity of the materials increase with the addition of the filler due to the creation of a three-dimensional network. The rheological percolation threshold was found to be 3% for PVDF/TPU/CB-PPy 38/62 vol% and 1% for PVDF/TPU/CB-PPy 50/50 vol%, suggesting that the addition of

higher amount of conductive filler could compromise the processability of the composites. Furthermore, the addition of CB-PPy leaded to a reduction on the T_g values of the composites due to a reduction of the mobility of the polymeric chains with the addition of the filler. DSC curves show that the melting temperature of the composites decreases with the addition of CB-PPy.

Moreover, piezoresistive responses were investigated and the best responses were found for compression molded PVDF/TPU/CB-PPy composites with 5% and 6% of CB-PPy. However, PVDF/TPU/CB-PPy 38/62 vol% with 6% and PVDF/TPU/CB-PPy 50/50 vol% with 5% of CB-PPy presented the highest sensitivity and gauge factor values, large pressure range and reproducible piezoresistive responses under 100 cycles.

Furthermore, the influence of blending, addition of filler and processing techniques on PVDF crystallinity and its β phase content was evaluated by DSC, FTIR and XRD. In general, the degree of crystallinity of the samples decreases with the addition of CB-PPy, thus suggesting that the conductive particles can hinder the crystallization of PVDF chains, although the percentage of β phase in PVDF increases with the addition CB-PPy. This effect is more pronounced in samples containing high concentration of filler (i.e. 6% or more). The piezoelectric coefficient d_{33} increases with the percentage of β phase value for all composites and the addition of CB-PPy in the composites seems to have a significant effect on the piezoelectric coefficient (d_{33}) of the composites when the filler concentration is higher than 6-7%.

The electromagnetic interference shielding effectiveness (EMI-SE) of PVDF/TPU/CB-PPy composites was also measured. Results show that the EMI-SE of the composites is directly related to their electrical conductivity. In fact, materials with higher electrical conductivity showed a better shielding of the electromagnetic waves since the amount of particles that can interact with the electromagnetic radiation is higher. For reaching the attenuation of at least -20 dB, 15% of CB-PPy is necessary for PVDF/TPU/CB-PPy 38/62 vol% composites, while 10% of CB-PPy is enough to reach the same value in co-continuous composites, thus indicating that composites based on the co-continuous blend displayed higher EMI shielding efficiency than composites prepared with a matrix with a PVDF/TPU ratio of 38/62 vol%. In addition,

the main EMI shielding mechanism found on the composites was the absorption, which is required for some applications.

In addition, the effects of two different processing techniques (compression molding and 3D printing by fused filament fabrication) on the main properties of the investigated materials were compared. 3D printed parts showed lower electrical conductivity when compared to compression molded composites with the same composition due to the presence of voids, defects and overlapping layers that can hinder the flow of electrons. In fact, the PVDF/TPU 38/62 vol% compression molded composite with 6% of CB-PPy displayed an electrical conductivity of $1.94x10^{-1}$ $S•m^{-1}$, while the 3D printed composite with same composition showed an electrical conductivity of $6.01x10^{-8}$ $S•m^{-1}$. On the other hand, the 3D printed co-continuous composite with 10% of CB-PPy presented a high value of electrical conductivity of $4.14×10^{0}$ $S•m^{-1}$ even after the printing process, thus indicating a potential use of this filament for electrically conductive applications.

Moreover, 3D printed composites of PVDF/TPU/CB-PPy 38/62 vol% with 5% and 6% of CB-PPy exhibited good piezoresistive response. However, only the composite with 6% of CB-PPy showed reproducible piezoresistive responses under 100 cycles. The results also show that the 3D printing process affect directly the phase transformation of PVDF and the piezoelectric coefficient of the materials. In fact, the β phase content and piezoelectric responses in PVDF is lower for samples prepared by FFF when compared to compression molded specimens with same composition. Diminished EMI-SE responses were found for specimens prepared by FFF due to the presence of voids and defect in 3D printed parts. Overall, the results suggest that the compression molding and fused filament fabrication are both proper techniques for the fabrication of piezoresistive pressure sensors based on PVDF/TPU/CB-PPy composites.

As a possible future development of this work, the preparation of electrically conductive filaments with different compositions would be interesting since the present activity was limited to a few compositions. In addition, the effect of other FFF printing parameters (such as printing directions, layer height, number of layers and infill density) on the mechanical and electrical properties of the composites would be worthwhile to be tested.

References

1. Jianwen Chen, Y.Z., Jinrui Huang, Jiaoxia Zhang, Duo Pan, Juying Zhou, and A.U. Jong E. Ryu, Zhanhu Guo, *Advances in Responsively Conductive Polymer Composites and Sensing Applications.* Polymer Reviews, 2021. **61**(1): p. 157-193.
2. Dios, J.R., et al., *Piezoresistive performance of polymer-based materials as a function of the matrix and nanofiller content to walking detection application.* Composites Science and Technology, 2019. **181**: p. 107678.
3. Ke, K., et al., *Highly sensitive capacitive pressure sensors based on elastomer composites with carbon filler hybrids.* Composites Part A: Applied Science and Manufacturing, 2019. **126**: p. 105614.
4. Rosa, B.d.S., et al., *Development of Poly (butylene adipate-co-terephthalate) Filled with Montmorillonite-Polypyrrole for Pressure Sensor Applications.* Materials Research, 2019. **22**(2).
5. Kim, H., et al., *3D Printing of BaTiO3/PVDF Composites with Electric In Situ Poling for Pressure Sensor Applications.* Macromolecular Materials and Engineering, 2017. **302**(11): p. 1700229.
6. Bertolini, M.C., et al., *Hybrid Composites Based on Thermoplastic Polyurethane With a Mixture of Carbon Nanotubes and Carbon Black Modified With Polypyrrole for Electromagnetic Shielding.* Frontiers in Materials, 2020. **7**.
7. Wan, Y., Y. Wang, and C.F. Guo, *Recent progresses on flexible tactile sensors.* Materials Today Physics, 2017. **1**: p. 61-73.
8. Kennedy, Z.C., et al., *3D-printed poly(vinylidene fluoride)/carbon nanotube composites as a tunable, low-cost chemical vapour sensing platform.* Nanoscale, 2017. **9**(17): p. 5458-5466.
9. Xiang, D., et al., *Enhanced performance of 3D printed highly elastic strain sensors of carbon nanotube/thermoplastic polyurethane nanocomposites via non-covalent interactions.* Composites Part B: Engineering, 2019. **176**: p. 107250.
10. Alsharari, M., B. Chen, and W. Shu, *3D Printing of Highly Stretchable and Sensitive Strain Sensors Using Graphene Based Composites.* Proceedings, 2018. **2**(13): p. 792.
11. Schmitz, D.P., et al., *Electromagnetic interference shielding effectiveness of ABS carbon-based composites manufactured via fused deposition modelling.* Materials Today Communications, 2018. **15**: p. 70-80.
12. Caminero, M.A., et al., *Additive Manufacturing of PLA-Based Composites Using Fused Filament Fabrication: Effect of Graphene Nanoplatelet Reinforcement on Mechanical Properties, Dimensional Accuracy and Texture.* Polymers (Basel), 2019. **11**(5).
13. de Leon, A.C., et al., *High performance polymer nanocomposites for additive manufacturing applications.* Reactive and Functional Polymers, 2016. **103**: p. 141-155.

14. Ahmed, K., et al., *Soft, conductive nanocomposites based on ionic liquids/carbon nanotubes for 3D printing of flexible electronic devices.* Polymer Journal, 2019. **51**(5): p. 511-521.
15. Christ, J.F., et al., *3D printed highly elastic strain sensors of multiwalled carbon nanotube/thermoplastic polyurethane nanocomposites.* Materials & Design, 2017. **131**: p. 394-401.
16. Simon J. Leigh1, R.J.B., Christopher P. Purssell, Duncan R. Billson, David A. Hutchins, *A Simple, Low-Cost Conductive Composite Material for 3D Printing of Electronic Sensors.* Plos One, 2012. **7**(11): p. 49365.
17. Daniel, F., et al., *Temperature-dependent electrical resistance of conductive polylactic acid filament for fused deposition modeling.* The International Journal of Advanced Manufacturing Technology, 2018. **99**(5-8): p. 1215-1224.
18. Ecco, L., et al., *Rapid Prototyping of Efficient Electromagnetic Interference Shielding Polymer Composites via Fused Deposition Modeling.* Applied Sciences, 2018. **9**(1): p. 37.
19. Viskadourakis, Z., et al., *Electromagnetic shielding effectiveness of 3D printed polymer composites.* Applied Physics A, 2017. **123**(12).
20. A. Paddubskaya, N.V., P. Kuzhir, K. Batrakov, S.Maksimenko, R. Kotsilkova, H. Velichkova, I. Petrova, I. Birò, K. Kertész, G. I.Mark, Z. E. Horvath and L. P. Birò, *Electromagnetic and thermal properties of three-dimensional printed multilayered nano-carbon_poly(lactic) acid structures.* Journal of Applied Physics, 2016. **119**: p. 135102.
21. Thomassin, J.-M., et al., *Polymer/carbon based composites as electromagnetic interference (EMI) shielding materials.* Materials Science and Engineering: R: Reports, 2013. **74**(7): p. 211-232.
22. Abedi, K., et al., *Evaluation of electromagnetic shielding properties of high-performance continuous carbon fiber composites fabricated by robotic 3D printing.* Additive Manufacturing, 2022. **54**: p. 102733.
23. Dul, S., et al., *Graphene/Carbon Nanotube Hybrid Nanocomposites: Effect of Compression Molding and Fused Filament Fabrication on Properties.* Polymers (Basel), 2020. **12**(1).
24. Wang, Y., et al., *3D-printing of segregated carbon nanotube/polylactic acid composite with enhanced electromagnetic interference shielding and mechanical performance.* Materials & Design, 2021. **197**: p. 109222.
25. Ramoa, S.D.A.S., et al., *Novel electrically conductive polyurethane/montmorillonite-polypyrrole nanocomposites.* Express Polymer Letters, 2015. **9**(10): p. 945-958.
26. Wu, H., et al., *Recent developments in polymers/polymer nanocomposites for additive manufacturing.* Progress in Materials Science, 2020. **111**: p. 100638.
27. Dorigato, A., et al., *Electrically conductive nanocomposites for fused deposition modelling.* Synthetic Metals, 2017. **226**: p. 7-14.
28. Menon, A.V., G. Madras, and S. Bose, *Magnetic Alloy-MWNT Heterostructure as Efficient Electromagnetic Wave Suppressors in Soft Nanocomposites.* ChemistrySelect, 2017. **2**(26): p. 7831-7844.

29. Desai, N.I.J.a.P.D., *Characterization of resistors created by fused filament fabrication*, in *28th Flexible Automation and Intelligent Manufacturing (FAIM2018) Conference.* 2018, Procedia Manufacturing. p. 37-44.
30. Sezer, H.K. and O. Eren, *FDM 3D printing of MWCNT re-inforced ABS nano-composite parts with enhanced mechanical and electrical properties.* Journal of Manufacturing Processes, 2019. **37**: p. 339-347.
31. Yadav, D., et al., *Optimization of FDM 3D printing process parameters for multi-material using artificial neural network.* Materials Today: Proceedings, 2020. **21**: p. 1583-1591.
32. M. Bera, U.S., A. Bhardwaj, P. K. Maji, *Reduced graphene oxide (RGO)-induced compatibilization and reinforcement of poly(vinylidene fluoride) (PVDF)–thermoplastic polyurethane (TPU) binary polymer blend.* Applied Polymers, 2019. **136**(5): p. 47010.
33. Chatham, C.A., et al., *Semi-Crystalline Polymer Blends for Material Extrusion Additive Manufacturing Printability: A Case Study with Poly(ethylene terephthalate) and Polypropylene.* Macromolecular Materials and Engineering, 2019. **304**(5): p. 1800764.
34. Al-Saleh, M.H. and U. Sundararaj, *An innovative method to reduce percolation threshold of carbon black filled immiscible polymer blends.* Composites Part A: Applied Science and Manufacturing, 2008. **39**(2): p. 284-293.
35. Liu, Y., et al., *Selective dispersion of silver nanowires in epoxy/polyetherimide binary composites with enhanced electrical conductivity: a study of curing kinetics and morphology.* Polymer Composites, 2019. **40**(11): p. 4390-4401.
36. Bluma G. Soares, L.F.C., Adriana A. Silva, Tamara Indrusiak, Guilherme M. O. Barra, Sebastien Livi, *Conducting melt blending of polystyrene and EVA copolymer with carbon nanotube assisted by phosphonium-based ionic liquid.* Journal of Applied Polymer Science, 2018. **135**(24).
37. Chen, J., et al., *Design of superior conductive polymer composite with precisely controlling carbon nanotubes at the interface of a co-continuous polymer blend via a balance of π-π interactions and dipole-dipole interactions.* Carbon, 2017. **114**: p. 441-448.
38. Lopes Pereira, E.C., et al., *Conductive heterogeneous blend composites of PP/PA12 filled with ionic liquids treated-CNT.* Polymer Testing, 2019. **74**: p. 187-195.
39. Brigandi, P.J., et al., *Influence of carbon black and carbon nanotubes on the conductivity, morphology, and rheology of conductive ternary polymer blends.* Polymer Engineering & Science, 2017. **57**(12): p. 1329-1339.
40. Bizhani, H., et al., *Double percolated MWCNTs loaded PC/SAN nanocomposites as an absorbing electromagnetic shield.* European Polymer Journal, 2018. **100**: p. 209-218.
41. Li, B., et al., *A highly stretchable, super-hydrophobic strain sensor based on polydopamine and graphene reinforced nanofiber composite for human motion monitoring.* Composites Part B: Engineering, 2020. **181**: p. 107580.

42. Shi, Y.-y., et al., *Selective localization of carbon nanotubes at the interface of Poly(L-lactide)/Ethylene-co-vinyl Acetate resulting in lowered electrical resistivity.* Composites Part B: Engineering, 2013. **55**: p. 463-469.
43. Laureto, J., et al., *Thermal properties of 3-D printed polylactic acid-metal composites.* Progress in Additive Manufacturing, 2017. **2**(1-2): p. 57-71.
44. Tomáš Tichý, O.Š., Petr Veselý and Tomáš Cápal, *Application Possibilities of FFF technology for high-voltage insulation systems*, in *42nd International Spring Seminar on Electronics Technology (ISSE)*. 2019.
45. Lorenzo-Bañuelos, M., A. Díaz, and I.I. Cuesta, *Influence of raster orientation on the determination of fracture properties of polypropylene thin components produced by additive manufacturing.* Theoretical and Applied Fracture Mechanics, 2020. **107**: p. 102536.
46. Momenzadeh, N., C.M. Stewart, and T. Berfield, *Mechanical and Thermal Characterization of Fused Filament Fabrication Polyvinylidene Fluoride (PVDF) Printed Composites.* 2019: p. 59-65.
47. Sánchez, D.M., et al., *Development of carbon fiber acrylonitrile styrene acrylate composite for large format additive manufacturing.* Materials & Design, 2020. **191**: p. 108577.
48. Rigotti, D., A. Dorigato, and A. Pegoretti, *3D printable thermoplastic polyurethane blends with thermal energy storage/release capabilities.* Materials Today Communications, 2018. **15**: p. 228-235.
49. Mora, A., P. Verma, and S. Kumar, *Electrical conductivity of CNT/polymer composites: 3D printing, measurements and modeling.* Composites Part B: Engineering, 2020. **183**: p. 107600.
50. Stansbury, J.W. and M.J. Idacavage, *3D printing with polymers: Challenges among expanding options and opportunities.* Dent Mater, 2016. **32**(1): p. 54-64.
51. Yamamoto, B.E., et al., *Development of multifunctional nanocomposites with 3-D printing additive manufacturing and low graphene loading.* Journal of Thermoplastic Composite Materials, 2018. **32**(3): p. 383-408.
52. Díaz-García, Á., et al., *Novel procedure for laboratory scale production of composite functional filaments for additive manufacturing.* Materials Today Communications, 2020. **24**: p. 101049.
53. Al-Saygh, A., et al., *Flexible Pressure Sensor Based on PVDF Nanocomposites Containing Reduced Graphene Oxide-Titania Hybrid Nanolayers.* Polymers (Basel), 2017. **9**(2).
54. Zheng, Q., et al., *Graphene-based wearable piezoresistive physical sensors.* Materials Today, 2020.
55. Chang, Y., et al., *State-of-the-art and recent developments in micro/nanoscale pressure sensors for smart wearable devices and health monitoring systems.* Nanotechnology and Precision Engineering, 2020. **3**(1): p. 43-52.
56. Sun, L., et al., *Realization of flexible pressure sensor based on conductive polymer composite via using electrical impedance tomography.* Smart Materials and Structures, 2020. **29**(5): p. 055004.
57. Gao, Y., et al., *Flexible Hybrid Sensors for Health Monitoring: Materials and Mechanisms to Render Wearability.* Adv Mater, 2020. **32**(15): p. e1902133.

58. Kennedy, Z.C., et al., *Enhanced anti-counterfeiting measures for additive manufacturing: coupling lanthanide nanomaterial chemical signatures with blockchain technology.* Journal of Materials Chemistry C, 2017. **5**(37): p. 9570-9578.
59. Muhammad Imran, S., et al., *Pressure-sensitive polymer nanocomposites: Carbon nanofiber-reinforced MWCNT-coated PMMA microbeads.* Polymer-Plastics Technology and Materials, 2019. **58**(16): p. 1793-1801.
60. Lathers, S., M. Mousa, and J. La Belle, *Additive Manufacturing Fused Filament Fabrication Three-Dimensional Printed Pressure Sensor for Prosthetics with Low Elastic Modulus and High Filler Ratio Filament Composites.* 3D Printing and Additive Manufacturing, 2017. **4**(1): p. 30-40.
61. Sugiyama, T.T.a.S., *Analysis of Piezoresistance in p-Type Silicon for mechanical sensors.* Journal of Microelectromechanical Systems, 2002. **11**(5): p. 598/604.
62. Thomas W. Tombler, C.Z., Leo Alexseyev, Jing Kong, Hongjie Dai, Lei Liu, C. S. Jayanthi, Meijie Tang and Shi-Yu Wu *Reversible electromechanical characteristics of carbon nanotubes underlocal-probe manipulation.* Nature, 2000. **405**: p. 769-772.
63. Bae, S.-H., et al., *Graphene-based transparent strain sensor.* Carbon, 2013. **51**: p. 236-242.
64. Wei, P., et al., *Reprocessable 3D-Printed Conductive Elastomeric Composite Foams for Strain and Gas Sensing.* ACS Applied Polymer Materials, 2019. **1**(4): p. 885-892.
65. Chen, Q., P.F. Cao, and R.C. Advincula, *Mechanically Robust, Ultraelastic Hierarchical Foam with Tunable Properties via 3D Printing.* Advanced Functional Materials, 2018. **28**(21): p. 1800631.
66. Wang, Z., et al., *Full 3D Printing of Stretchable Piezoresistive Sensor with Hierarchical Porosity and Multimodulus Architecture.* Advanced Functional Materials, 2019. **29**(11): p. 1807569.
67. Roh, E., et al., *A Solution-Processable, Omnidirectionally Stretchable, and High-Pressure-Sensitive Piezoresistive Device.* Adv Mater, 2017. **29**(42).
68. Yao, H.B., et al., *A flexible and highly pressure-sensitive graphene-polyurethane sponge based on fractured microstructure design.* Adv Mater, 2013. **25**(46): p. 6692-8.
69. Merlini, C., et al., *Electrically pressure sensitive poly(vinylidene fluoride)/polypyrrole electrospun mats.* RSC Adv., 2014. **4**(30): p. 15749-15758.
70. Liu, R., K. Xu, and Y. Zhang, *Nanomaterial-based wearable pressure sensors: A minireview.* Instrumentation Science & Technology, 2020. **48**(4): p. 459-479.
71. Souza, F.G., R.C. Michel, and B.G. Soares, *A methodology for studying the dependence of electrical resistivity with pressure in conducting composites.* Polymer Testing, 2005. **24**(8): p. 998-1004.
72. Max B Kirkpatrick, J.A.T., and Tue Le, *Characterization of 3D printed piezoelectric sensors_ Determiniation of d_inf_33__inf_ piezoelectric coefficient for 3D printed polyvinylidene fluoride sensors.pdf>.* IEEE SENSORS, 2016: p. 1-3.

73. Bencomo, J.A., S.T. Iacono, and J. McCollum, *3D printing multifunctional fluorinated nanocomposites: tuning electroactivity, rheology and chemical reactivity.* Journal of Materials Chemistry A, 2018. **6**(26): p. 12308-12315.
74. Mao, Y.-J., et al., *Effective electromagnetic interference shielding properties of micro-truss structured CNT/Epoxy composites fabricated based on visible light processing.* Composites Science and Technology, 2022. **221**: p. 109296.
75. Ma, H., et al., *Rheological Behavior and Morphologies of Reactively Compatibilized PVDF/TPU Blends.* Macromolecular Chemistry and Physics, 2011. **212**(3): p. 252-258.
76. Elnabawy, E., et al., *Piezoelastic PVDF/TPU Nanofibrous Composite Membrane: Fabrication and Characterization.* Polymers (Basel), 2019. **11**(10).
77. Chen, C., et al., *3D printing of electroactive PVDF thin films with high β-phase content.* Smart Materials and Structures, 2019. **28**(6): p. 065017.
78. Wu, L., et al., *Power generation by PVDF-TrFE/graphene nanocomposite films.* Composites Part B: Engineering, 2019. **164**: p. 703-709.
79. Behera, M., *Study of Optical, Thermal, Mechanical and Microstructural Properties of Fullerene/Poly (vinylidene fluoride) Polymer Nanocomposites.* Biointerface Research in Applied Chemistry, 2022. **13**(2): p. 121.
80. Shoorangiz, M., Z. Sherafat, and E. Bagherzadeh, *CNT loaded PVDF-KNN nanocomposite films with enhanced piezoelectric properties.* Ceramics International, 2022. **48**(11): p. 15180-15188.
81. Fakhri, P., et al., *Improved electroactive phase content and dielectric properties of flexible PVDF nanocomposite films filled with Au- and Cu-doped graphene oxide hybrid nanofiller.* Synthetic Metals, 2016. **220**: p. 653-660.
82. Yan, J., et al., *Performance enhancements in poly(vinylidene fluoride)-based piezoelectric nanogenerators for efficient energy harvesting.* Nano Energy, 2019. **56**: p. 662-692.
83. Seena, M., J. Husna, and V. Prasad, *Dielectric properties of hot-pressed Poly(vinylidene fluoride)/Functionalized carbon nanotube composites.* Materials Chemistry and Physics, 2022. **285**: p. 126134.
84. Wu, C.M. and M.H. Chou, *Acoustic–electric conversion and piezoelectric properties of electrospun polyvinylidene fluoride/silver nanofibrous membranes.* Express Polymer Letters, 2020. **14**(2): p. 103-114.
85. Kim, H., et al., *Fabrication and characterization of 3D printed BaTiO3/PVDF nanocomposites.* Journal of Composite Materials, 2017. **52**(2): p. 197-206.
86. Tarbuttona, J., et al., *Phase Transformation and Shock Sensor Response of Additively Manufactured Piezoelectric PVDF.* Procedia Manufacturing, 2017. **10**: p. 982-989.
87. You, M.-H., et al., *A self-powered flexible hybrid piezoelectric–pyroelectric nanogenerator based on non-woven nanofiber membranes.* Journal of Materials Chemistry A, 2018. **6**(8): p. 3500-3509.
88. Kim, H., et al., *Enhanced dielectric properties of three phase dielectric MWCNTs/BaTiO3/PVDF nanocomposites for energy storage using fused*

deposition modeling 3D printing. Ceramics International, 2018. **44**(8): p. 9037-9044.
89. Wang, X., et al., *Tactile-Sensing Based on Flexible PVDF Nanofibers via Electrospinning: A Review.* Sensors (Basel), 2018. **18**(2).
90. Wu, L., et al., *Improved piezoelectricity of PVDF-HFP/carbon black composite films.* Journal of Physics D: Applied Physics, 2014. **47**(13): p. 135302.
91. Dhatarwal, P. and R.J. Sengwa, *Tunable β-phase crystals, degree of crystallinity, and dielectric properties of three-phase PVDF/PEO/SiO2 hybrid polymer nanocomposites.* Materials Research Bulletin, 2020. **129**: p. 110901.
92. Lederle, F., C. Härter, and S. Beuermann, *Inducing β phase crystallinity of PVDF homopolymer, blends and block copolymers by anti-solvent crystallization.* Journal of Fluorine Chemistry, 2020. **234**: p. 109522.
93. M. Arjun Hari, S.C.K., Soney Varghese, Lintu Rajan, *Performance Enhancement of Flexible and Self-Powered PVDF-ZnO Based Tactile Sensors.* IEEE sensors journal, 2022. **22**(10).
94. Georgousis, G., et al., *Strain sensing in polymer/carbon nanotube composites by electrical resistance measurement.* Composites Part B: Engineering, 2015. **68**: p. 162-169.
95. Yuan, X., et al., *A poling-free PVDF nanocomposite via mechanically directional stress field for self-powered pressure sensor application.* Nano Energy, 2022. **98**: p. 107340.
96. Villanueva, R., D. Ganta, and C. Guzman, *Mechanical, in-situ electrical and thermal properties of wearable conductive textile yarn coated with polypyrrole/carbon black composite.* Materials Research Express, 2018. **6**(1): p. 016307.
97. Raman, S. and A. Ravi Sankar, *Intrinsically conducting polymers in flexible and stretchable resistive strain sensors: a review.* Journal of Materials Science, 2022. **57**(28): p. 13152-13178.
98. Dul, S., A. Pegoretti, and L. Fambri, *Fused Filament Fabrication of Piezoresistive Carbon Nanotubes Nanocomposites for Strain Monitoring.* Frontiers in Materials, 2020. **7**.
99. Wang, M.-J., et al., *Carbon black*, in *Kirk-Othmer Encyclopedia of Chemical Technology*. 2003. p. 761-803.
100. Merlini, C., et al., *Development of a novel pressure sensing material based on polypyrrole-coated electrospun poly(vinylidene fluoride) fibers.* Materials Science and Engineering: B, 2014. **179**: p. 52-59.
101. Jiang, L., et al., *Sensing characteristics of polypyrrole–poly(vinyl alcohol) methanol sensors prepared by in situ vapor state polymerization.* Sensors and Actuators B: Chemical, 2005. **105**(2): p. 132-137.
102. Li, M., et al., *Stretchable conductive polypyrrole/polyurethane (PPy/PU) strain sensor with netlike microcracks for human breath detection.* ACS Appl Mater Interfaces, 2014. **6**(2): p. 1313-9.
103. S. Hossein Hosseini, A.A.E., *Conducting polymer blends of polypyrrole with polyvinyl acetate, polystyrene, and polyvinyl chloride based toxic gas sensors.* Journal of Applied Polymer Science, 2003. **90**: p. 49–62.

104. Brady, S., D. Diamond, and K.-T. Lau, *Inherently conducting polymer modified polyurethane smart foam for pressure sensing.* Sensors and Actuators A: Physical, 2005. **119**(2): p. 398-404.
105. Tjahyono, A.P., K.C. Aw, and J. Travas-Sejdic, *A novel polypyrrole and natural rubber based flexible large strain sensor.* Sensors and Actuators B: Chemical, 2012. **166-167**: p. 426-437.
106. Ilicheva, N.S., et al., *Synthesis and Properties of Electroconductive Polymeric Composite Material Based on Polypyrrole.* ISRN Polymer Science, 2012. **2012**: p. 1-7.
107. Merlini, C., et al., *The effect of compressive stress on the electrically resistivity of poly(vinylidene fluoride)/polypyrrole blends.* Synthetic Metals, 2014. **196**: p. 186-192.
108. Stauffer, D., Aharony, A., *Introduction To Percolation Theory*. Second edition ed. 1994, FL: Boca Raton.
109. Gutierrez, B.J.A., et al., *Investigation of the Effects of Multi-Wall and Single-Wall Carbon Nanotubes Concentration on the Properties of ABS Nanocomposites.* C, 2021. **7**(2): p. 33.
110. Wei, X., et al., *3D Printable Graphene Composite.* Sci Rep, 2015. **5**: p. 11181.
111. Gnanasekaran, K., et al., *3D printing of CNT- and graphene-based conductive polymer nanocomposites by fused deposition modeling.* Applied Materials Today, 2017. **9**: p. 21-28.
112. Zhang, D., et al., *Fabrication of highly conductive graphene flexible circuits by 3D printing.* Synthetic Metals, 2016. **217**: p. 79-86.
113. Lopes Pereira, E.C., et al., *Influence of Protonic Ionic Liquid on the Dispersion of Carbon Nanotube in PLA/EVA Blends and Blend Compatibilization.* Frontiers in Materials, 2019. **6**.
114. Wang, X., et al., *Silk-molded flexible, ultrasensitive, and highly stable electronic skin for monitoring human physiological signals.* Adv Mater, 2014. **26**(9): p. 1336-42.
115. Rinaldo Gregorio Junior, N.C.P.d.S.N., *Effect of PMMA addition on the solution cristalizattion of alpha and beta phase of PVDF.* Journal of Physics D: Applied Physics, 1995. **28**: p. 432/436.
116. Atanassov, A., et al., *Properties of clay nanocomposites based on poly(vinylidene fluoride-co- hexafluoropropylene).* Journal of Thermoplastic Composite Materials, 2012. **27**(1): p. 126-141.
117. Al-Saleh, M.H. and U. Sundararaj, *A review of vapor grown carbon nanofiber/polymer conductive composites.* Carbon, 2009. **47**(1): p. 2-22.

Publications on peer reviewed journals

- Bertolini M. C., Dul S., Barra G. M. O, Pegoretti A., "Poly(vinylidene fluoride)/thermoplastic polyurethane flexible and 3D printable conductive composites", Journal of Applied Polymer Science, Vol. 138, (2020).

- Bertolini M. C., Dul S., Pereira E. C. L., Soares B. G., Barra G. M. O, Pegoretti A., "Fabrication and characterization of piezoresistive flexible pressure sensors based on poly(vinylidene fluoride)/thermoplastic polyurethane filled with carbon black-polypyrrole", Polymer Composites, Vol. 12, (2021), p. 6621-6634.

- Bertolini M.C., Zamperlin N., Barra G. M. O, Pegoretti A., "Development of poly(vinylidene fluoride)/thermoplastic polyurethane/carbon black-polypyrrole composites with enhanced piezoelectric properties". In preparation.

- Bertolini M. C., Ramoa S. D. A. S., Soares B. G., Barra G. M. O., Pegoretti A., "Poly(vinylidene fluoride) and thermoplastic polyurethane composites filled with carbon black-polypyrrole for electromagnetic shielding applications". In preparation.

Acknowledgements

I would like to gratefully thank my supervisor Prof. Alessandro Pegoretti and my supervisor abroad Prof. Guilherme Barra for guiding me during this journey, for all the knowledge shared and support during these years. I could not have undertaken this journey without them. I would also like to thank the University of Trento and the Universidade Federal de Santa Catarina for the opportunity and the Italian Ministry of University and Research (MUR) for the financial support. I kindly thank Dr. Sithiprumnea Dul who taught me so much and spent his time helping me in many occasions. I truly thank the technicians Alfredo Casagranda and Claudia Gavazza for their support on some experimental activities. I am very grateful also to Prof. Bluma Soares and Dr. Eliane Lopes (Department of Metallurgical and Material Engineering, Universidade Federal do Rio de Janeiro) for helping with the rheology and electromagnetic interference shielding analysis. I thank Laboratório Labmat (Department of Mechanical Engineering, Universidade Federal de Santa Catarina) for the collaboration, especially Fabiana for her help. My sincere thank also goes to Nico Zamperlini, who helped me with the piezoelectric measurements. I kindly thank all my colleagues in the PC Lab (UniTn) and in Policom (UFSC) for their shares, help and friendship, especially Leonardo, Debora, Silvia, whom were always helping me. My special thank go to the friends I made during this period in Italy, they became a family for me when mine was so far in another continent, mainly for Marta, Anča, Ali, Samy, Flavia and so many others. I gratefully thank all my family and friends for their love and support. My parents for always believing in me. And a very special and grateful thank to my husband who took such a good care of our soon so I could reach this goal, also for his encouragement and support. Thank to they both for their love.